TECHNISCHE UNIVERSITÄT MÜNCHEN
Lehrstuhl für Angewandte Mechanik

Control of a Rubbing Rotor
using an
Active Auxiliary Bearing

Dipl.-Ing. Univ. Lucas Bernhard Ginzinger

Acknowledgment – Danksagung

Contents

1 Introduction

Since men invented the wheel, rotating shafts have been part of our day to day life. Rotors play an import role in many technical applications. Among other applications, they are used for power generation and transmission, in drive systems, electrical machines and in the processing industry. Efficiency is a major objective in power generation and drive systems, so rotors have to cope with high requirements. Numerous and extensive studies have been made to improve the effectiveness and to reduce the probability of failure. By reducing unwanted vibrations, higher rotating speeds can be reached. At the same time constructions have become lighter. Those are only some reasons why the demands have been growing rapidly for the last decades.

On the one hand, the current concern in modern turbomachinery is reliability and safety. On the other hand, efficiency is a main matter of current research and development, especially concerning fuel efficiency. In rotating machinery, increased efficiency is often achieved by tightening operation clearances. This fact increases the risk of a contact between rotating parts and stationary parts of the machine, which is called rubbing. According to a report of the ALLIANZ insurance company [2], rotor rubbing is the primary failure mode at steam turbines - 22 percent of the damages are caused by rubbing.

1.1 Problem Formulation

If a rotor system is not operating under normal conditions and the rotor deflection increases, the stationary and rotating elements are in danger of coming into contact. There are many reasons for the occurrence of rotor-to-stator rubbing:

- Remaining unbalance

- Arising unbalance

- Thermal influences

- Misalignment

- Stator/Casing motion

- External excitation

- Approaching a critical frequency during "speeding-up" or "coast-down"

Rubbing may occur under abnormal operation, but it also may arise under normal conditions, such as during speeding-up or coast-down, in the vicinity of a critical frequency. Conventional auxiliary bearings (also called backup bearings or retainer bearings) limit large response amplitudes and prevent direct rotor-to-stator contact, but do not stabilize the rotor system. Using this type of support leads to various states of rubbing between rotor and auxiliary bearing in case of a failure. Destructive states and very high impact forces are possible. Auxiliary bearings are used in many systems, like various types of turbines (e.g. at the aircraft engine BR710, Rolls-Royce, see Figure 1.1), centrifuges or fail-safe systems at magnetic bearings.
 A contact between rotor and stator is a highly nonlinear event. One and the same

(a) 3D drawing (Rolls-Royce)   (b) Sectional drawing [39], [69]
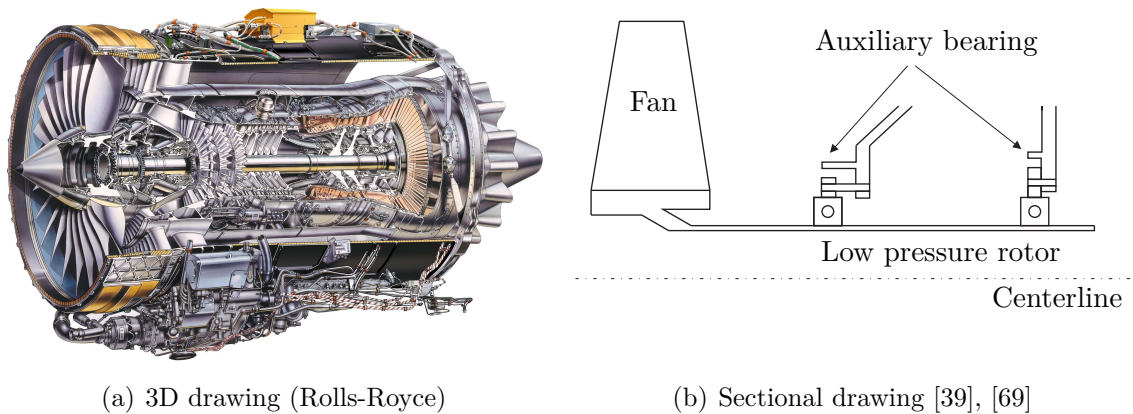
Figure 1.1: Aircraft engine: Rolls-Royce, BR710

excitation may cause a completely different response of such a nonlinear system. After a contact, various motion patterns with different degrees of destructiveness may arise at a rotor system. In the present work, three patterns of them are surveyed:

- *Synchronous Full Annular Rub:* A motion pattern, which is least dangerous. Every point of the rotor runs at a circle with the same angular velocity as the drive system. The bending stress of the shaft is constant. Consequently, the material of the shaft has a static load. There is a permanent contact between rotor and auxiliary bearing. At many rotor systems, this kind of rubbing can be tolerated for a short time without damage.

- *Partial Rub:* In this dangerous state, the rotor has multiple impacts in the auxiliary bearing. There are high impact forces.

- *Backward Whirl:* This motion pattern is one of the most dangerous ones and has to be absolutely avoided. The center of the shaft rotates with another frequency as the drive system. The direction of rotation of this motion is opposite to the one of the drive system. The frequency is often very high. The bending stress changes periodically. In many cases a severe damage is inevitable, if this rubbing state occurs.

The main goal of this work is to develop and verify a control system to reduce the severity of rubbing in auxiliary bearings. For this reason a rubbing state of *Synchronous Full Annular Rub* should be assured with very low contact forces and hardly any impacts. All other rubbing states - including the most destructive *Backward Whirl* - have to be avoided.

The control force is applied indirectly using the auxiliary bearing, only in case of rotor rubbing. During the normal operation state, the feedback control does not interfere with the rotor system at all. The control system should be activated shortly before the occurrence of the first impact, if a contact between rotor and the auxiliary bearing is inevitable. As soon as the load has disappeared, the auxiliary bearing should separate from the rotor again and the normal operation mode should be continued. In case of a permanent error/excitation, the control concept should allow a safe shut-down. Furthermore, the controller has to assure at all times that the rotor deflection does not exceed the initial air gap of the auxiliary bearing, to keep its general purpose in mind - the limitation of the deflection.

1.2 Literature Survey

Numerous and extensive research work has been done in the various fields of rotordynamics over the last decades. In literature, multiple books give a good survey of rotordynamics, e.g. [15], [18], [24] and [59]. The present project is related to various fields of mechanical engineering. Two important fields are treated in the literature survey, the dynamics of rubbing rotors and the active vibration control of rotor systems.

Many publications regard the dynamics of rubbing rotors. But, no mainstream could be determined. Mostly, the research projects and the related publications have been dedicated to particular applications and cases. A selection in chronological order is given here.

One of the first papers regarding this topic has been written by BLACK [5]. In this study synchronous whirling interaction between rotor and stator has been analyzed. Rotor and stator have been regarded as linear multi-degree-of-freedom systems including damping and dry friction. The analysis offers an approach to fairly quickly predict the kind and the range of interaction to be expected in any particular case.

CHILDS [14] presented a mathematical examination of the hypotheses, that circumferential stiffness variations induced by rubbing over a portion of a rotor's orbit can lead to parametric excitation of half-speed whirl at a rotor's natural frequency. The results indicate that potential rubbing surfaces should be lubricated and the local casing stiffness should be substantially lower than the rotor at potential rubbing locations.

SZCZYGIELSKI [58] investigated the rubbing phenomena, which occur between fast rotating rotors and rigid boundaries. A mechanical model has been developed, which

comprises the movement in several phases: free motion, impact and gliding or rolling contact phases. The results have been validated experimentally.

Muszynska [40] gave a general survey on the physical phenomena occurring during rotor-to-stator rubs and a literature survey on the subject of rub.

Isaksson [30] developed a basic model of the rotor-to-stator contact. The objective was to simulate the dynamical behavior of a rotor interacting with non-rotating parts, such as stator housing and seals. The results have not been verified using experimental data.

Bartha [4] presented a valuable insight into how to avoid dry friction backward whirl. The considerable factors are given and recommendations for protecting the rotor are proposed. In this study, a theoretical and experimental investigation into dry friction backward whirl is also presented. The simulation results are compared and verified with experiments. The simulation gives a close approximation of the excitation needed to trigger dry friction backward whirl and helps to identify relevant influencing variables.

Ecker [16] investigated the steady-state behavior of an active magnetic bearing supported single mass rotor contacting an auxiliary bearing with offset center position.

Markert [37] showed that a variety of simple contact models can be used for the computation of the transient dynamics of rotors in retainer bearings without resulting in any differences except for considerations in a very small time-scale.

Sawicki [47] presented an analytical and numerical simulation of an unbalanced multi-disk rotor with rubbing. By employing nonlinear vibration theory, many of the phenomena evolving out of rub-impact in rotating systems have been addressed.

Lawen [32] investigated the application of synchronous interaction dynamics methodology proposed by Black [5] to the problem of auxiliary bearing design. A series of experimental parameter variation studies have been performed, focusing on the overall effects of various auxiliary bearing clearance and stiffness values, which show the effectiveness of the analysis technique. Provided that the assumption of purely synchronous vibration is reasonably satisfied, Black's method for identifying regions of synchronous interaction is shown to be a versatile tool for the analysis of rotor systems with auxiliary clearance bearings.

Wegener [69] presented a comprehensive investigation on the possible use of flexible retainer bearings to limit the amplitude of an unbalanced rotor during the run-up and run-down through the entire frequency range. Many parameter analyses have been performed and practically utilizable design recommendations have been obtained.

Jiang [31] investigated the possibilities to model the friction force between the rotating and stationary components during rubbing and provided an overall picture on the dynamics and stability of rubbing rotor systems.

FENG [19] discussed rubbing phenomena in rotor-stator contact caused by initial perturbation, which is obtained by an instantaneous change of the radial velocity of the rotor. Friction is taken into account. It was found, that rubbing does not occur at subcritical speed if the clearance is larger than the steady-state excursion of the rotor. At supercritical speed, the minimum clearance to avoid full rubbing may exceed the steady-state rotor excursion at the rotor resonance.

VON GROLL [67] analyzed the occurrence of subharmonic vibration frequencies in cases of a rotor/stator contact. Under normal operating conditions the shaft speed is the dominant frequency in rotating machinery. Contrary to that are the dominant subharmonics in the measured cases of abnormal conditions. A possible geometric eccentricity of the rotor and the stator is an important part of the model for these frequency components to appear. The ratio of the resonance frequency of the rotor/stator system to the shaft speed has been found to be substantial to determine the frequency pattern. Accordingly, a possible mechanism for the occurrence of subharmonics could be the correlation with a low-frequency mode of the supporting structure.

WATANABE [68] presented a theoretical and experimental study of the rotor vibration due to the rubbing against casing, for high-speed regimes and different configurations of the casing. The casing dynamics have been taken into account.

EHEHALT [17] validated the motion patterns of an elastic rotor rubbing against the stator. This comprehensive experimental study gives a survey of effects and phenomena of rotor rubbing.

LEGRAND [33] gave a new full 3D strategy for direct contacts between bladed disks and surrounding casing to provide a framework for simulation. It involves reduced computational costs and a robust contact methodology to account for high relative displacements at the contact interface.

YOUNAN [72] presented a work dedicated to the design of auxiliary bearings for the primary magnetic system in a fluid film bearing test rig. A three mass model for the rig is used to conduct the transient analysis of the rotor drop. The contact is described using the theory of Hertz. The analysis included different sets of auxiliary bearing and different levels of damping.

Various approaches have been developed for the active vibration control of flexible rotors. ULBRICH [66] gave a comprehensive outlook of various possibilities of active vibration control.

Many works have investigated concepts with control forces acting directly on the rotor without contact using magnetic bearings, e.g. SCHWEITZER [50], [51] and ULBRICH [64]. The so-called active magnetic bearing systems have been proven in many applications over the last 30 years. Nevertheless, the main disadvantage of this concept is the required space for the magnetic bearings.

Therefore, concepts have been developed to use actuators acting via bearing housings and thereby indirectly on the rotor in opposition to magnet bearings, e.g.

FUERST [23], MOORE [38], STANWAY [56] and ULBRICH [61], [63]. This method yields the advantage that the actuators do not have to be installed at sometimes hardly accessible places.

Only few publications deal with control structures especially for the problem of controlling rubbing rotors. CHAVEZ [12], [13] presented theoretical investigations on an approach to control a rubbing rotor using an active auxiliary bearing. The simulations of a sliding mode control and cross coupled feedback of the presented rotor system with an active auxiliary bearing show the possibilities of reducing the impact forces and decreasing the lateral and torsional vibrations.

GINZINGER [25] presented the first experimental verification of an active auxiliary bearing controlling a rubbing rotor.

ABULRUB [1] and SAHINKAYA [46] investigated the problem of controlling a rubbing rotor in magnetic bearings. In this study, the so-called Recursive Open Loop Adaptive Controller (ROLAC) is introduced. ROLAC uses the magnetic bearings to apply the control force. The control system should prevent contact or it should recover the rotor position quickly with minimum impact damage if contact occurs. For the proposed control system, it is required that the magnetic bearings are fully operational at any time.

CADE [11] gave an introduction into a recent research project regarding an application for an active auxiliary bearing especially for magnetic bearing systems. The auxiliary bearing is piezo actuated using a closed hydraulic coupling.

The literature provides many contributions dedicated to the dynamics of rubbing rotors. Nevertheless there is no well-defined interpretation and the results are not consistent in general. But the effects of the three rubbing states - *Backward Whirling*, *Partial Rub* and *Synchronous Full Annular Rub*, which are of interest in this work, are well investigated.

There is no general approach for the design of an auxiliary bearing. Only recommendations for particular cases can be found.

Active vibration control of rotors has been an ongoing research topic during the last decades. But, there has been hardly any research activity in the field of actively controlling a rubbing rotor. To our best knowledge, the concept of an active auxiliary bearing, which is presented in this work, was the first approach of this type.

1.3 Outline

At first the development of the feedback control system for an active auxiliary bearing is discussed in general in Chapter 2. Our concept to control a rubbing rotor is presented. The control force is applied using the active auxiliary bearing. Two unidirectional actuators enhance the capability of the auxiliary bearing. The target

of the control system and the desired rubbing state is defined. The particular phases of the control concept are discussed.

The modeling of the rotor and the active auxiliary bearing, which is necessary for the controller development, is performed. The equations of motion are derived separately for rotor and the active auxiliary bearing. Then the modeling of the active elements of the rotor system is introduced: actuators and drive system. At last, the contact model, which is used to couple the rotor and the auxiliary bearing, is presented.

A cascade control is developed, which consists of two parts, the feedback controller of the actuators and the computation of the target trajectory. Three control concepts for the actuators have been designed: PID, sliding mode control and feedback linearization. Using the derived equations of motion, an efficient to calculate simulation has been developed to investigate the control concept and to ensure stability. The simulation results suggest using the feedback linearization for the experimental verification.

The concept of an active auxiliary bearing is verified and analyzed experimentally. The design of the test rig is presented in Chapter 3. Two assemblies have been analyzed - one with a very slender shaft and one with a thick shaft. For both configurations, the main parameters are investigated and discussed. Details on the electromagnetic actuators and on the real-time hardware are given.

In Chapter 4, a comprehensive experimental investigation of the proposed control system is presented. Various experiments with both assemblies show the success of the control strategy. "Speeding-up", "arising unbalance" as well as "impact load" are investigated. For every experiment the contact force which arises between rotor and stator is used as a main indicator of the success.

Finally Chapter 5 introduces an advanced simulation environment, which allows configuring the proposed active auxiliary bearing for future applications. The simulation library MBSim is used for the simulation. A comparison between experimental result and simulation closes this chapter.

2 Development of the Feedback Controller

Given a physical system to be controlled, one typically goes, according to SLOTINE [53], through a standard procedure to design the feedback control system, possibly with a few iterations:

1. Specify the desired behavior, and select actuators and sensors;

2. Model the physical plant by a set of differential equations;

3. Design a control law for the system;

4. Analyze and simulate the resulting control system;

5. Implement the control system in hardware.

This procedure is performed in the following. In Section 2.1 the desired behavior is defined. Section 2.2 is dedicated to the mechanical model of a rotor system with an active auxiliary bearing. In the following the control concept is designed and analyzed. The implementation of the control concept on a developed test rig is discussed in Chapter 3.

2.1 Concept

A basic rotor system has been taken as an example to show the possibilities how to control the dynamics of a rubbing rotor using an active auxiliary bearing , Figure 2.1. The system consists of an elastic rotor with one disc, which is mounted with two isotropic ball bearings. The auxiliary bearing is attached to the foundation via two unidirectional magnetic actuators.

Two types of auxiliary bearings (also called backup bearings or retainer bearings) may be used to prevent rotor systems from failure: rolling element bearings and bushing type bearings. Problems may arise with both concepts and are caused by high impacts and contact forces as well as high rotational frequencies. The presented rotor system uses a bushing type bearing. Dry friction experiments also have been performed, which is of interest for systems in no-oil environments.

The control force is applied indirectly by the auxiliary bearing. The advantages of this concept are the following: If the rotor system runs in its common way, the active auxiliary bearing does not take effect, so the original design of the rotor system can be kept unchanged. Additionally, the auxiliary bearing does not only limit an extreme response amplitude of the rotor and prevents the rotor/blades and
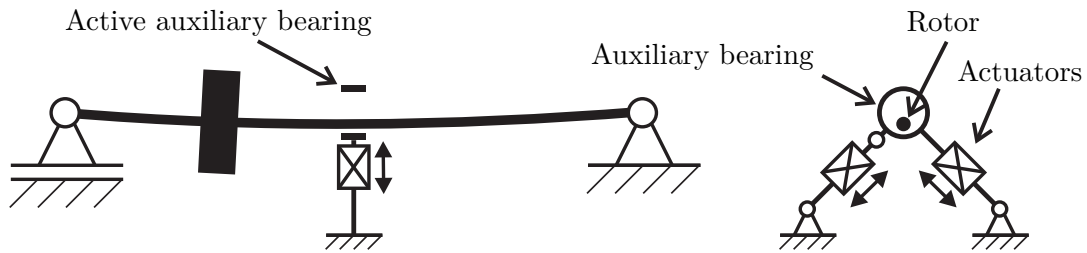
Figure 2.1: Rotor system with an active auxiliary bearing

the casing/seals from direct contact, but also effectively reduces the rubbing sever-ity. Especially the occurrence of destructive rubbing instabilities is avoided. The capability of existing auxiliary bearings, i.e. as safety bearings in active magnetic bearing systems or as run-through resonance support, can be well extended from this concept by introducing active control.

A three-phase control strategy has been developed, which guarantees a smooth tran-sition from free rotor motion to the state of full annular rub. The controller is activated if the rotor deflection exceeds the normal operating condition. In the first phase, the movement of the auxiliary bearing is synchronized with the rotor orbit followed by a smooth transition to a contact. In the second phase the feedback control assures a permanent contact and a minimal contact force. In case of a short-time additional load, the contact is separated in the third phase if the rotor goes to normal operation condition again.
There are three main effects of the proposed control concept, which improve the dynamics of a rubbing rotor system:

1. The avoidance of destructive rubbing states and multiple impacts reduces the load on the system significantly.

2. The control concept introduces additional external damping into the rotor system.

3. The permanent contact between the rotor and the auxiliary bearing leads to a sudden change in the stiffness of the whole system. There is a shift of the resonant frequencies of a rubbing rotor running at a critical speed.

There are several possibilities of supporting a rotor system using an active auxiliary bearing. In case of a suddenly arising unbalance, the controller is activated auto-matically if the rotor response exceeds a certain level. The active control stabilizes the rotor and keeps the load on the whole system low, so that a safe coast-down is possible. On the other hand, it is also possible to use the control system to run safely through a resonance frequency.

To reduce the contact force in the auxiliary bearing the following conditions should be satisfied:

- A smooth transition from the free rotor motion to a permanent contact state.

- Reduction of the first impact.

- The pattern of the rubbing movement is "synchronous full annular rub".

- Prevention of multiple impacts (which means a state of a permanent contact).

To keep the principal purpose in mind, the control scheme also has to limit the rotor amplitude, just as a passive auxiliary bearing does.

The possibilities to control a rubbing rotor with the help of an auxiliary bearing have been investigated theoretically during the last years, see [62]. After a preliminary investigation, a force control turned out to be inappropriate. Usually, force measurement systems have a latency being too long for the present application. In addition to this, a very high sampling rate is needed to gather the high frequency impacts correctly. For these reasons a position control is the better approach for this controller.

2.2 Modeling

In this section, the modeling of the rotor and the active auxiliary bearing is presented. This mathematical model of the system is used for the development of the feedback controller, which requires the equations of motion. At first a mechanical model of the elastic rotor is derived, followed by the modeling of the active auxiliary bearing. The chosen electromagnetic actuators are modeled. Then, a contact model to couple the active auxiliary bearing and the rotor is discussed.

2.2.1 Elastic Rotor

For the development of the mechanical model a well-proven method has been used. Many books deal with the modeling of hybrid multibody systems [8, 9, 60]. Some publications examine especially the modeling and dynamics of elastic rotor systems [3,13,65,71]. Because of the high relevance, the derivation of the equations of motion will be discussed in the following.

Real elastic structures have infinite degrees of freedom. Using a modal transformation, it is possible to reduce the complexity of the equations of motion of such systems to the relevant degrees of freedom, because most of the modal degrees of freedom are outside the investigated frequency range.

Assumptions and Requirements

Taking into account the following assumptions and requirements, the modeling of the regarded rotor system is simplified:

- The rotor is modeled as an elastic, continuous and rotation-symmetric EULER-BERNOULLI beam.

- There is no coupling between bending and torsion.

- The deformations are small (of 1st order).

- The Kelvin-Voigt model is used for the material of the rotor shaft.

- The unbalance is small (of 1st order).

- Only constant angular acceleration is considered.

The modeling of the elastic rotor structure includes the inertia for translation and rotation, gyroscopic effects and internal damping. The formulation of the equations representing the dynamics takes two compulsory steps: kinematics and kinetics, see for example [52].

Kinematics

The task of kinematics is to provide a unitary description of the positions, the velocities and the accelerations for all points of the body. This geometric aspect of the motion is developed in several steps: various coordinate systems are introduced and the relative kinematics of the coordinate systems is derived. The elastic rotor shaft is modeled using infinitesimal elements.

Coordinate Systems   Four coordinate systems are introduced to describe the kinematics of an infinitesimal elements of the rotor shaft, see Figure 2.2.

- I: The inertial coordinate system, the $_I z$ axis coincides with the undeformed rotor shaft.

- B: A coordinate system which rotates about the $_I z$ axis with the angular velocity Ω_B. The $_B z$ axis coincides with the $_I z$ axis.

- R: A coordinate system which rotates about the $_I z$ axis with the angular velocity of the rotor shaft Ω. The $_R z$ axis coincides with the $_I z$ axis.

- K: A body-fixed coordinate system which is fixed to an element of the elastic rotor shaft. The origin of the coordinate system is fixed in the shear center of the element.
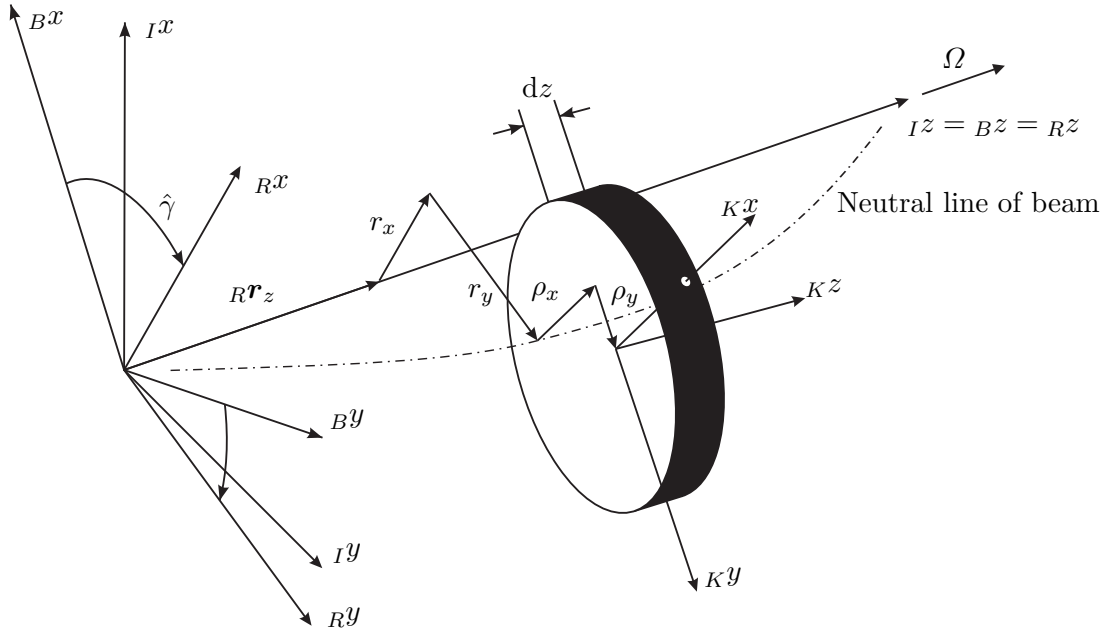
Figure 2.2: Element of the elastic rotor shaft

The introduction of the coordinate system B is done for a more general description, which might be useful for multi-shaft systems [3]. To describe such systems, it is possible to choose Ω_B in a way that the line of action of tangential forces is constant. In the present work, the rotor system is coupled to a fixed environment, so $\Omega_B = 0$.

The angular velocity of the coordinate system R is $\boldsymbol{\omega}_0$, which is given by

$$\boldsymbol{\omega}_0 = \begin{Bmatrix} 0 \\ 0 \\ \Omega \end{Bmatrix}. \tag{2.1}$$

The rotation of a shaft element relative to the reference system R is described using cardan angles. Assuming only small rotations and neglecting terms of higher order, the transformation matrix $\mathbf{A}_{RK}$ (transformation from K to R) can be written as

$$\mathbf{A}_{RK} = {}_R\tilde{\boldsymbol{\varphi}} + \boldsymbol{E}_3 = \begin{bmatrix} 1 & -\vartheta & \beta \\ \vartheta & 1 & -\alpha \\ -\beta & \alpha & 1 \end{bmatrix} \qquad \text{with} \qquad {}_R\boldsymbol{\varphi} = \begin{Bmatrix} \alpha \\ \beta \\ \vartheta \end{Bmatrix}. \tag{2.2}$$

$\boldsymbol{E}_3$ is the identity matrix of the dimension $\mathbb{R}^{3\times3}$. The tilde symbol $\widetilde{(\ )}$ represents the cross product:

$$\mathbf{a} \times \mathbf{b} = \tilde{\mathbf{a}}\,\mathbf{b}. \qquad \mathbf{a} = \begin{Bmatrix} a_1 \\ a_2 \\ a_3 \end{Bmatrix}, \text{ which leads to } \tilde{\mathbf{a}} = \begin{bmatrix} 0 & -a_3 & a_2 \\ a_3 & 0 & -a_1 \\ -a_2 & a_1 & 0 \end{bmatrix}.$$

Position and Velocity   The position vector to the center of gravity of an element of the elastic rotor shaft can be written down as

$$_R\boldsymbol{r} = {}_R\boldsymbol{r}_z + {}_R\bar{\boldsymbol{r}} + (\tilde{\boldsymbol{\varphi}} + \boldsymbol{E}_3) \, {}_K\boldsymbol{\varrho} \tag{2.3}$$

with (see also 2.2)

$$
\begin{aligned}
{}_R\boldsymbol{r}_z &= \left\{ 0 \quad 0 \quad z \right\}^T & &\in \mathbb{R}^3: \text{ vector to element of undeformed shaft,} \\
{}_R\bar{\boldsymbol{r}} &= \left\{ r_x \quad r_y \quad 0 \right\}^T & &\in \mathbb{R}^3: \text{ vector of deformation,} \\
{}_K\boldsymbol{\varrho} &= \left\{ \rho_x \quad \rho_y \quad 0 \right\}^T & &\in \mathbb{R}^3: \text{ vector from neutral line to center of gravity.}
\end{aligned}
$$

The vectors $\boldsymbol{r}_z$ and $\boldsymbol{\varrho}$ are constant in time. The vectors $\bar{\boldsymbol{r}}$ and $\boldsymbol{\varphi}$ describe the deformation of the elastic shaft and therefore are time- and position-dependent.

The velocity vector of an element of the shaft is obtained by the time derivation of (2.3) and is given in the coordinate system R as

$$
\begin{aligned}
{}_R\boldsymbol{v} = {}_R\dot{\boldsymbol{r}} &= \frac{d}{dt}{}_R\boldsymbol{r} + \boldsymbol{\omega}_0 \times {}_R\boldsymbol{r} \\
&= \dot{\bar{\boldsymbol{r}}} + \dot{\tilde{\boldsymbol{\varphi}}}\,\boldsymbol{\varrho} + \tilde{\boldsymbol{\omega}}_0\,\bar{\boldsymbol{r}} + \tilde{\boldsymbol{\omega}}_0\,\tilde{\boldsymbol{\varphi}}\,\boldsymbol{\varrho} + \tilde{\boldsymbol{\omega}}_0\,\boldsymbol{\varrho} \\
&= \underbrace{\dot{\bar{\boldsymbol{r}}} + \tilde{\boldsymbol{\varrho}}^T\dot{\boldsymbol{\varphi}} + \tilde{\boldsymbol{\omega}}_0\,\bar{\boldsymbol{r}} + \tilde{\boldsymbol{\omega}}_0\,\tilde{\boldsymbol{\varrho}}^T\,\boldsymbol{\varphi}}_{R\bar{\boldsymbol{v}}} + \tilde{\boldsymbol{\omega}}_0\,\boldsymbol{\varrho},
\end{aligned}
\tag{2.4}
$$

where $_R\bar{\boldsymbol{v}}$ is the time varying part and $\tilde{\boldsymbol{\omega}}_0\,\boldsymbol{\varrho}$, which is constant.

The angular velocity vector of a shaft-element in reference to the coordinate system R can be written as

$$
\begin{aligned}
{}_K\boldsymbol{\omega} &= \boldsymbol{\omega}_0 + \dot{\boldsymbol{\varphi}} - \tilde{\boldsymbol{\varphi}}\,\boldsymbol{\omega}_0 - \tilde{\boldsymbol{\varphi}}\,\dot{\boldsymbol{\varphi}} \\
&= \boldsymbol{\omega}_0 + \underbrace{\dot{\boldsymbol{\varphi}} + \tilde{\boldsymbol{\omega}}_0\,\boldsymbol{\varphi} - \tilde{\boldsymbol{\varphi}}\,\dot{\boldsymbol{\varphi}}}_{K\bar{\boldsymbol{\omega}}}.
\end{aligned}
\tag{2.5}
$$

Also the angular velocity can be split in a constant and varying part. $\boldsymbol{\omega}_0$ is the reference (frame) motion and $_K\bar{\boldsymbol{\omega}}$ the superposed oscillation.

Minimal Coordinates and Minimal Velocities   The full state of a system can be described by the position and the velocity of each body. Because of constraints these coordinates of the system are usually not independent. Minimal velocities are used instead, which are a combination of independent position and velocity information. The minimal velocities need not to be the time derivation of the minimal coordinates, because of the mentioned independence.

The superposed parts of the translational and the angular velocities can always be

expressed as a linear combination of the minimal velocities (see [8]):

$$\begin{Bmatrix} _R\bar{\boldsymbol{v}} \\ _K\bar{\boldsymbol{\omega}} \end{Bmatrix} = \boldsymbol{F}\,\dot{\boldsymbol{s}}, \qquad \boldsymbol{F} \in \mathbb{R}^{6 \times n_{el}},\ \dot{\boldsymbol{s}} \in \mathbb{R}^{n_{el}}. \tag{2.6}$$

The matrix $\boldsymbol{F}$ in (2.6) is called the derivative matrix. $\boldsymbol{F}$ as well as the minimal velocities $\dot{\boldsymbol{s}}$ have to be determined in the following. $n_{el} \in \mathbb{N}$ is the number of degrees of freedom of the elastic rotor, which is defined by the modeling of the elastic rotor.

In the next step the general decomposition of the velocities in a product of the derivative matrix and the minimal velocities (2.6) has to be carried out for the presented rotor system. Summarizing $_R\bar{\boldsymbol{v}}$ and $_K\bar{\boldsymbol{\omega}}$ from the equations (2.4) and (2.5) one can write down

$$\begin{Bmatrix} _R\bar{\boldsymbol{v}} \\ _K\bar{\boldsymbol{\omega}} \end{Bmatrix} = \begin{bmatrix} \boldsymbol{E} & \tilde{\boldsymbol{\varrho}}^T \\ 0 & \boldsymbol{E} - \tilde{\boldsymbol{\varphi}} \end{bmatrix} \begin{Bmatrix} \dot{\bar{\boldsymbol{r}}} \\ \dot{\boldsymbol{\varphi}} \end{Bmatrix} + \begin{bmatrix} \tilde{\boldsymbol{\omega}}_0 & \tilde{\boldsymbol{\omega}}_0\,\tilde{\boldsymbol{\varrho}}^T \\ 0 & \tilde{\boldsymbol{\omega}}_0 \end{bmatrix} \begin{Bmatrix} \bar{\boldsymbol{r}} \\ \boldsymbol{\varphi} \end{Bmatrix}, \tag{2.7}$$

where $\tilde{\boldsymbol{\varphi}}\,\dot{\boldsymbol{\varphi}}$ and $\boldsymbol{\varrho}$ have been neglected due to higher order. $\bar{\boldsymbol{r}}$ and $\boldsymbol{\varphi}$ are time-dependent, which leads to a partial differential equation. Such equations cannot be solved analytically in general. For this reason the RITZ-method is used for approximation.

The symmetry of the rotation of the shaft allows using the same ansatz function for $r_x(z,t)$ and $r_y(z,t)$ for the deformation of the rotor:

$$r_x(z,t) = \boldsymbol{u}^T(z)\,\boldsymbol{q}_x(t), \tag{2.8}$$
$$r_y(z,t) = \boldsymbol{u}^T(z)\,\boldsymbol{q}_y(t), \tag{2.9}$$

with $\boldsymbol{u},\,\boldsymbol{q}_x,\,\boldsymbol{q}_y \in \mathbb{R}^{n_B}$.

The number of ansatz functions in x- and y-direction is n_B. For the approximation of the torsion we can write down

$$\vartheta(z,t) = \mathbf{w}^T(z)\,\boldsymbol{q}_\vartheta(t) \qquad \text{with } \mathbf{w},\,\boldsymbol{q}_\vartheta \in \mathbb{R}^{n_T}. \tag{2.10}$$

n_T is the number of chosen ansatz functions. The overall number of elastic degrees of freedom is composed of

$$n_{el} = 2\,n_B + n_T.$$

A short introduction to the ansatz functions is presented later.

Using the small-angle approximation the components of $\boldsymbol{\varphi}$ are

$$\alpha = -\frac{\partial r_y}{\partial z} = -r'_y \qquad \text{and} \qquad \beta = \frac{\partial r_x}{\partial z} = r'_x. \tag{2.11}$$

Summarizing the time-variant functions $\boldsymbol{q}_x$, $\boldsymbol{q}_y$ and $\boldsymbol{q}_\vartheta$ from the equations (2.8) and (2.10) to the vector of generalized coordinates $\boldsymbol{q}_e$ and considering (2.11), one can

write down

$$\begin{Bmatrix} \bar{r} \\ \varphi \end{Bmatrix} = \begin{bmatrix} J_T \\ J_R \end{bmatrix} q_e \tag{2.12}$$

with

$$q_e = \begin{Bmatrix} q_x \\ q_y \\ q_\vartheta \end{Bmatrix} \in \mathbb{R}^{n_{el}}, \qquad J_T = \begin{bmatrix} u^T & 0 & 0 \\ 0 & u^T & 0 \\ 0 & 0 & 0 \end{bmatrix}, \quad J_R = \begin{bmatrix} 0 & -u'^T & 0 \\ u'^T & 0 & 0 \\ 0 & 0 & \mathbf{w}^T \end{bmatrix} \in \mathbb{R}^{3 \times n_{el}}. \tag{2.13}$$

J_T and J_R are the JACOBIAN-matrices of Translation (index T) and rotation (index R). Using this equation together with (2.7) and neglecting $\tilde{\varphi}\,\dot{\varphi}$ yields to

$$\begin{Bmatrix} _R\bar{v} \\ _K\bar{\omega} \end{Bmatrix} = \begin{bmatrix} J_T \\ J_R \end{bmatrix} \dot{q}_e + \begin{bmatrix} \tilde{\omega}_0 & 0 \\ 0 & \tilde{\omega}_0 \end{bmatrix} \begin{bmatrix} J_T \\ J_R \end{bmatrix} q_e \overset{!}{=} F\,\dot{s}. \tag{2.14}$$

By using

$$\tilde{\omega}_0\,J_{T,R} = J_{T,R} \begin{bmatrix} 0 & -\Omega\,E_{n_B} & 0 \\ \Omega\,E_{n_B} & 0 & 0 \\ 0 & 0 & 0 \end{bmatrix} = J_{T,R}\,W, \qquad W \in \mathbb{R}^{n_{el} \times n_{el}}$$

one can finally write down the equation (2.6) in a very compact form:

$$F = \begin{bmatrix} J_T \\ J_R \end{bmatrix} \qquad\qquad\qquad\qquad\qquad \in \mathbb{R}^{6 \times n_{el}} \tag{2.15}$$

$$\dot{s} = \dot{q}_e + W\,q_e \qquad\qquad\qquad\qquad\qquad \in \mathbb{R}^{n_{el}}. \tag{2.16}$$

Kinetics

Based on the LAGRANGIAN principle, BREMER [8] gives the equations of motion for a multibody system in the following form:

$$\sum_{i=1}^{n} \left\{ \left[\frac{\partial v}{\partial \dot{s}} \right]^T \{\dot{\mathbf{p}} + \tilde{\omega}\,\mathbf{p} - f^e\} + \left[\frac{\partial \omega}{\partial \dot{s}} \right]^T \{\dot{\mathbf{L}} + \tilde{\omega}\,\mathbf{L} - l^e\} \right\}_i = \mathbf{0}. \tag{2.17}$$

f^e are the external forces and l^e are the external moments. This formulation is valid for a reference system, which has an angular velocity of ω and hence is applicable for the present multibody system. The partial derivatives of v and ω with respect to the vector of the minimal velocities $\dot{s}$ constitute the JACOBIAN-matrices.

To adopt the equation (2.17) to be applicable for an elastic rotor system, we have to add the elastic deformation potential V and the RAYLEIGH-function R, which includes the inner structural damping. As discussed at the beginning, we split up the elastic shaft in infinitesimal thin elements, which have the shape of a disk. For

that reason, the sigma sign is replaced by the integral. By neglecting terms of higher order the equations of motion can be written as

$$\sum_{i=1}^{n}\int_{K_i}\left\{\begin{bmatrix}\frac{\partial \boldsymbol{v}}{\partial \dot{\boldsymbol{s}}}\\[4pt]\frac{\partial \boldsymbol{\omega}}{\partial \dot{\boldsymbol{s}}}\end{bmatrix}^{T}\left\{{}_R\!\begin{pmatrix}m^*\dot{\boldsymbol{v}} & + & m^*\tilde{\boldsymbol{\omega}}_0\,\boldsymbol{v} & - & \mathrm{d}\boldsymbol{f}^e\end{pmatrix}\atop {}_K\!\begin{bmatrix}\boldsymbol{I}^*\dot{\boldsymbol{\omega}} & + & \left(\tilde{\boldsymbol{\omega}}_0\,\boldsymbol{I}^* - \widetilde{\boldsymbol{I}^*\boldsymbol{\omega}_0}\right)\bar{\boldsymbol{\omega}} & + & \boldsymbol{g}_R - \mathrm{d}\boldsymbol{l}^e\end{bmatrix}\right\}\right.$$

$$\left.+\left\{\frac{\partial V}{\partial \boldsymbol{q}_e}\right\}^{T}+\left\{\frac{\partial R}{\partial \dot{\boldsymbol{q}}_e}\right\}^{T}\right\}_i=\boldsymbol{0}. \quad (2.18)$$

$\boldsymbol{g}_R$ is called the gyroscopic vector and comprises of the magnitudes which result from the reference motion.

$$\boldsymbol{g}_R = \boldsymbol{I}^*\dot{\boldsymbol{\omega}}_0 + \tilde{\boldsymbol{\omega}}_0\,\boldsymbol{I}^*\,\boldsymbol{\omega}_0. \quad (2.19)$$

$\mathrm{d}\boldsymbol{f}^e$ and $\mathrm{d}\boldsymbol{l}^e$ are the active forces and moments, which act on the specific element, e.g. weight and centrifugal forces.

In the rotating coordinate system R the length-specific mass m^* is constant and the length-specific mass moment of inertia is constant in the body-fixed system K:

$$m^* = \frac{\partial m}{\partial z}\,\mathrm{d}z = \rho\,A\,\mathrm{d}z, \quad (2.20)$$

$$\boldsymbol{I}^* = \frac{\partial \boldsymbol{I}}{\partial z}\,\mathrm{d}z = \rho\begin{bmatrix}I_x & 0 & 0\\0 & I_y & 0\\0 & 0 & I_p\end{bmatrix}\mathrm{d}z, \quad (2.21)$$

where ρ is the density, A the cross-sectional area, I_x and I_y are the axial moment of inertia and I_p the polar moment of inertia.

Regarding $\frac{\partial \boldsymbol{v}}{\partial \dot{\boldsymbol{s}}}$ and $\frac{\partial \boldsymbol{\omega}}{\partial \dot{\boldsymbol{s}}}$ under consideration of (2.14) it turns out, that only the small superposed velocities $\bar{\boldsymbol{v}}$ and $\bar{\boldsymbol{\omega}}$ have influence on the minimal velocity $\dot{\boldsymbol{s}}$. All other terms of (2.4) and (2.5) are regarded as time-constant. Therefore we can write

$$\begin{bmatrix}\frac{\partial \boldsymbol{v}}{\partial \dot{\boldsymbol{s}}}\\[4pt]\frac{\partial \boldsymbol{\omega}}{\partial \dot{\boldsymbol{s}}}\end{bmatrix}=\begin{bmatrix}\frac{\partial \bar{\boldsymbol{v}}}{\partial \dot{\boldsymbol{s}}}\\[4pt]\frac{\partial \bar{\boldsymbol{\omega}}}{\partial \dot{\boldsymbol{s}}}\end{bmatrix}=\boldsymbol{F}, \quad (2.22)$$

Summarizing (2.18) yields

$$\boldsymbol{M}_i\,\ddot{\boldsymbol{s}}_i + \boldsymbol{G}_i\,\dot{\boldsymbol{s}}_i = \boldsymbol{h}_i \quad (2.23)$$

with

$$\boldsymbol{M} = \int_K \boldsymbol{F}^T\begin{bmatrix}\boldsymbol{E}_3\,m^* & 0\\0 & \boldsymbol{I}^*\end{bmatrix}\boldsymbol{F}$$

$$\boldsymbol{G} = \int_K \boldsymbol{F}^T\begin{bmatrix}\tilde{\boldsymbol{\omega}}_0\,m^* & 0\\0 & \tilde{\boldsymbol{\omega}}_0\,\boldsymbol{I}^* - \widetilde{\boldsymbol{I}^*\boldsymbol{\omega}_0}\end{bmatrix}\boldsymbol{F}$$

$$
\boldsymbol{h} = \int_{K} \boldsymbol{F}^{T} \left\{ \begin{matrix} \mathrm{d}\boldsymbol{f}^{e} - \left(\dot{\tilde{\boldsymbol{\omega}}}_{0} + \tilde{\boldsymbol{\omega}}_{0}\,\tilde{\boldsymbol{\omega}}_{0} \right) m^{*}\,\boldsymbol{\varrho} \\ \mathrm{d}\boldsymbol{l}^{e} - \boldsymbol{g}_{R} \end{matrix} \right\} - \left\{ \frac{\partial V}{\partial \boldsymbol{q}_{e}} \right\}^{T} - \left\{ \frac{\partial R}{\partial \dot{\boldsymbol{q}}_{e}} \right\}^{T} .
$$

Using the equations (2.13) and (2.15) we can write down the mass matrix $\boldsymbol{M}$ and the gyroscopic matrix $\boldsymbol{G}$:

$$
\boldsymbol{M} = \rho \int_{0}^{l} A\left(z\right) \begin{bmatrix} \boldsymbol{u}\,\boldsymbol{u}^{T} & 0 & 0 \\ 0 & \boldsymbol{u}\,\boldsymbol{u}^{T} & 0 \\ 0 & 0 & 0 \end{bmatrix} \mathrm{d}z + \rho \int_{0}^{l} I_{x}\left(z\right) \begin{bmatrix} \boldsymbol{u}'\,\boldsymbol{u}'^{T} & 0 & 0 \\ 0 & \boldsymbol{u}'\,\boldsymbol{u}'^{T} & 0 \\ 0 & 0 & 0 \end{bmatrix} \mathrm{d}z +
$$

$$
+ \rho \int_{0}^{l} I_{p}\left(z\right) \begin{bmatrix} 0 & 0 & 0 \\ 0 & 0 & 0 \\ 0 & 0 & \mathbf{w}\,\mathbf{w}^{T} \end{bmatrix} \mathrm{d}z, \quad (2.24)
$$

$$
\boldsymbol{G} = \rho\,\Omega \int_{0}^{l} A\left(z\right) \begin{bmatrix} 0 & -\boldsymbol{u}\,\boldsymbol{u}^{T} & 0 \\ \boldsymbol{u}\,\boldsymbol{u}^{T} & 0 & 0 \\ 0 & 0 & 0 \end{bmatrix} \mathrm{d}z +
$$

$$
+ \rho\,\Omega \int_{0}^{l} \left(I_{x}\left(z\right) - I_{p}\left(z\right) \right) \begin{bmatrix} 0 & -\boldsymbol{u}'\,\boldsymbol{u}'^{T} & 0 \\ \boldsymbol{u}'\,\boldsymbol{u}'^{T} & 0 & 0 \\ 0 & 0 & 0 \end{bmatrix} \mathrm{d}z. \quad (2.25)
$$

Forces resulting from Elastic Deformation   Under the assumption of a linear stress-strain relation the bending potential V and inner damping R (RAYLEIGH-damping) can be given as

$$
\begin{aligned}
V &= \frac{1}{2}\,\boldsymbol{\varphi}'^{T}\,\mathbf{H}_{V}\,\boldsymbol{\varphi}', \\
R &= \frac{1}{2}\,d_{i}\,\boldsymbol{\varphi}'^{T}\,\mathbf{H}_{V}\,\boldsymbol{\varphi}', \qquad \mathbf{H}_{V} = \mathrm{diag}\left\{ E\,I_{x} \quad E\,I_{y} \quad G\,I_{p} \right\},
\end{aligned} \qquad (2.26)
$$

where E is the modulus of elasticity, G the shear modulus and d_{i} the inner damping. Shear deformation is not considered.

Using

$$
\boldsymbol{\varphi}' = \left\{ \begin{matrix} \alpha' \\ \beta' \\ \vartheta' \end{matrix} \right\} = \begin{bmatrix} 0 & -\boldsymbol{u}''^{T} & 0 \\ \boldsymbol{u}''^{T} & 0 & 0 \\ 0 & 0 & \mathbf{w}'^{T} \end{bmatrix} \boldsymbol{q}_{e}
$$

one can derive the vector of the elastic bending potential as follows:

$$
\int_{K} \left\{ \frac{\partial V}{\partial \boldsymbol{q}_{e}} \right\}^{T} = \left(E \int_{0}^{l} I_{x}\left(z\right) \begin{bmatrix} \boldsymbol{u}''\,\boldsymbol{u}''^{T} & 0 & 0 \\ 0 & \boldsymbol{u}''\,\boldsymbol{u}''^{T} & 0 \\ 0 & 0 & 0 \end{bmatrix} \mathrm{d}z +
$$

$$+G \int\limits_0^l I_p\left(z\right) \begin{bmatrix} 0 & 0 & 0 \\ 0 & 0 & 0 \\ 0 & 0 & \mathbf{w}' \, \mathbf{w}'^T \end{bmatrix} \mathrm{d}z \Bigg) \boldsymbol{q}_e = \boldsymbol{K}_V \, \boldsymbol{q}_e \quad (2.27)$$

where $\boldsymbol{K}_V$ is the stiffness matrix. The damping matrix $\boldsymbol{D}_R$ can be derived from

$$\int\limits_K \left\{ \frac{\partial R}{\partial \dot{\boldsymbol{q}}_e} \right\}^T = d_i \, \boldsymbol{K}_V \, \dot{\boldsymbol{q}}_e = \boldsymbol{D}_R \, \dot{\boldsymbol{q}}_e. \tag{2.28}$$

External Forces Finally, we have to consider the external forces $\boldsymbol{f}^e$ and moments $\boldsymbol{l}^e$, which act on the discrete locations z_{F_i}. In the following we use the DIRAC-function δ, which is defined as

$$\delta\left(x\right) = \begin{cases} +\infty & \text{if } x = 0 \\ 0 & \text{else} \end{cases} \qquad \text{and} \qquad \int\limits_{-\infty}^{+\infty} \delta\left(x\right) \, \mathrm{d}x = 1.$$

These forces and moments can be given as

$$\boldsymbol{f}^e = \sum_i \int\limits_0^l \frac{\partial \boldsymbol{f}_i}{\partial z} \delta\left(r - r_{F_i}\right) \mathrm{d}z \qquad \text{and} \qquad \boldsymbol{l}^e = \sum_i \int\limits_0^l \frac{\partial \boldsymbol{l}_i}{\partial z} \delta\left(r - r_{M_i}\right) \mathrm{d}z. \tag{2.29}$$

Using this the particular parts of the vector $\boldsymbol{h}$, it can be simplified to

$$\int\limits_K \boldsymbol{F}^T \left\{ \begin{matrix} \mathrm{d}\boldsymbol{f}^e \\ \mathrm{d}\boldsymbol{l}^e \end{matrix} \right\} = \sum_{i=1}^{n_F} \boldsymbol{F}_{F_i}^T \left\{ \begin{matrix} \boldsymbol{f}_i \\ \boldsymbol{l}_i \end{matrix} \right\} \qquad \text{with} \qquad \boldsymbol{F}_{F_i} = \begin{bmatrix} \boldsymbol{J}_{T_{F_i}} \\ \boldsymbol{J}_{R_{F_i}} \end{bmatrix}, \tag{2.30}$$

where n_F is the number of the acting forces and moments, $\boldsymbol{F}_{F_i}$ the derivative matrix, $\boldsymbol{J}_{T_{F_i}}$ the JACOBIAN matrix of translation and $\boldsymbol{J}_{R_{F_i}}$ the JACOBIAN matrix of rotation - each at the location i.

For a given mounting, the deflection $\boldsymbol{r}_{L_i}$ of the rotor besides the bearing and the according deflection $\boldsymbol{r}_{K_i}$ of the bearing can be used to determine the forces, which are acting on the rotor:

$$\boldsymbol{f}_{L_i}^e = - \underbrace{\begin{bmatrix} c_{xx} & c_{xy} & 0 \\ c_{yx} & c_{yy} & 0 \\ 0 & 0 & 0 \end{bmatrix}}_{\boldsymbol{C}_{el_i}} \left(\boldsymbol{r}_{L_i} - \boldsymbol{r}_{K_i}\right) - \underbrace{\begin{bmatrix} d_{xx} & d_{xy} & 0 \\ d_{yx} & d_{yy} & 0 \\ 0 & 0 & 0 \end{bmatrix}}_{\boldsymbol{D}_{el_i}} \left(\dot{\boldsymbol{r}}_{L_i} - \dot{\boldsymbol{r}}_{K_i}\right), \tag{2.31}$$

where $\boldsymbol{C}_{el_i}$ and $\boldsymbol{D}_{el_i}$ are the stiffness and damping matrices of the bearing i. In the same way we can derive the discrete moments using the vector of rotation $\boldsymbol{\varphi}$ instead of the vector of translation $\boldsymbol{r}$. By neglecting the terms of higher order, the stiffness and damping matrices for the bearing i can be given using (2.31) together

with (2.12) and (2.18):

$$\boldsymbol{K}_{L_i} = \boldsymbol{J}_{T_{L_i}}^T \, \boldsymbol{C}_{el_i} \, \boldsymbol{J}_{T_{L_i}} \qquad \text{and} \qquad \boldsymbol{D}_{L_i} = \boldsymbol{J}_{T_{L_i}}^T \, \boldsymbol{D}_{el_i} \, \boldsymbol{J}_{T_{L_i}}, \tag{2.32}$$

where $\boldsymbol{J}_{T_{L_i}}$ is the JACOBIAN matrix. For a detailed description of the derivation of the stiffness and damping matrices refer to [54], [55].

Transformation of the Moment Equation in the Reference System   The terms of the linear momentum are given in the rotating R-system, whereas the terms of the angular momentum are given in the body-fixed K-system. To derive the complete set of equations of motion we have to transform all parts of it into one single coordinate system. Here, the R-system has been chosen.

$\tilde{\boldsymbol{\varphi}}$ (2.2) only consists of terms of 1st order. As a consequence, the left part of the differential equation (2.23) remains unchanged because we neglect terms of 2nd order. The only term which is added, is derived of $\boldsymbol{g}_R$ of the vector $\boldsymbol{h}$. Using

$$\int_K \boldsymbol{F}^T \begin{bmatrix} 0 \\ -\mathbf{A}_{RK}\,\boldsymbol{g}_R \end{bmatrix} = -\int_K \boldsymbol{F}^T \begin{bmatrix} 0 \\ \boldsymbol{g}_R + \tilde{\boldsymbol{g}}_R\,\boldsymbol{\varphi} \end{bmatrix} \mathrm{d}z \tag{2.33}$$

and the equations (2.12) and (2.19) the non-conservative matrix $\boldsymbol{N}_B$ - which is caused by the angular acceleration $\dot{\Omega}$ - is derived:

$$\boldsymbol{N}_B = \dot{\Omega}\,\rho \int_K I_p(z) \begin{bmatrix} 0 & \boldsymbol{u}'\,\boldsymbol{u}'^T & 0 \\ -\boldsymbol{u}'\,\boldsymbol{u}'^T & 0 & 0 \\ 0 & 0 & 0 \end{bmatrix} \mathrm{d}z. \tag{2.34}$$

Concluding we can write down the full set of equations of motion of the elastic rotor as

$$\left._R\left\{ \boldsymbol{M}\,\ddot{\boldsymbol{s}} + \underbrace{\left(\boldsymbol{G} + \boldsymbol{D}_R + \boldsymbol{D}_L\right)}_{\boldsymbol{P}}\,\dot{\boldsymbol{s}} + \underbrace{\left[\boldsymbol{K}_L + \boldsymbol{K}_V + \boldsymbol{N}_B - \left(\boldsymbol{D}_R + \boldsymbol{D}_L\right)\boldsymbol{W}\right]}_{\boldsymbol{Q}}\,\boldsymbol{q}_e = \boldsymbol{h} \right\}.\right. \tag{2.35}$$

Parts of the damping (2.28) and (2.32) are proportional to the position level, because of the dependency on $\dot{\boldsymbol{q}}_e$ in combination with the equation (2.16). The vector $\boldsymbol{h}$ comprises of unbalance forces, external forces (e.g. control forces) and forces which act across the system boundary by spring-/damper-elements.

Ansatz Functions

The modeling of the elastic beam is performed using the RITZ method. Within this method, the vectors which are time- and position-dependent are split up into

independent factors. Suitable ansatz functions have to be chosen to determine the matrices and vectors of the equation (2.35). There are the following requirements, according to [8]

- The geometrical boundary conditions have to be fulfilled.

- The functions have to be independent from each other.

- The determined system of functions has to be a complete set of functions, i.e. it must be able to represent the complete manifold of all possible solutions.

It is not possible to fulfill the last requirement, as for this it would be necessary to choose an infinite number of ansatz functions. For this reason we have to strike a balance between high accuracy caused by a huge number of functions and a good performance, which implies a limited number of functions.

For the present work *B-Spline* ansatz functions have been chosen. These piecewise by polynomials defined functions have been successfully applied on elastic structures in many cases, e.g. [45]. The polynomial functions are continuous at the connecting points. The main advantage is that the order of the polynomial functions can be kept low, due to the independence of the functions.

B-Spline functions of order 3 and 5 have been compared regarding convergence of the RITZ-ansatz. The assumption of a better convergence of the B-Splines of the 5th order has not yet been confirmed. Therefore, B-Splines of 3rd order with 320 equidistant supporting points have been chosen for the modeling of the flexible rotor shaft. The functions are two times continuously differentiable. The ansatz functions have been computed using MAPLE. For a detailed description of the derivation of B-Splines see [6] and [48]. For general introduction to B-Splines see [7].

System Reduction

Due to the low order of the ansatz functions many ansatz functions are required for a good system description. Consequently, the resulting order of the overall system is high, which causes a high computational effort for simulating the system. For this reason a modal transformation is performed to reduce the order of the system.

The modal transformation is based on the assumption of linear independent movement patterns of elastic systems. It is assumed that the movement of the system can be approximated by the eigenmodes of translation and rotation. The oscillation modes of the transformed system are fully decoupled. For a detailed discussion of modal analysis and transformation in general see [35].

Starting with the equations (2.24), (2.27) and (2.31) we can derive the eigenmodes of translation and rotation of the static and undamped system according to the

following approach:

$$\boldsymbol{M}_{u,B}\,\ddot{\boldsymbol{q}}_{u,B} + \underbrace{\left(\boldsymbol{K}_{u,V,B} + \boldsymbol{K}_{u,L,B}\right)}_{\boldsymbol{K}_{u,B}}\,\boldsymbol{q}_{u,B} = \boldsymbol{0} \tag{2.36}$$

and

$$\boldsymbol{M}_{u,T}\,\ddot{\boldsymbol{q}}_{u,T} + \underbrace{\left(\boldsymbol{K}_{u,V,T} + \boldsymbol{K}_{u,L,T}\right)}_{\boldsymbol{K}_{u,T}}\,\boldsymbol{q}_{u,T} = \boldsymbol{0}, \tag{2.37}$$

with

$$\boldsymbol{M}_{u,B} = \rho \int_0^l A\left(z\right)\boldsymbol{u}\,\boldsymbol{u}^T\,\mathrm{d}z + \rho \int_0^l I_x\left(z\right)\boldsymbol{u}'\,\boldsymbol{u}'^T\,\mathrm{d}z \qquad \boldsymbol{M}_{u,T} = \rho \int_0^l I_p\left(z\right)\mathbf{w}\,\mathbf{w}^T\,\mathrm{d}z$$

$$\boldsymbol{K}_{u,V,B} = E \int_0^l I_x\left(z\right)\boldsymbol{u}''\,\boldsymbol{u}''^T\,\mathrm{d}z \qquad\qquad \boldsymbol{K}_{u,V,T} = G \int_0^l I_p\left(z\right)\mathbf{w}'\,\mathbf{w}'^T\,\mathrm{d}z$$

$$\boldsymbol{K}_{u,L,B} = \sum_{i=1}^{n_{\text{Bearing}}} \boldsymbol{u}\left(z_i\right)c_{xx,i}\,\boldsymbol{u}\left(z_i\right)^T \qquad\qquad \boldsymbol{K}_{u,L,T} = \boldsymbol{0}.$$

n_{Bearing} is the number of supporting points. It is assumed that the support forces act in one direction only, which means that $c_{xy} = c_{yx} = 0$.

Now we can calculate the eigenvalues of bending $\lambda_{B,i}$ and torsion $\lambda_{T,i}$ and the associated eigenvectors $\boldsymbol{x}_{B,i}$ and $\boldsymbol{x}_{T,i}$. To perform the modal transformation we summarize f_B eigenmodes of bending from bottom to top and f_T eigenmodes of torsion and can write down the reduced modal matrix $\tilde{\tilde{\mathbf{X}}}$:

$$\tilde{\tilde{\mathbf{X}}} = \begin{bmatrix} \tilde{\tilde{\mathbf{X}}}_B & 0 & 0 \\ 0 & \tilde{\tilde{\mathbf{X}}}_B & 0 \\ 0 & 0 & \tilde{\tilde{\mathbf{X}}}_T \end{bmatrix} \qquad \tilde{\tilde{\mathbf{X}}} \in \mathbb{R}^{n_{el} \times 2\,f_B + f_T}. \tag{2.38}$$

with

$$\tilde{\tilde{\mathbf{X}}}_B = \begin{bmatrix} \boldsymbol{x}_{B,1} & \boldsymbol{x}_{B,2} & \dots & \boldsymbol{x}_{B,f_B} \end{bmatrix} \qquad \tilde{\tilde{\mathbf{X}}}_B \in \mathbb{R}^{n_B \times f_B}$$

$$\tilde{\tilde{\mathbf{X}}}_T = \begin{bmatrix} \boldsymbol{x}_{T,1} & \boldsymbol{x}_{T,2} & \dots & \boldsymbol{x}_{T,f_T} \end{bmatrix} \qquad \tilde{\tilde{\mathbf{X}}}_T \in \mathbb{R}^{n_T \times f_T}$$

.

We have simplified the system of equations drastically, because after expanding the matrix products $\mathbf{X}_{B/R}^T\,\boldsymbol{M}_{u,B/R}\,\mathbf{X}_{B/R}$ and $\mathbf{X}_{B/R}^T\,\boldsymbol{K}_{u,B/R}\,\mathbf{X}_{B/R}$ all resulting matrices are diagonal matrices. This is a result of the discussed decoupling. To avoid CPU-intensive numerical inversion, we normalize the eigenvectors so that the mass matrix becomes an identity matrix, for a detailed discussion of this strategy see [48].

Equations of Motion

In the following the last steps to receive the equations of motion are performed. After a transformation to the reference system B we can summarize the equations of motion for any coordinate system which is rotating with the angular velocity Ω_B.

In a compact form the system of equations is given by

$$
_B\left\{ \bar{\boldsymbol{M}}\,\ddot{\bar{\boldsymbol{s}}} + \underbrace{\left(\bar{\boldsymbol{G}} + \bar{\boldsymbol{D}}_R + \bar{\boldsymbol{D}}_L\right)}_{\bar{\boldsymbol{P}}}\,\dot{\bar{\boldsymbol{s}}} + \underbrace{\left(\bar{\boldsymbol{K}}_V + \bar{\boldsymbol{K}}_L + \bar{\boldsymbol{N}}_B + \bar{\boldsymbol{N}}_D\right)}_{\bar{\boldsymbol{Q}}}\,\bar{\boldsymbol{q}}_e = \bar{\boldsymbol{h}}\right\}, \quad (2.39)
$$

where the bars indicate that the matrices and vectors have been transformed to the modal space and with

$$
\dot{\bar{\boldsymbol{s}}} = \dot{\bar{\boldsymbol{q}}}_e + \bar{\boldsymbol{W}}\,\bar{\boldsymbol{q}}_e \qquad \text{with} \qquad \bar{\boldsymbol{W}} = \begin{bmatrix} 0 & -\Omega_B\,\boldsymbol{E}_{f_B} & 0 \\ \Omega_B\,\boldsymbol{E}_{f_B} & 0 & 0 \\ 0 & 0 & 0 \end{bmatrix}. \qquad (2.40)
$$

The comprised matrices are listed in the following.

Mass Matrix

$$
\bar{\boldsymbol{M}} = \begin{bmatrix} \bar{\boldsymbol{M}}_B & 0 & 0 \\ 0 & \bar{\boldsymbol{M}}_B & 0 \\ 0 & 0 & \bar{\boldsymbol{M}}_T \end{bmatrix} = \boldsymbol{E}_{2\,f_B + f_T} \qquad (2.41)
$$

$$
\text{with} \quad \bar{\boldsymbol{M}}_B = \rho \int_l \left(A\,\bar{\boldsymbol{u}}\,\bar{\boldsymbol{u}}^T + I_x\,\bar{\boldsymbol{u}}'\,\bar{\boldsymbol{u}}'^T \right)\,\mathrm{d}z = \boldsymbol{E}_{f_B}
$$

$$
\text{and} \quad \bar{\boldsymbol{M}}_T = \rho \int_l I_p\,\bar{\mathbf{w}}\,\bar{\mathbf{w}}^T\,\mathrm{d}z = \boldsymbol{E}_{f_T}.
$$

Gyroscopic Damping Matrix

$$
\bar{\boldsymbol{G}} = \begin{bmatrix} 0 & \bar{\boldsymbol{G}}_B & 0 \\ -\bar{\boldsymbol{G}}_B & 0 & 0 \\ 0 & 0 & 0 \end{bmatrix} \qquad (2.42)
$$

$$
\text{with} \quad \bar{\boldsymbol{G}}_B = \Omega\,\rho \int_l I_p\,\bar{\boldsymbol{u}}'\,\bar{\boldsymbol{u}}'^T\,\mathrm{d}z - \Omega_B\,\bar{\boldsymbol{M}}_B.
$$

Rayleigh-Damping of the Elastic Structure

$$\bar{D}_R = \begin{bmatrix} \bar{D}_{R,B} & 0 & 0 \\ 0 & \bar{D}_{R,B} & 0 \\ 0 & 0 & \bar{D}_{R,T} \end{bmatrix} \tag{2.43}$$

$$\text{with} \quad \bar{D}_{R,B} = d_i\,\bar{K}_{V,B} \quad \text{and} \quad \bar{D}_{R,T} = d_i\,\bar{K}_{V,T}.$$

Damping of the Supporting Points

$$\bar{D}_L = \begin{bmatrix} \bar{D}_{L,B} & 0 & 0 \\ 0 & \bar{D}_{L,B} & 0 \\ 0 & 0 & \bar{D}_{L,T} \end{bmatrix} \tag{2.44}$$

$$\text{with} \quad \bar{D}_{L,B} = \sum_{i=1}^{n_{\text{Bearing}}} d_{xx,i}\,\bar{u}\left(z_i\right)\,\bar{u}\left(z_i\right)^T$$

$$\text{and} \quad \bar{D}_{L,T} = \sum_{i=1}^{n_{\text{Bearing}}} d_{\vartheta\vartheta,i}\,\bar{\mathbf{w}}\left(z_i\right)\,\bar{\mathbf{w}}\left(z_i\right)^T.$$

Stiffness of the Elastic Structure

$$\bar{K}_V = \begin{bmatrix} \bar{K}_{V,B} & 0 & 0 \\ 0 & \bar{K}_{V,B} & 0 \\ 0 & 0 & \bar{K}_{V,T} \end{bmatrix} \tag{2.45}$$

$$\text{with} \quad \bar{K}_{V,B} = E\int_l I_x\,\bar{u}''\,\bar{u}''^T\,\mathrm{d}z \quad \text{and} \quad \bar{K}_{V,T} = G\int_l I_p\,\bar{\mathbf{w}}'\,\bar{\mathbf{w}}'^T\,\mathrm{d}z.$$

Stiffness of the Supporting Points

$$\bar{K}_L = \begin{bmatrix} \bar{K}_{L,B} & 0 & 0 \\ 0 & \bar{K}_{L,B} & 0 \\ 0 & 0 & \bar{K}_{L,T} \end{bmatrix} \tag{2.46}$$

$$\text{with} \quad \bar{K}_{L,B} = \sum_{i=1}^{n_{\text{Bearing}}} c_{xx,i}\,\bar{u}\left(z_i\right)\,\bar{u}\left(z_i\right)^T \quad \text{and} \quad \bar{K}_{L,T} = \mathbf{0}.$$

Non-conservative Matrix of Acceleration

$$\bar{N}_B = \begin{bmatrix} 0 & \bar{N}_{B,B} & 0 \\ -\bar{N}_{B,B} & 0 & 0 \\ 0 & 0 & 0 \end{bmatrix} \tag{2.47}$$

$$\text{with} \quad \bar{N}_{B,B} = \dot{\Omega}\,\rho\int_l I_p\,\bar{u}'\,\bar{u}'^T\,\mathrm{d}z \quad .$$

Non-conservative Part of the Damping

$$\bar{\boldsymbol{N}}_D = \begin{bmatrix} 0 & \bar{\boldsymbol{N}}_{D,B} & 0 \\ -\bar{\boldsymbol{N}}_{D,B} & 0 & 0 \\ 0 & 0 & 0 \end{bmatrix} - \bar{\boldsymbol{W}}\,\bar{\boldsymbol{D}}_L \tag{2.48}$$

$$\text{with} \quad \bar{\boldsymbol{N}}_{D,B} = \Omega\,\bar{\boldsymbol{D}}_{R,B}.$$

Due to the modal transformation, $\bar{\boldsymbol{K}}_{V,B}$ and $\bar{\boldsymbol{K}}_{V,T}$ can be written as

$$\bar{\boldsymbol{K}}_{V,B} + \bar{\boldsymbol{K}}_{L,B} = \mathrm{diag}\left\{ -\lambda_{B,1}^2 \quad -\lambda_{B,2}^2 \quad \ldots \quad -\lambda_{B,f_B}^2 \right\}, \tag{2.49}$$

$$\bar{\boldsymbol{K}}_{V,T} + \bar{\boldsymbol{K}}_{L,T} = \mathrm{diag}\left\{ -\lambda_{T,1}^2 \quad -\lambda_{T,2}^2 \quad \ldots \quad -\lambda_{T,f_T}^2 \right\}. \tag{2.50}$$

The modal input matrix is given by

$$\bar{\boldsymbol{h}} = \sum_{i=1}^{n_{\mathrm{Input}}} \bar{\boldsymbol{F}}\,(z_i)^T \left\{ \begin{matrix} \boldsymbol{f}_i \\ \boldsymbol{l}_i \end{matrix} \right\} + \rho \int_l A\,\varepsilon \left\{ \begin{matrix} \left(\Omega^2\,\cos\Phi + \dot{\Omega}\,\sin\Phi\right)\bar{\boldsymbol{u}} \\ \left(\Omega^2\,\sin\Phi - \dot{\Omega}\,\cos\Phi\right)\bar{\boldsymbol{u}} \\ 0 \end{matrix} \right\} \mathrm{d}z \tag{2.51}$$

$$\text{with} \quad \bar{\boldsymbol{F}}\,(z)^T = \begin{bmatrix} \bar{\boldsymbol{u}}\,(z) & 0 & 0 & 0 & \bar{\boldsymbol{u}}'\,(z) & 0 \\ 0 & \bar{\boldsymbol{u}}\,(z) & 0 & -\bar{\boldsymbol{u}}'\,(z) & 0 & 0 \\ 0 & 0 & 0 & 0 & 0 & \bar{\mathbf{w}}\,(z) \end{bmatrix},$$

$$\varepsilon = \sqrt{\rho_x^2 + \rho_y^2},$$

$$\text{and} \quad \Phi = \hat{\gamma} + \arctan\frac{\rho_y}{\rho_x} \quad \text{with} \quad \hat{\gamma} = \Omega - \Omega_B.$$

The deflection and torsion of the shaft at the position of z_i is derived by a reverse transformation out of the modal space:

$$\left\{ \begin{matrix} \bar{\boldsymbol{r}}\,(z_i) \\ \boldsymbol{\varphi}\,(z_i) \end{matrix} \right\} = \bar{\boldsymbol{F}}\,(z_i)\,\bar{\boldsymbol{q}}_e. \tag{2.52}$$

2.2.2 Active Auxiliary Bearing

The kinematics and the kinetics of the active auxiliary bearing are derived in the following. A linearization of the equations of motion completes its modeling.

Kinematics

Figure 2.3 shows the geometry of the active auxiliary bearing. There are three joints and five bodies, only four bodies can move independently. The left lower body and the right lower body are the stationary masses of the actuators, which only rotate

by the joints A and B. The upper masses of the actuators are symbolized by two bodies, which rotate by the joints A and B and move along the linear guiding of the actuators. The fifth body is the auxiliary bearing which is rigidly fixed to the right upper mass and coupled to the left upper mass by the joint C. The kinetics of the system is discussed in the following.
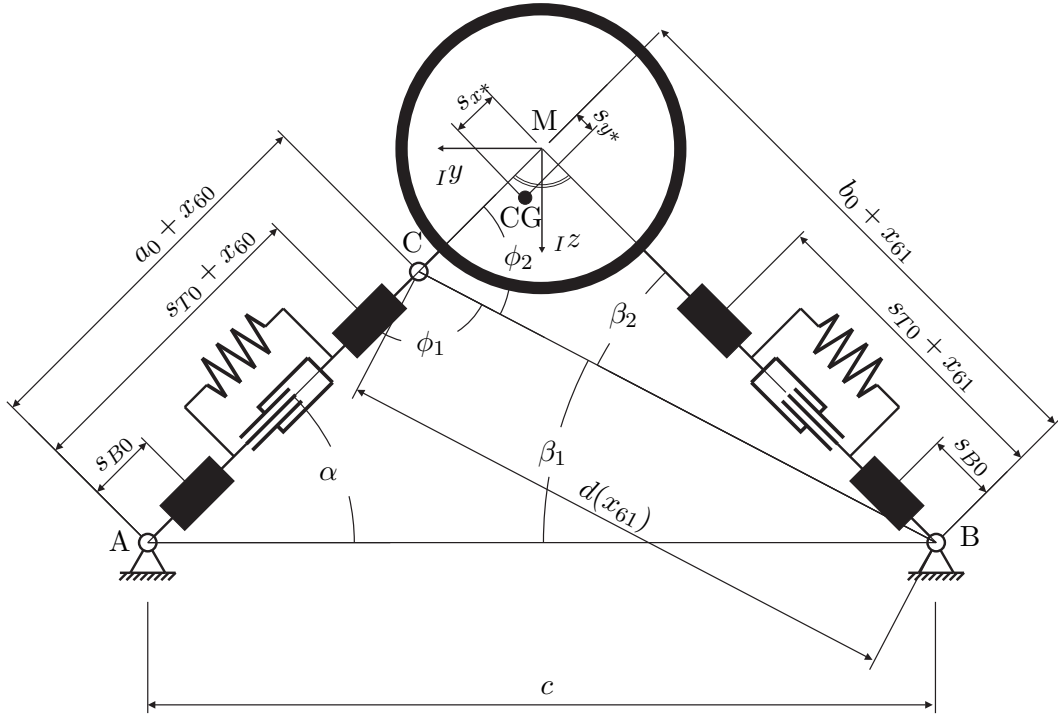

Figure 2.3: Kinematics of the active auxiliary bearing

The derivation of the kinematic relations is performed in the inertial coordinate system $_I y$-$_I z$. s_{B0} is the distance from the lower joints A or B to the center of gravity of both lower bodies. x_{60} is the displacement of the left actuator, x_{61} denotes the displacement of the right one. The choice of identifier of the actuators "60" and "61" result from the serial numbers of the actuators. $s_{T0} + x_{60}$ is the distance between the joint A and the center of gravity of the left upper mass. $s_{T0} + x_{61}$ denotes the distance between the joint B and the right upper mass. $a_0 + x_{60}$ is the distance between the left lower joint A and the upper joint C and $b_0 + x_{61}$ is the distance between the joint B and the hole of the auxiliary bearing, M. s_{x*} and s_{y*} define the position of the center of gravity (CG) of the auxiliary bearing with respect to the center of the hole M. $d(x_{61})$ is the distance between the right lower joint B and the upper joint C. Several angles are indicated: $\alpha, \beta_1, \beta_2, \phi_1, \phi_2$.

The following assumptions are made:

- $\phi_1 + \phi_2 = 180$ for the initial position, which means that $x_{60} = x_{61} = 0$. In this position the auxiliary bearing is concentric with the non-rotating rotor shaft.

- In this initial position $\overline{AM} = \overline{BM} = b_0$.

- The distance $\overline{CM}$ can be approximated in the operational range by $\overline{CM} = b_0 - a_0$.

Using the theorem of Pythagoras, d, which depends on x_{61}, is given by

$$d(x_{61}) = \overline{BC} = \sqrt{(b_0 - a_0)^2 + (b_0 + x_{61})^2}. \tag{2.53}$$

The following trigonometric relations are made:

$$\cos \beta_1 = \frac{-(a_0 + x_{60})^2 + c^2 + d(x_{61})^2}{2\, c\, d(x_{61})}, \tag{2.54}$$

$$\sin \beta_2 = \frac{b_0 - a_0}{d(x_{61})}, \tag{2.55}$$

$$\cos \alpha = \frac{(a_0 + x_{60})^2 + c^2 - d(x_{61})^2}{2\, c\, (a_0 + x_{60})}, \tag{2.56}$$

where 2.54 and 2.56 are derived from the law of cosines. Using these equations we can derive α, β_1, β_2, ϕ_1 and ϕ_2. β is introduced by $\beta = \beta_1 + \beta_2$. A Taylor expansion is used to approximate and simplify the angles α, β_1, β_2, ϕ_1 and ϕ_2 for the ongoing derivation of the equations of motion.

Using the derived relations for the angles, the position vectors, the velocities and angular velocities of the five bodies are set up.

Kinetics, Equations of Motion

The method of LAGRANGE 2 [8] is used to derive the equations of motion for this multibody system

$$\frac{d}{dt}\left(\frac{\partial T}{\partial \dot{\boldsymbol{q}}}\right) - \left(\frac{\partial T}{\partial \boldsymbol{q}}\right) + \left(\frac{\partial V}{\partial \boldsymbol{q}}\right) = \boldsymbol{Q}_{NC}, \tag{2.57}$$

where T is the sum of the kinetic energy and V the sum of the potential energy of all bodies. $\boldsymbol{Q}_{NC}$ is the vector of the non-conservative forces acting on the system. The generalized coordinates are composed of the actuator coordinates:

$$\boldsymbol{q} = \begin{Bmatrix} x_{60} \\ x_{61} \end{Bmatrix}. \tag{2.58}$$

Energy Terms   The mass forces and inertia forces are taken into account in the kinetic energy. For an arbitrary mounted, mass-conservative body the kinetic energy can be written as

$$T \quad = \quad \underbrace{\frac{1}{2}\, m\, \dot{\boldsymbol{r}}_{O'}^{T}\, \dot{\boldsymbol{r}}_{O'}}_{\text{translational part}} + \quad m\, \dot{\boldsymbol{r}}_{O'}^{T}\, \boldsymbol{\omega} \times \boldsymbol{r}_{O'S} \quad + \underbrace{\frac{1}{2}\, \boldsymbol{\omega}^{T}\, \boldsymbol{\Theta}\, \boldsymbol{\omega}}_{\text{rotational part}} , \tag{2.59}$$

where m is the mass of the body, $\dot{\boldsymbol{r}}_{O'}$ the velocity of the reference point, $\boldsymbol{\omega}$ the angular velocity of the body, $\boldsymbol{r}_{O'S}$ the vector from the reference point to the center of gravity and $\boldsymbol{\Theta}$ the inertia tensor at the reference point.

The potential energy includes the conservative forces and is given by

$$V = \quad \underbrace{-m\, \boldsymbol{r}_{S}^{T}\, \boldsymbol{g}}_{\text{potential of inertia}} + \quad \underbrace{\frac{1}{2}\, c_S\, \Delta s^2}_{\text{potential of elasticity}} . \tag{2.60}$$

$\boldsymbol{r}_S$ is the position vector to the center of gravity of the body, $\boldsymbol{g}$ the vector of gravity, c_S the stiffness and Δs the deflection of the spring. By using the center of gravity as a reference point the equation is simplified by $\boldsymbol{r}_{O'S} = \boldsymbol{0}$ and the part in the middle becomes equal to zero.

By using the equations above and the kinematic relations of the auxiliary bearing, the terms of energy are derived. There are many examples for such a multibody system in literature, so the discussion of the derivation is neglected here, e.g. [8], [52], [60].

The mechanical model of the active auxiliary bearing is shown in Figure 2.4. The system boundary is drawn at the joints to the baseplate and at the contact between auxiliary bearing and rotor.

m_{AuxB}, m_{ActT} and m_{ActB} are the masses of the bodies and I_{AuxB}, I_{ActT} and I_{ActB} the inertia tensors. c_{60} and c_{61} are the stiffness of the membranes of the actuators. M_{FricA}, M_{FricB} and M_{FricC} denote the joint friction. F_{em60} and F_{em61} are the forces which are applied by the actuators. These forces comprise of the electromagnetic forces and the permanent-magnetic forces. F_{cy} and F_{cz} are the components of a possible contact forces and M_{cx} is the moment of the contact reaction caused by the friction.

Non-Conservative Forces   Using JACOBIAN-matrices the non-conservative forces are transformed to the generalize coordinates. The sum of the non-conservative forces $\boldsymbol{Q}_{NC}$ is given by

$$\boldsymbol{Q}_{NC} = \sum_{i=1}^{m} \left[\frac{\partial \boldsymbol{v}_i}{\partial \dot{\boldsymbol{q}}}\right]^{T} \boldsymbol{F}_{NC,i} + \sum_{i=1}^{n} \left[\frac{\partial \boldsymbol{\omega}_i}{\partial \dot{\boldsymbol{q}}}\right]^{T} \boldsymbol{M}_{NC,i}. \tag{2.61}$$

In the present case $\boldsymbol{Q}_{NC}$ comprises of the forces of the actuators, the friction and
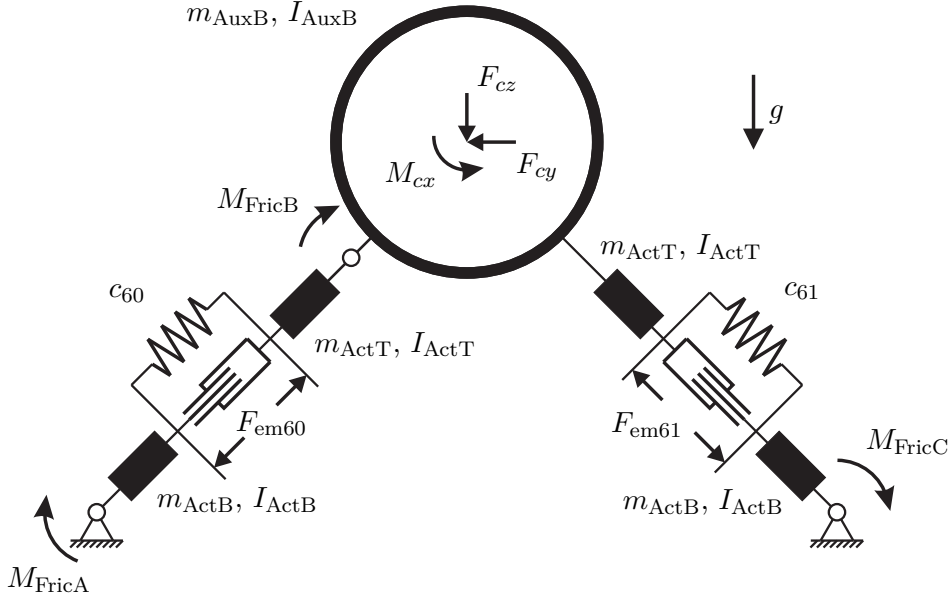
Figure 2.4: Mechanical model of the active auxiliary bearing

the contact force between rotor and auxiliary bearing. The forces of the actuators act directly in the direction of the generalized coordinates, so one can write $\boldsymbol{Q}_{NC}$, which is equal to the vector of the actuator forces $\boldsymbol{F}_{Act}$:

$$\boldsymbol{Q}_{NC,\,Act} = \boldsymbol{F}_{Act} = \begin{Bmatrix} F_{em60} \\ F_{em61} \end{Bmatrix}. \tag{2.62}$$

The contact force between the rotor and auxiliary bearing is included to get a general description. The center of the auxiliary bearing has been taken as the reference point, so the non-conservative forces are given by

$$\boldsymbol{Q}_{NC,\,Contact} = \left[\frac{\partial \boldsymbol{v}_M}{\partial \dot{\boldsymbol{q}}}\right]^T \begin{Bmatrix} 0 \\ F_{Cy} \\ F_{Cz} \end{Bmatrix} + \left[\frac{\partial \boldsymbol{\omega}_{AuxB}}{\partial \dot{\boldsymbol{q}}}\right]^T \begin{Bmatrix} M_{Cx} \\ 0 \\ 0 \end{Bmatrix}. \tag{2.63}$$

The joint friction is approximated to be proportional to the angular velocity:

$$\boldsymbol{Q}_{NC,\,Joints} = -\left[\frac{\partial \boldsymbol{\omega}_A}{\partial \dot{\boldsymbol{q}}}\right]^T d_A\,\boldsymbol{\omega}_A - \left[\frac{\partial \boldsymbol{\omega}_B}{\partial \dot{\boldsymbol{q}}}\right]^T d_B\,\boldsymbol{\omega}_B - \left[\frac{\partial \boldsymbol{\omega}_C}{\partial \dot{\boldsymbol{q}}}\right]^T d_C\,\boldsymbol{\omega}_C, \tag{2.64}$$

where $\boldsymbol{\omega}_A$, $\boldsymbol{\omega}_B$ and $\boldsymbol{\omega}_C$ are the relative angular velocities of the joints and d_A, d_B and d_C the damping i.e. friction coefficients of the particular joints. Note that for the present case $d_A = d_B$.

We can write down the sum of the non-conservative forces

$$\boldsymbol{Q}_{NC} = \boldsymbol{Q}_{NC,\,Act} + \boldsymbol{Q}_{NC,\,Contact} + \boldsymbol{Q}_{NC,\,Joints}. \tag{2.65}$$

Summarizing, this yields to the nonlinear equations of motion of the auxiliary bearing

$$\boldsymbol{M}_{AB}\ddot{\boldsymbol{q}} = \boldsymbol{h}_{AB}(\dot{\boldsymbol{q}},\boldsymbol{q},t), \tag{2.66}$$

where $\boldsymbol{M}_{AB}$ is the mass matrix of the auxiliary bearing and $\boldsymbol{h}_{AB}$ contains all external, internal and gyroscopic forces.

Because of the trigonometrical constraints, the equations of motion are nonlinear of higher order. For certain feedback control strategies a linearized model of the auxiliary bearing is required. Because of the small actuator deflection compared to the dimensions of the system we linearize the equation at the initial and static position of the system. In this position the auxiliary bearing is concentric to the undeformed rotor shaft. After performing a TAYLOR expansion and considering only linear terms, the equations of motion are given by

$$\boldsymbol{M}_{AB,lin}\,\ddot{\boldsymbol{q}} + \boldsymbol{D}_{AB,lin}\,\dot{\boldsymbol{q}} + \boldsymbol{C}_{AB,lin}\,\boldsymbol{q} = \boldsymbol{F}_{Act} + \boldsymbol{Q}_{NC,Contact}, \tag{2.67}$$

where $\boldsymbol{M}_{AB,lin}$, $\boldsymbol{D}_{AB,lin}$ and $\boldsymbol{C}_{AB,lin}$ are the linearized mass matrix, linearized damping matrix and linearized stiffness matrix, respectively.

2.2.3 Active Elements

Actuators

Electromagnetic actuators, which have been developed at the Institute of Applied Mechanics, have been selected for our experiment. These actuators are discussed in Section 3.3 in detail. The performed modeling for feedback controller development of the actuators comprises of the stiffness of the membranes, the mass inertia and the acting forces which are applied to the mechanism. These acting forces consist of the electromagnetic ones, which are controlled, and the permanent ones, which are non-controlled.

Drive System

The drive system has been modeled including a moment of inertia and a PID controller, which applies a torque on the motor shaft. To reduce the complexity for the SIMULINK® simulation presented in Section 2.6, the PID controller directly controls the rotational speed, instead of the torque.

The torque, which drives the rotor, is applied to the shaft of the drive system. This shaft and the elastic rotor shaft are coupled. The torque does not act directly on the rotor shaft, but arises due to torsion of the coupling. The resulting relation should be discussed using an analogous model, which is shown in Figure 2.5. c_K is the stiffness of the coupling and d_K the damping. J_R describes the torque of inertia

of the rotor and J_M the one of the drive system. M_M is the torque, which is applied by the drive system. φ_R is the rotation angle of the rotor and φ_M is the angle of the drive system.
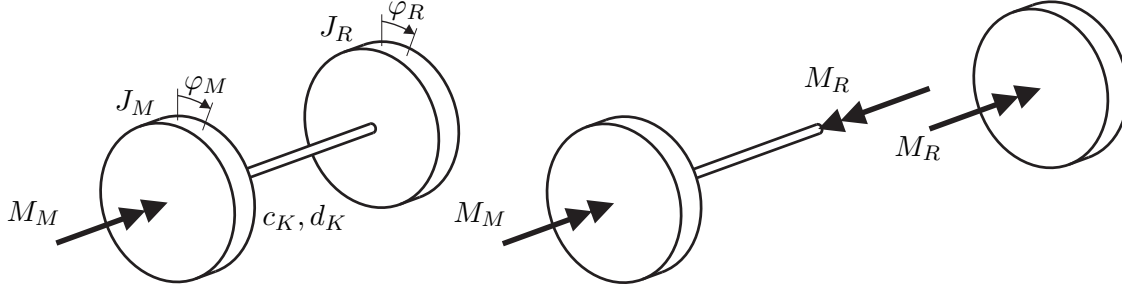

Figure 2.5: Analogous model of the shaft coupling

The system has two rotational degrees of freedom, φ_M and φ_R. The equations of motion of this system can be denoted as

$$\begin{Bmatrix} M_M \\ 0 \end{Bmatrix} = \begin{bmatrix} J_M & 0 \\ 0 & J_R \end{bmatrix} \begin{Bmatrix} \ddot{\varphi}_M \\ \ddot{\varphi}_R \end{Bmatrix} + \begin{bmatrix} d_K & -d_K \\ -d_K & d_K \end{bmatrix} \begin{Bmatrix} \dot{\varphi}_M \\ \dot{\varphi}_R \end{Bmatrix} + \begin{bmatrix} c_K & -c_K \\ -c_K & c_K \end{bmatrix} \begin{Bmatrix} \varphi_M \\ \varphi_R \end{Bmatrix}. \quad (2.68)$$

By cutting free the coupling between drive system and rotor, the acting torque can be determined:

$$M_R = d_K \left(\dot{\varphi}_M - \dot{\varphi}_R \right) - c_K \left(\varphi_M - \varphi_R \right). \quad (2.69)$$

2.2.4 Contact Model

To simulate the rotor system during a state of rubbing, the separate systems *active auxiliary bearing* and *rotor* are coupled. In the course of the feedback controller development a SIMULINK® simulation has been developed which uses this coupling. For this purpose the contact law of HUNT & CROSSLEY [29] has been selected. For a detailed description of the relative kinematics see [48].

Using the contact law of HUNT & CROSSLEY the elasticity and damping of the contact is modeled by nonlinear and isotropic force laws. In general the contact force depends on the depth and velocity of penetration:

$$\boldsymbol{F}_C = \boldsymbol{F}_C \left(\delta_e, \dot{\delta}_e \right) = \begin{Bmatrix} 0 \\ F_{Cy} \\ F_{Cz} \end{Bmatrix}, \quad (2.70)$$

where $\boldsymbol{F}_C$ is the force acting at the contact point in normal direction, δ_e the depth of penetration and $\dot{\delta}_e$ the relative velocity of the penetrating bodies at the contact point in the direction perpendicular to the contact plane. In general, the amount of

the normal component of the contact force $\boldsymbol{F}_C$ is given by

$$F_N = \underbrace{f_N\left(\delta_e\right)}_{\text{elasticity}} + \underbrace{g_N\left(\delta_e,\,\dot{\delta}_e\right)}_{\text{damping}} + \underbrace{F_P\left(\delta_e,\,\dot{\delta}_e\right)}_{\text{dissipation}}. \tag{2.71}$$

The dissipative part allows including plastic deformation. In the present case plastic deformation is neglected, so this part is set to zero.

The elastic part f_N is a nonlinear function of the depth of the penetration. This allows simulating a progressive increase of the force by increasing penetration depth. This part is calculated according to

$$f_N = c_c\,\delta_e^n. \tag{2.72}$$

The stiffness of the contact c_c is very large compared to the stiffness of the overall system, which is important for the simulation of impacts. Besides, the penetration of the contacting bodies should be kept low, as it is in reality.

The damping is carried out by energy dissipation of the impacts and is given by

$$g_N = \frac{3}{2}\,\alpha\,c_c\,\delta_e^n\,\dot{\delta}_e. \tag{2.73}$$

The damping coefficient α depends on the coefficient of restitution. Due to the dependence on the elastic part there is an additional increase of the damping force with increasing penetration depth. According to the HERTZIAN theory of contact pressure the exponent n is set to $\frac{3}{2}$. Summarizing we can write down the contact force in normal direction in complex notation as

$$\boldsymbol{F}_C = c_c\,\delta_e^{\frac{3}{2}}\left(1 + \frac{3}{2}\,\alpha\,\dot{\delta}_e\right)\mathrm{e}^{\mathrm{j}\,\vartheta_c}. \tag{2.74}$$

Caused by the friction in the contact point there is also a tangential force, which is modeled using the COULOMB friction law. The force is directed opposite to the relative movement of the contacting bodies in the contact points. The tangential force acting on the auxiliary bearing is given by

$$\boldsymbol{F}_{C,T} = \mu\,\left|\boldsymbol{F}_C\right|\,\mathrm{e}^{\mathrm{j}\left(\vartheta_c + \frac{\pi}{2}\,\mathrm{sgn}\,\omega_{rel}\right)} \qquad\text{,with}\qquad \omega_{rel} = -\omega_{AuxB} + \Omega, \tag{2.75}$$

where μ is the friction coefficient, ϑ_c the polar angle of the vector from the center of the rotor to the center of the auxiliary bearing, ω_{AuxB} the angular velocity of the auxiliary bearing and Ω the angular velocity of the rotor. To avoid problems in the numerical simulation we smooth the sgn function by using a sat function:

$$\mathrm{sat}\,x = \begin{cases} \mathrm{sgn}\,x & |x| > 1 \\ x & |x| \le 1 \end{cases}. \tag{2.76}$$

Therefore, we can write down the tangential contact force as

$$\boldsymbol{F}_{C,T} = \mu \; |\boldsymbol{F}_C| \; e^{j\left(\vartheta_c + \frac{\pi}{2} \text{sat} \{n_c \, \omega_{rel}\}\right)}, \tag{2.77}$$

where n_c is a coefficient to adopt an optimal behavior of the sat function. The action line of the tangential forces does not go through the center of the auxiliary bearing, so we have to include a moment of the tangential force as mentioned above. This moment is calculated according

$$M_{Cx} = \frac{d_F}{2} \; |\boldsymbol{F}_{C,T}| \; \text{sat} \{n_c \, \omega_{rel}\}, \tag{2.78}$$

where d_F is the inner diameter of the auxiliary bearing.

2.3 Cascade Control

The control concept uses a cascade control, see Figure 2.6. $\mathbf{q}_a$ is the measured position of the auxiliary bearing and $\mathbf{q}_{ad}$ the desired one, $\mathbf{q}_r$ are the coordinates of the rotor, $\mathbf{i}_c$ is the control current to drive the actuators and p a Boolean variable to activate and deactivate the control system. The trajectory computation provides the target trajectory for the auxiliary bearing. The activation routine observes the movement of the rotor and for instance in case of a suddenly arising unbalance the controller is activated automatically if the rotor response is too large. In the following the feedback control of the actuators and the trajectory computation are discussed separately.
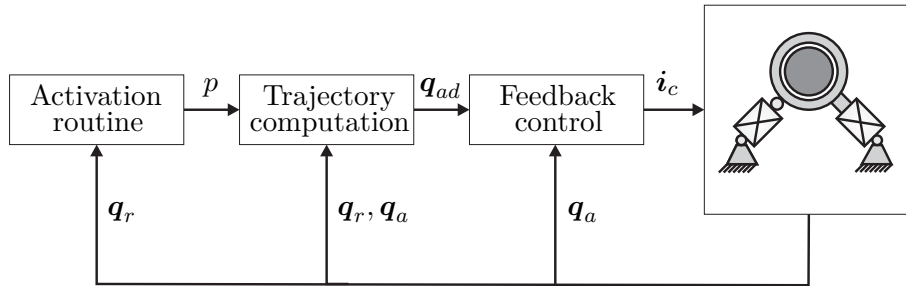
Figure 2.6: Cascade control

There are several challenges to the feedback control concept regarding the proposed system. The electromagnetic actuators have a very high power output and a high bandwidth, but the negative stiffness results in a bad controllability. Of course, also these high-power actuators have a limitation in force, frequency and stroke. Like every real-time hardware, the selected hardware has a limited computational power, which results in a limit of the sample time, depending on the computational effort of the controller. Especially regarding the unilateral contact [44] between rotor and auxiliary bearing, the time-discrete sampling is a big problem for stability. Therefore,

stability can be ensured analytically only for a state without contact. For a detailed investigation of stability of the feedback controller of the present system see [26].

Several strategies for the control of the actuators - linear as well as nonlinear feedback control techniques - have been investigated:

- PID Controller

- Sliding Mode Control

- Feedback Linearization

First of all, a PID controller was developed, which turned out to be applicable in general, but with the drawback of a low control quality. The main advantage is the very low real-time computational effort, which makes implementing the control strategy on a low-cost microcontroller easier, see [43]. The PID controller is discussed in section 2.4.1. A general introduction to this common linear feedback control concept is given in [22].

The second approach was a sliding mode control. This concept has been adapted to the present system [26]. Although this robust control technique considers inaccuracies of the model, it is unsuitable for the proposed control concept. The reason for this is the inherent switching condition. Even if this condition is smoothed using a saturation function, the chattering still disturbs the aimed permanent contact. Therefore, this concept is not discussed in the following.

The third concept is the feedback linearization, which was subject to a large amount of research in the last years. This method turned out to be superior in control quality for the present case and is discussed in detail in section 2.4.2. Most of the experiments have been carried out using this feedback controller.

The development of the trajectory computation followed no established scheme and is an all-new development. This part of the control system is discussed in section 2.5.

2.4 Feedback Control of the Actuators

2.4.1 PID Controller

One big challenge in the control of the electromagnetic actuators is its stability. The utilization of strong permanent magnets to generate the bias flux leads to a strong negative system-stiffness, which results in a bad controllability of the system. Furthermore, the actuator shows a nonlinear force behavior in relation to the control current and the axial position of the pull-disk. To linearize the nonlinear system in the whole operating range a nonlinear feed forward mechanism to compensate the nonlinear effects is applied. Thus, the system gets a linear force characteristic
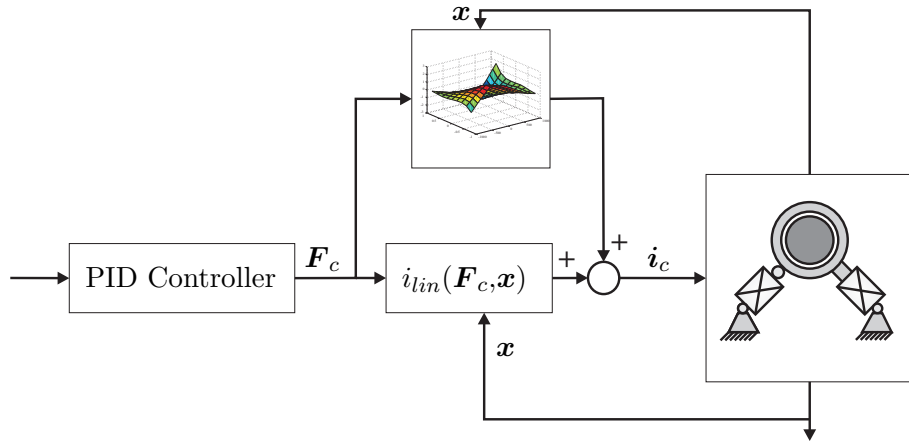
Figure 2.7: Feed forward mechanism, compensation of nonlinearity

related to the control current, which is independent to the displacement of the movable pull-disks.

The feed forward mechanism shown in Figure 2.7 is based on the feedback controller for the used electromagnetic actuators developed by OBERBECK [42]. $\boldsymbol{F}_c$ is the desired control force, which has been determined by the PID controller, $i_{lin}(\boldsymbol{F}_c,\boldsymbol{x})$ is the linear part of the force-current correlation, $\boldsymbol{x}$ is the displacement of the actuators and $\boldsymbol{i}_c$ is the control current.

The nonlinearity of the actuator is canceled using a map of the force-displacement-current correlation. This map, see Figure 2.8, contains only the nonlinear part of the correlation. The linear part is treated with the $i_{lin}(\boldsymbol{F}_c,\boldsymbol{x})$-function, see Figure 2.7. The map was gained by static measurements, which gave the supporting points of the field.

Depending on the used real-time hardware, a big disadvantage of the usage of this map might be the very high computational effort of interpolation. Especially for the present case using the dSPACE real-time hardware, the computational effort of interpolation is very high. This fact is unacceptable, because a controller sample rate as high as possible is preferable. A surface fit has been done to gain a polynomial function to represent the measured map. The function is of the type

$$i(F_c,x) = a + bx + cx^2 + dx^3 + eF_c + fF_cx + gF_cx^2 + hF_cx^3 + iF_c^2 + jF_c^2x + kF_c^2x^2 + lF_c^2x^3,$$
(2.79)

where F_c is the desired actuator force, x the displacement of the actuators and i the control current. a, b, c, d, e, f, g, h, i, j, k and l are the constant coefficients. The coefficients of this function have been determined using the online surface fit tool *ZunZun.com* [1]. The map, which is given by the determined function, is plotted in Figure 2.9.
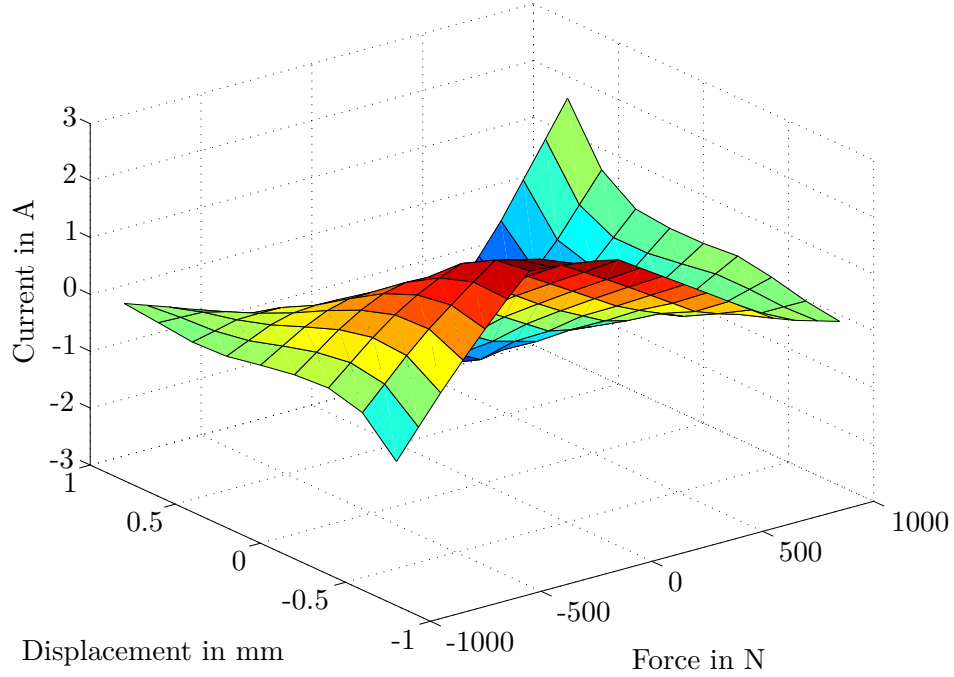
---

1 http://www.zunzun.com

Figure 2.8: Measured map of the force-displacement-current correlation of the actuator

Using this fitted map the computational effort for the feed forward mechanism has been reduced by 70 percent.

The linearized equations of motion (2.67), which are derived in Section 2.2, are simplified by neglecting the contact reactions $\boldsymbol{Q}_{NC,Contact}$, because the contact forces should be on a low level during a controlled state of rubbing:

$$\boldsymbol{M}_{AB,lin}\,\ddot{\boldsymbol{q}} + \boldsymbol{D}_{AB,lin}\,\dot{\boldsymbol{q}} + \boldsymbol{C}_{AB,lin}\,\boldsymbol{q} = \boldsymbol{F}_{Act}. \tag{2.80}$$

These linear decoupled equations of motion have two degrees of freedom, which correspond to the two actuators. The control force $\boldsymbol{F}_{Act}$ is given by

$$\boldsymbol{F}_{Act} = \begin{Bmatrix} F_{em60} \\ F_{em61} \end{Bmatrix}. \tag{2.81}$$

In this approach we design two decoupled PID feedback controller for a linear system. A common PID controller follows the equation:

$$F_{emi} = Pe + D\frac{de}{dt} + I\int e\,dt \qquad \text{with } i = 60, 61, \tag{2.82}$$

where F_{emi} is the calculated control force, P, D and I are coefficients and e the tracking error:

$$e = y_d - y \tag{2.83}$$
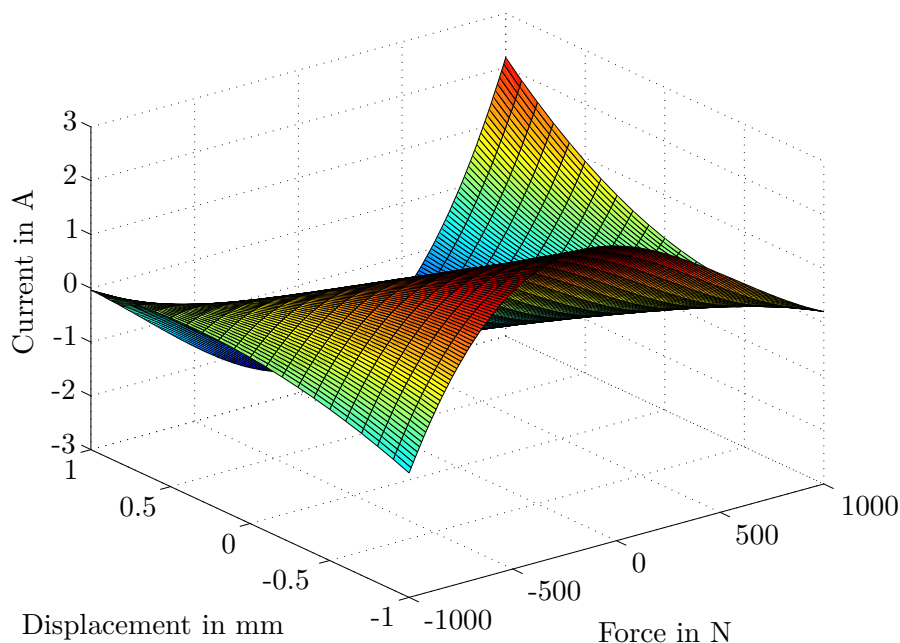
Figure 2.9: Fitted map of the force-displacement-current correlation of the actuator

where y_d is the desired and y the measured position of the actuator. The coefficients of the control law are chosen for the linearized system according to the Hurwitz polynomial [22] and were optimized experimentally. Note that in case of contact the coefficient I for the integral control part is switched to zero.

2.4.2 Feedback Linearization Control

Although linear control is a well-proven method and has a long history of success-ful industrial applications, we cannot neglect that the present system has strong nonlinearities. Over the last years much effort has been put into developing several nonlinear control strategies to improve feedback controllers for nonlinear systems. The method of feedback linearization has been chosen for present system. A de-tailed description can be found in [53].
Designing a control system mostly starts with deriving a meaningful model of the plant, i.e., a model that captures the key dynamics of the plant in the operational range of interest. Feedback linearization deals with a technique that transforms orig-inal system models into equivalent models of a simpler form. This differs entirely from conventional linearization. Feedback linearization is achieved by exact state transformations and feedback, rather than by linear approximations of the dynam-ics. The idea, that the form and complexity of a system model depend considerably on the choice of reference frames or coordinate systems, is well known in mechanics.

Therefore, we transform the nonlinear model into a linear system, and then use the well-known and powerful linear design techniques to complete the control design. The feedback linearization method has been successfully applied to address some practical control problems, including the control of helicopters, high performance aircrafts, industrial robots and biomedical devices.

Mathematical Tools

At first some mathematical tools from differential geometry are shortly introduced. For a detailed description please refer to standard literature in differential geometry.

To be consistent with the terminology of this field of mathematics, we shall call a vector function $\boldsymbol{f} : \boldsymbol{R}^n \to \boldsymbol{R}^n$ a vector field in $\boldsymbol{R}^n$. Furthermore we only investigate smooth vector fields, which means, that the function $\boldsymbol{f}(\boldsymbol{x})$ has continuous partial derivates of any required order.

The gradient of a scalar function $h(\mathbf{x})$ is given by

$$\nabla h = \frac{\partial h}{\partial \mathbf{x}} = \begin{bmatrix} \frac{\partial h}{\partial x_1} & \frac{\partial h}{\partial x_2} & \cdots & \frac{\partial h}{\partial x_n} \end{bmatrix} \qquad \dim \nabla h = 1 \times n. \tag{2.84}$$

Similarly, given a vector field $\mathbf{f}(\mathbf{x})$, the JACOBIAN of $\boldsymbol{f}$ is denoted by

$$\nabla \mathbf{f} = \frac{\partial \mathbf{f}}{\partial \mathbf{x}} = \begin{bmatrix} \frac{\partial f_1}{\partial x_1} & \frac{\partial f_1}{\partial x_2} & \cdots & \frac{\partial f_1}{\partial x_n} \\ \frac{\partial f_2}{\partial x_1} & \frac{\partial f_2}{\partial x_2} & \cdots & \frac{\partial f_2}{\partial x_n} \\ \vdots & \vdots & \ddots & \vdots \\ \frac{\partial f_n}{\partial x_1} & \frac{\partial f_n}{\partial x_2} & \cdots & \frac{\partial f_n}{\partial x_n} \end{bmatrix} \qquad \dim \nabla \mathbf{f} = n \times n. \tag{2.85}$$

The basis for the development of a direct Input- / Output- Relation (e.g. Linearization) is the so-called Lie derivative. The Lie derivative of a smooth scalar function $h(\boldsymbol{x}), \mathbb{R}^n \to \mathbb{R}$ with $\boldsymbol{x} \in \mathbb{R}^n$ with respect to the smooth vector field $\boldsymbol{f}(\boldsymbol{x}), \mathbb{R}^n \to \mathbb{R}^n$ is defined as

$$L_{\boldsymbol{f}} h = \nabla h \, \boldsymbol{f}. \tag{2.86}$$

Thus, the Lie derivative $L_{\boldsymbol{f}} h$ is simply the directional derivative of h along the direction of the vector $\boldsymbol{f}$. Repeated Lie derivatives can be defined recursively

$$L_{\boldsymbol{f}}^0 h = h \qquad L_{\boldsymbol{f}}^1 h = \nabla h \, \boldsymbol{f} \qquad L_{\boldsymbol{f}}^i h = L_{\boldsymbol{f}} \left(L_{\boldsymbol{f}}^{i-1} h \right) = \nabla \left(L_{\boldsymbol{f}}^{i-1} h \right) \boldsymbol{f}.$$

If $\boldsymbol{g}$ is another vector field, then the scalar function $L_{\boldsymbol{g}} L_{\boldsymbol{f}} h(\boldsymbol{x})$ is

$$L_{\boldsymbol{g}} L_{\boldsymbol{f}} h = \nabla \left(L_{\boldsymbol{f}} h \right) \boldsymbol{g}.$$

Using these mathematical tools, it is easy to perform the input-output-linearization even for complex systems.

Theory of the Input-Output Linearization

A system of equations of motion with m inputs $\boldsymbol{u}$ and the outputs $\boldsymbol{h}$ can be written in the canonical form

$$\dot{\boldsymbol{x}} = \boldsymbol{f}(\boldsymbol{x}) + \boldsymbol{G}(\boldsymbol{x})\,\boldsymbol{u} = \boldsymbol{f}(\boldsymbol{x}) + \sum_{j=1}^{m} \boldsymbol{g}(\boldsymbol{x})\,u_j. \tag{2.87}$$

The output equation is given by

$$\boldsymbol{y} = \boldsymbol{h}(\boldsymbol{x}). \tag{2.88}$$

There is no further requirement to the structure of the vectors $\boldsymbol{f}$ and $\boldsymbol{h}$ and the matrix $\boldsymbol{G}$. Therefore, the vectors and the matrix may contain nonlinear terms.

To perform the input-output linearization of (2.87), we have to apply the Lie derivative to each output y_i repeatedly until the break condition

$$L_{\boldsymbol{g}_j}\left[L_{\boldsymbol{f}}^{r_i-1} h_i(\boldsymbol{x})\right] \neq 0 \tag{2.89}$$

is fulfilled for at least one $j = 1 \ldots m$. The superscript index r_i indicates the r_i-th derivative of the i-th output. Performing this for every output of the system, an explicit relation of each input to one output is obtained. The equation of the direct input-output relation can be denoted as

$$\left\{\begin{array}{c} y_1^{(r_1)} \\ \vdots \\ y_m^{(r_m)} \end{array}\right\} = \underbrace{\left\{\begin{array}{c} L_{\boldsymbol{f}}^{r_1} h_1(\boldsymbol{x}) \\ \vdots \\ L_{\boldsymbol{f}}^{r_m} h_m(\boldsymbol{x}) \end{array}\right\}}_{\boldsymbol{a}(\boldsymbol{x})} + \underbrace{\left[\begin{array}{ccc} L_{\boldsymbol{g}_1}\left[L_{\boldsymbol{f}}^{r_1-1} h_1(\boldsymbol{x})\right] & \cdots & L_{\boldsymbol{g}_m}\left[L_{\boldsymbol{f}}^{r_1-1} h_1(\boldsymbol{x})\right] \\ \vdots & \ddots & \vdots \\ L_{\boldsymbol{g}_1}\left[L_{\boldsymbol{f}}^{r_m-1} h_m(\boldsymbol{x})\right] & \cdots & L_{\boldsymbol{g}_m}\left[L_{\boldsymbol{f}}^{r_m-1} h_m(\boldsymbol{x})\right] \end{array}\right]}_{\boldsymbol{E}(\boldsymbol{x})} \left\{\begin{array}{c} u_1 \\ \vdots \\ u_m \end{array}\right\}. \tag{2.90}$$

Here, with $i = 1..2$ each output has to be differentiated twice, so $r_i = 2$:

$$\left[\begin{array}{c} y_1^{r_1} \\ y_2^{r_2} \end{array}\right] = \left[\begin{array}{c} L_{\boldsymbol{f}}^{r_1} h_1(\mathbf{x}) \\ L_{\boldsymbol{f}}^{r_2} h_2(\mathbf{x}) \end{array}\right] + \mathbf{E}(\mathbf{x}) \left[\begin{array}{c} u_1 \\ u_2 \end{array}\right] \tag{2.91}$$

The matrix $E(x)$ is called the decoupling matrix and for notation simplification $a(x)$ has been introduced.

If the control input u is chosen according to

$$\mathbf{u} = E^{-1}(\mathbf{x})[\mathbf{v} - \mathbf{a}(\mathbf{x})], \tag{2.92}$$

where v is the new control input to be determined, the nonlinearity of the system is canceled and a simple linear double integrator relationship between the output and the new input v is obtained.

Development of the Feedback Controller using the Input-Output Linearization

For the design of the feedback controller we use the equations of motion (2.66) of the auxiliary bearing, which has the dimension 2. To keep the controller as simple as possible we define the displacement of the actuators as the output of the system, instead of the position of the auxiliary bearing in y and z.

The control error for each output is defined as

$$\tilde{y}_i = y_i - y_{i,d} \qquad \text{and} \qquad \dot{\tilde{y}}_i = \dot{y}_i - \dot{y}_{i,d} \qquad i = 1, 2, \tag{2.93}$$

where y_i is the actual output and $y_{i,d}$ the desired output.

The main purpose of the feedback controller is to minimize this control error. A pole-assignment method according to [49] has been chosen for the design process.

Pole-Assignment

By defining a control law for every output $i = 1, 2$

$$\nu = -k_1 \, \dot{\tilde{y}} - k_0 \, \tilde{y}, \tag{2.94}$$

the equations of motion of the closed loop system using the feedback linearization are given by

$$\begin{aligned}
\ddot{y} &= -k_1 \, \dot{\tilde{y}} - k_0 \, \tilde{y} \\
&= -k_1 \, (\dot{y} - \dot{y}_d) - k_0 \, (y - y_d).
\end{aligned} \tag{2.95}$$

With the help of the LAPLACE-transformation the transfer function of the closed loop is derived:

$$\frac{Y}{Y_d} = \frac{s \, k_1 + k_0}{s^2 + s \, k_1 + k_0}. \tag{2.96}$$

The system is stable if all poles of the transfer function are in the left half s-plane, i.e., all the poles have negative real parts. Solving the characteristic equation, the poles can be determined in general:

$$s_{1,2} = \frac{-k_1 \pm \sqrt{-k_1^2 - 4 \, k_0}}{2}. \tag{2.97}$$

Table 2.1: Poles of the designed control system

	a	b
Actuator 60	-270	50
Actuator 61	-270	50

By defining the coefficients k_0 and k_1 according

$$k_0 = a^2 + b^2 \qquad \text{and} \qquad k_1 = -2\,a \tag{2.98}$$

the poles $a \pm \mathrm{j}\,b$ can be arbitrarily assigned. The quality of control increases by placing the poles to the left, but this causes high control forces which may lead to instability. For the present system various simulations and experiments have been made to determine the optimal poles as given in Table 2.1.

2.5 Computation of the Target Trajectory

The computation of the target trajectory has to obey the control principle, which has been discussed in Section 2.1. The three-phase control strategy should guarantee a smooth catching of the rotor followed by a state of "synchronous rubbing". To keep the principal purpose of an auxiliary bearing in mind, the control scheme also has to limit the rotor amplitude as a passive auxiliary bearing does. The controller only needs the position of the auxiliary bearing, the position of the rotor shaft inside the auxiliary bearing and the information from the shaft encoder as an input.

The operation phases of the control concept are shown in Figure 2.10. The controller is not activated during normal operation condition (the rotor deflection r_N is smaller than a defined limit r_{limit}). As soon as the rotor deflection becomes too large, e.g. due to a suddenly arising unbalance, and r_N exceeds r_{limit}, the controller is activated. In the first control phase, the movement of the auxiliary bearing is synchronized with the rotor orbit followed by a smooth transition to a contact. In the second phase, the feedback control assures a permanent contact in the rubbing state of "synchronous full annular rub" and a low contact force. The second phase is active as long as the additional load is present. In the third phase the rotor is separated from the auxiliary bearing after the additional load has disappeared.
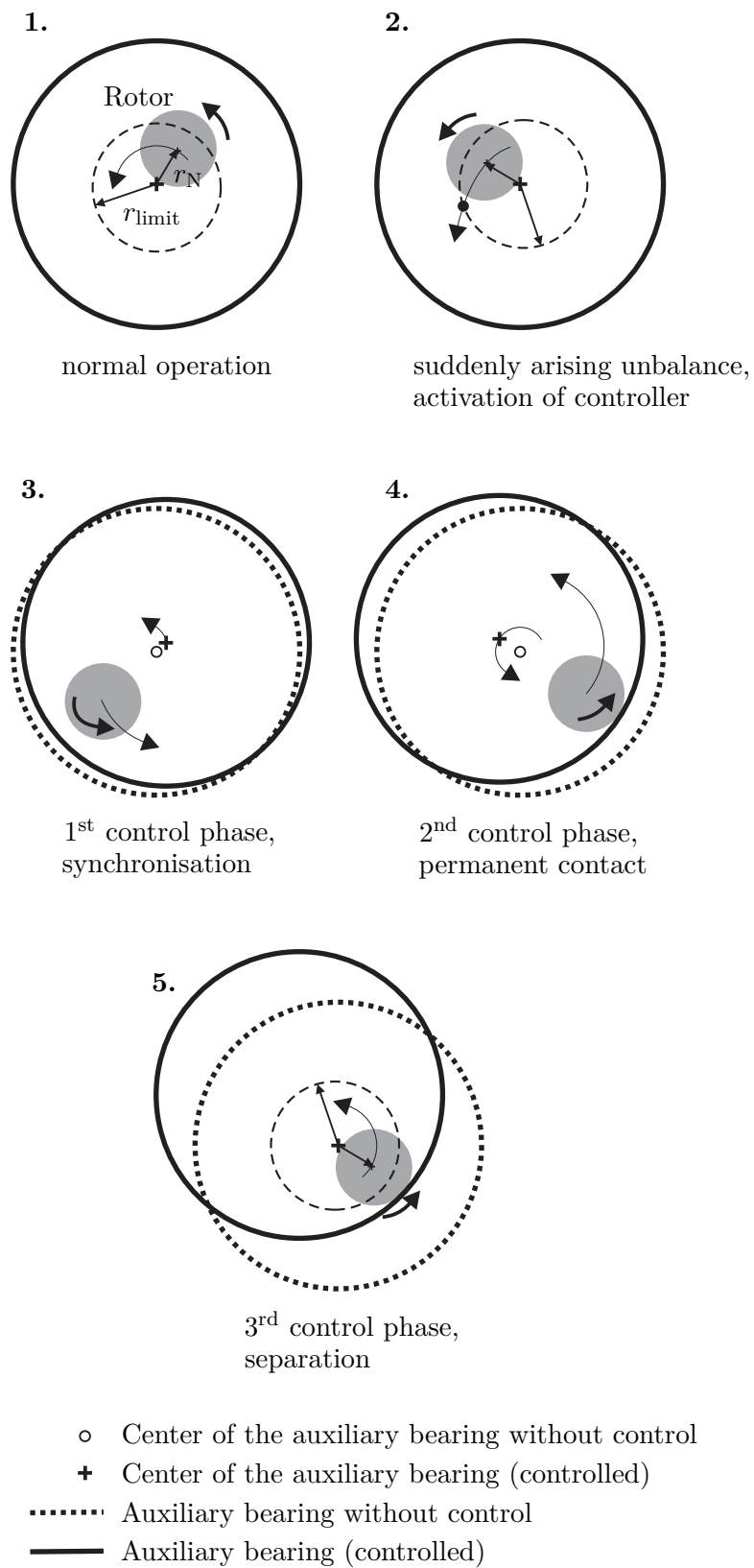
Figure 2.10: Principle of the control concept

In order to define the essential geometrical variables, a cross section of the auxiliary bearing and the rotor is shown schematically in Figure 2.11. The origin of the coordinate system coincides with the center of the undeformed rotor, $\mathbf{r}_r$ is the position vector to the center of the deformed rotor (in the cross section) and $\mathbf{r}_a$ to the center of the auxiliary bearing. The air gap in the auxiliary bearing is δ_0 and $\mathbf{r}_N$ represents the vector from the center of the auxiliary bearing to the center of the rotor. Modified polar coordinates are used, which allow a negative radius. The angles φ_a, φ_r and radii r_a, r_r, r_N of the vectors $\mathbf{r}_a$, $\mathbf{r}_r$ and $\mathbf{r}_N$ are introduced.
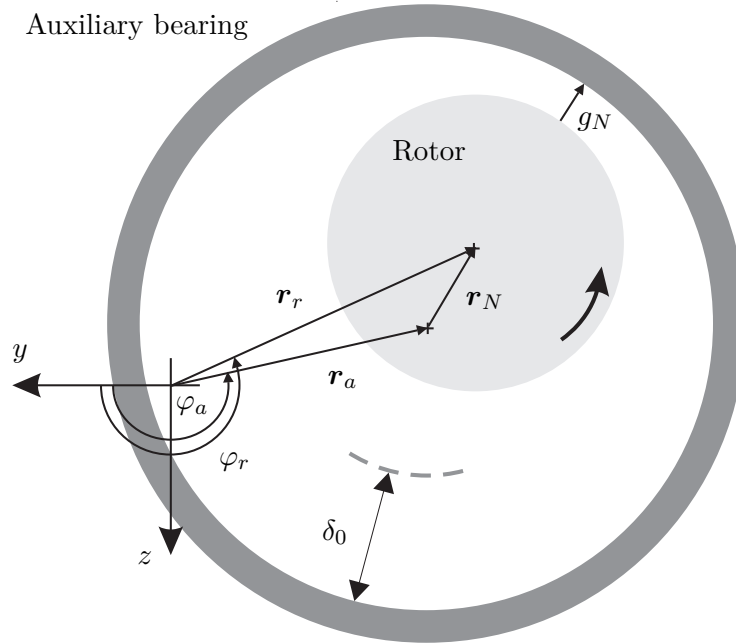
Figure 2.11: Contact kinematics

The overall control target of the first and second phase can be specified as

$$\mathbf{q}_{ad} = \begin{array}{c} arg\ min \\ (\ddot{\mathbf{q}},\dot{\mathbf{q}},\mathbf{q}) \end{array} \left\{ \begin{array}{c} g_N \\ \dot{g}_N \end{array} \right. , \tag{2.99}$$

with $arg\ min$ being defined as the values of $\ddot{\mathbf{q}},\dot{\mathbf{q}},\mathbf{q}$ that minimizes g_N and $\dot{g}_N$. The vector $\mathbf{q}$ corresponds to the generalized coordinates of the rotor and the auxiliary bearing, g_N is the distance between the contact points and $\mathbf{q}_{ad}$ the target trajectory for the auxiliary bearing. Equation (2.99) implies that the relative distance becomes zero to get a permanent contact and the relative velocity in normal direction should be as small as possible to get a smooth transition from free rotor motion to the state of full annular rub.

In the first two phases of the control scheme, the desired position of the auxiliary bearing is chosen in a way such that the movement of the auxiliary bearing is synchronized with the orbit of the rotor and the contact point coincides with the

point of the surface of the rotor which is farthest from the origin of coordinate system, Figure 2.11. This means that

$$\varphi_{a\ desired} = \varphi_r \ .$$

(2.100)

In case of contact this results in a movement pattern of "synchronous full annular rub". The destructive "backward whirl" is avoided.

Furthermore, the desired radius $r_{N\ desired}$ is needed to determine the desired position of the auxiliary bearing according the equation

$$\mathbf{r}_{a\ desired} = \begin{pmatrix} \varphi_a \\ r_a \end{pmatrix} = \begin{pmatrix} \varphi_r \\ r_r - r_{N\ desired} \end{pmatrix}.$$

(2.101)

Therefore, the 2D problem to control the orbit has turned into a 1D control problem of the radius $r_{N\ desired}$. In the first control phase (free rotor motion), which means $|r_N| < \delta_0$, the target position of the auxiliary bearing follows

$$r_{N\ desired} = r_N + \int (\mathrm{v}_{pmax} - \dot{r}_N)dt = r_N + \int (A\ e^{\alpha|r_r|} - \dot{r}_N)dt,$$

(2.102)

where v_{pmax} is the maximum relative velocity of the contact points. The constant factors A and α are chosen in such a way that first impact is kept small but also that the amplitude of the rotor does not exceed δ_0, to meet the principal purpose of an auxiliary bearing.

In the case of a contact (second control phase), which means $|r_N| = \delta_0$, the radius $r_{N\ desired}$ is calculated as

$$r_{N\ desired} = \delta_0 + \frac{1}{K_P} f_{perm}.$$

(2.103)

f_{perm} is the desired contact force during the permanent contact and $\frac{1}{K_P}$ is a conversion coefficient. Note that it is necessary to choose a desired contact force, which is large enough to ensure a permanent contact despite of the uncertainties of the measurement and control system. As soon as the additional load is over, the rotor deflection decreases.

The permanent contact is separated when the deflection falls below the limit r_{limit}. Then, the auxiliary bearing is moved to a position concentric to the undeformed rotor shaft.

Another challenge is the latency of the measurement system. Depending on the size of the time step we have to calculate the position of the rotor from the measured one, using the velocity:

$$\varphi_r = \varphi_{r\ measured} + l\ \Delta t\ \dot{\varphi}_{r\ measured}$$

(2.104)

$$r_r = r_{r\ measured} + l\ \Delta t\ \dot{r}_{r\ measured} \tag{2.105}$$

The constant factor l accounts for the latency induced by the measurement system.

2.6 SIMULINK® Simulation

For the initial development of the feedback controller a simulation is developed in SIMULINK®, which should represent the real system as realistically as possible. The simulation comprises of the nonlinear characteristics of the active auxiliary bearing and the rotor, the time and the magnitude discretization and the contact between the rotor and the auxiliary bearing. Figure 2.12 shows the model, which has been implemented in this simulation. Besides the components, which have been discussed in Section 2.2, an active magnetic bearing, which is used to apply various excitations on the rotor, has been included:
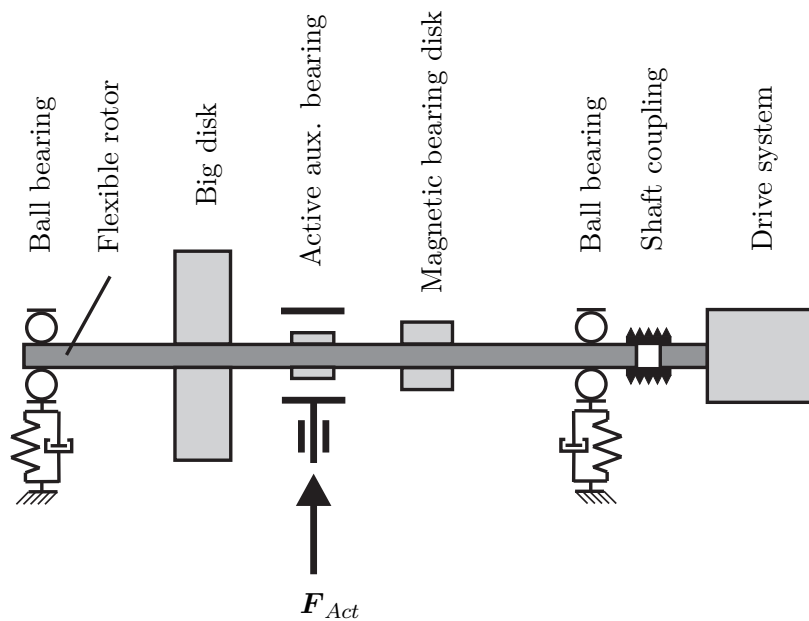
Figure 2.12: Mechanical model of the rotor system for the SIMULINK® simulation

- The elastic rotor
- A big disk (rigid)
- A disk, which runs inside the active auxiliary bearing (rigid)
- A disk, which runs inside the active magnetic bearing (rigid)
- The drive system
- The shaft coupling
- The auxiliary bearing

- The electromagnetic actuators

- The contact between the rotor and the auxiliary bearing

- The developed cascade control

The signals, which are measured in reality, are superposed by white noise. The simulation runs in multitasking mode, which means, that the rotor and auxiliary bearing is calculated with another sample frequency than the control system to better fit reality. A detailed description of the simulation can be found in [48].

2.6.1 Simulation Results without Contact

At first, the feedback control concepts of the actuators are simulated without rotor-to-stator (i.e. auxiliary bearing) contact. Using the Simulink® model a circular motion of the auxiliary bearing is simulated. The parameters of the target motion are summarized in Table 2.2. The frequency is 50 Hz and the radius of the desired circle is 0.4 mm. The air gap in auxiliary bearings is 0.3 mm, as discussed in Chapter 3. Regarding the developed "computation of the target trajectory", the maximum radius of the auxiliary bearing is a little larger than the nominal air gap and the motion is a circular motion with the angular velocity of the rotor shaft.

Table 2.2: Parameters of the target motion

Circular motion	
Frequency	50 Hz
Amplitude (radius)	0.4 mm

Using this target motion, the two control concepts are compared. In Table 2.3, the parameters of the PID controller are given. In Table 2.4, the feedback linearization controller parameters are listed, respectively.

Table 2.3: Parameters of the PID controller

Coefficients	P	I	D
Actuator 60	600 N/mm	1000 N/mms*	1.2 Ns/mm
Actuator 61	1200 N/mm	1000 N/mms*	2.4 Ns/mm
Sample time	0.0002 s		

* This coefficient is set to zero in case of contact

The parameters of the PID controller of the actuator 60 and of the actuator 61 differ from each other, because the system is nonlinear and the actuator 61 has to handle a higher load. In contrast, the feedback linearization controller is applied on a linearized system, and for that reason, the same poles have been used for both actuators. Both control systems are simulated at a sample time of 0.0002 s.

Table 2.4: Parameters of the feedback linearization controller

Poles	a	b
Actuator 60	-270	50
Actuator 61	-270	50
Sample time	0.0002 s	

To prove and assure the robustness of the controller, disturbance forces are applied to the auxiliary bearing in some simulations. These forces match the contact forces, which arise during the state of controlled rubbing.

PID Controller without Disturbance

The simulation results show the PID controller without disturbance. In Figure 2.13 the target movement ($x_{60\ \text{desired}}$ and $x_{61\ \text{desired}}$) and the simulated movement (x_{60} and x_{61}) of the actuator coordinates are plotted. Actuator 60 matches the target very good, but actuator 61 does not match the target. As the controller already operates close to the stability limit, it is not possible to increase the coefficients of this actuator any more, in order to improve the control quality.
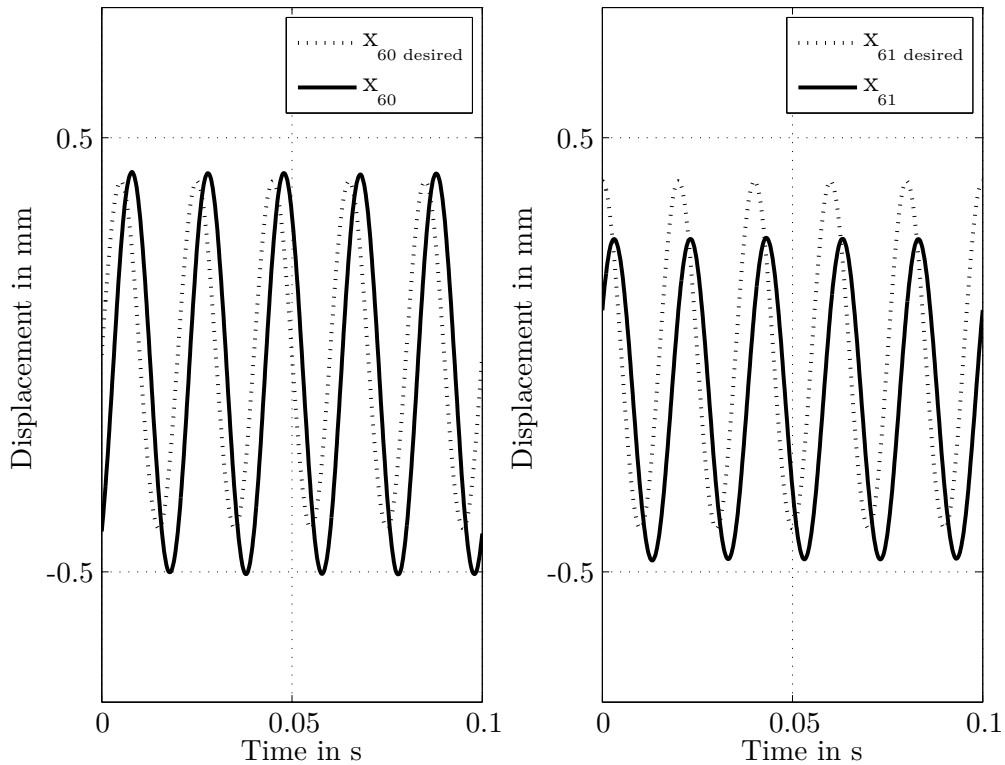
Figure 2.13: Simulation, PID controller, position

PID Controller with Disturbance

Now the disturbance, which should simulate the contact force during rubbing, is applied to the same simulation of the PID controller. Figure 2.14 shows the comparison of the movement of the auxiliary bearing, Figure 2.15 shows the applied disturbance forces and Figure 2.16 the actuator forces. The controller is stable despite of the disturbance. Also the forces of the actuators stay within the possible operation range.
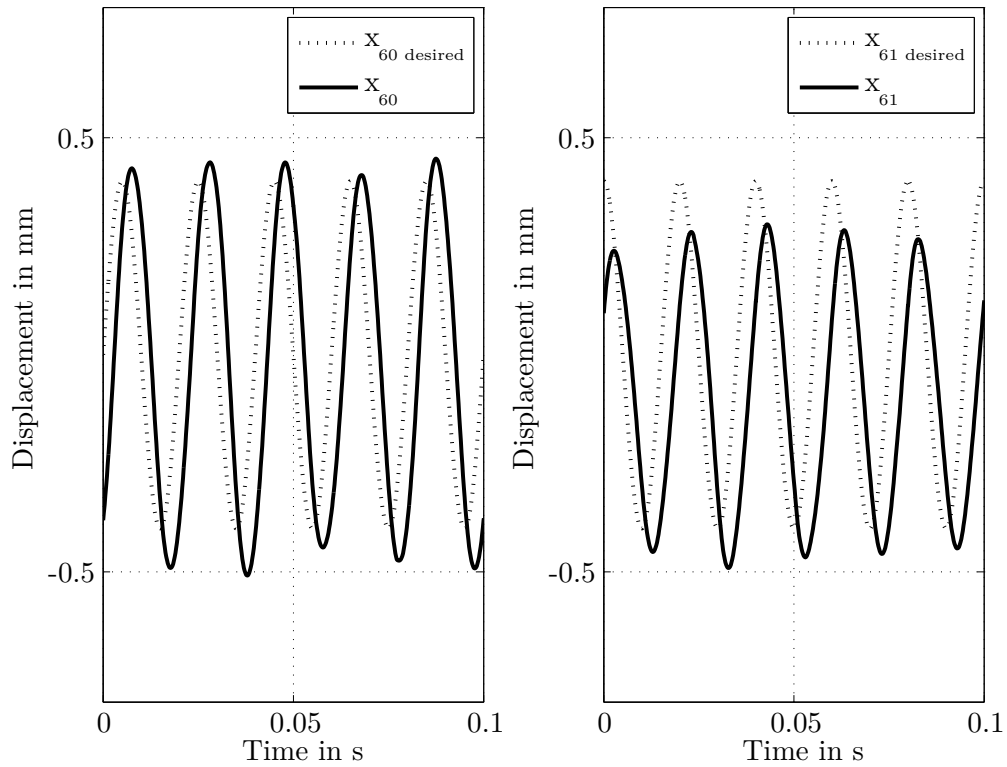
Figure 2.14: Simulation, PID controller with disturbance, position
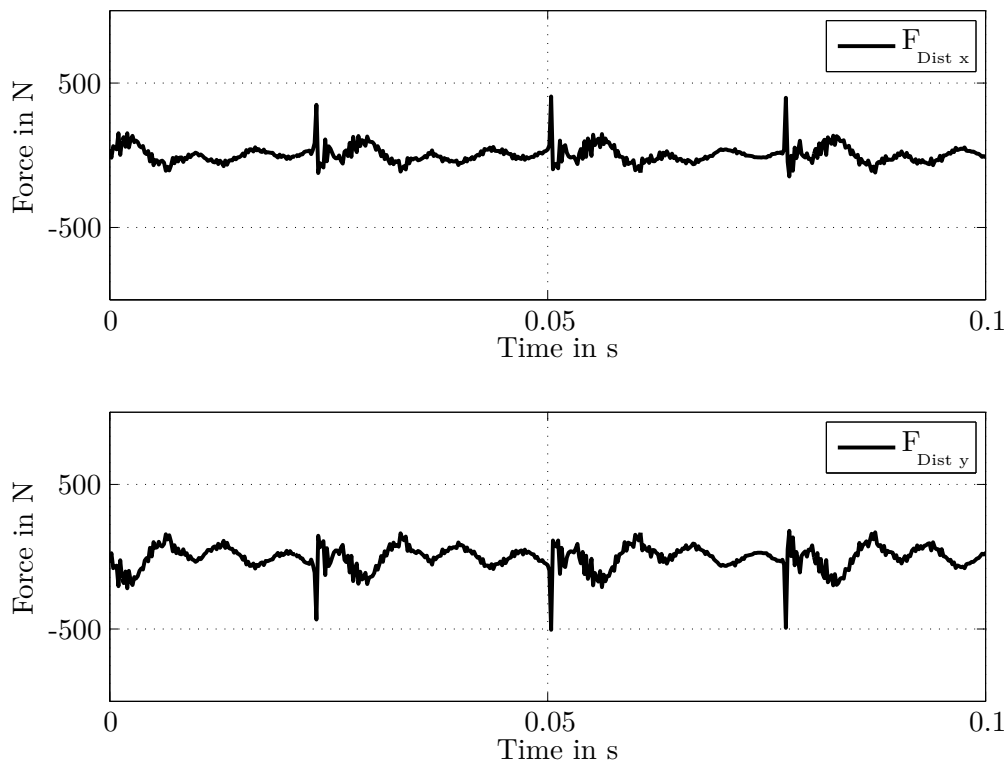
Figure 2.15: Simulation, PID controller with disturbance, disturbance forces
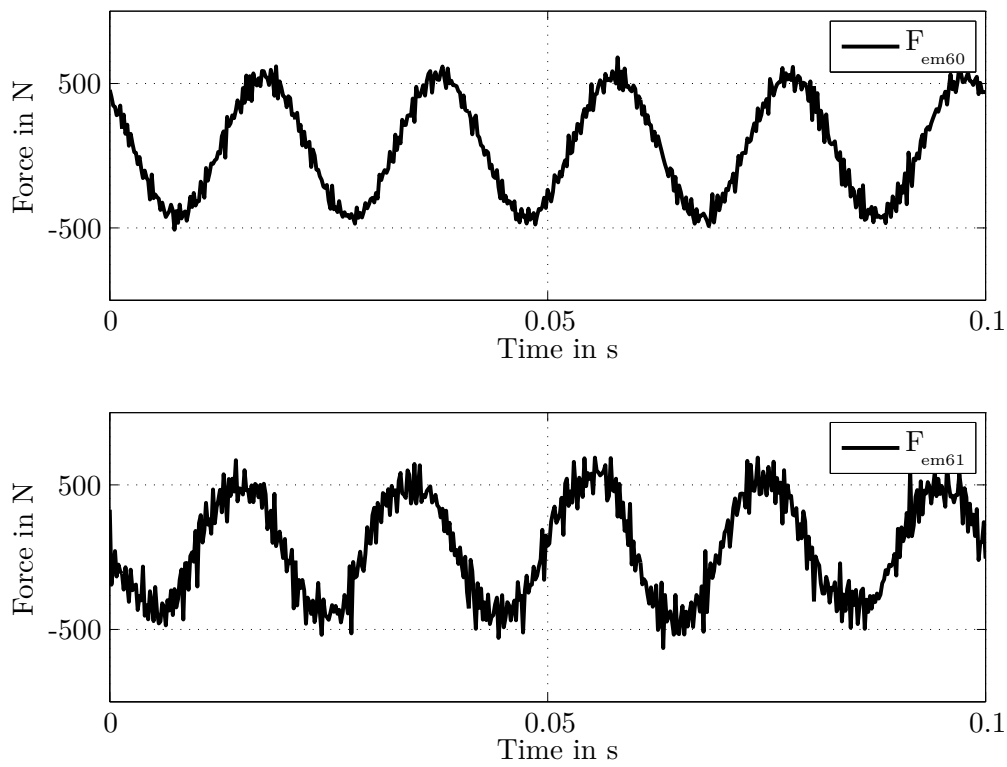
Figure 2.16: Simulation, PID controller with disturbance, actuator forces

Feedback Linearization Controller without Disturbance

The same two simulation scenarios (without and with disturbance) have been re-
peated using the feedback linearization controller. We obtain a much better control
quality in general. The control error is almost equal at both actuators, which is
very important. Otherwise, a smooth circular motion during a controlled state of
rubbing is not possible. Figure 2.17 shows a comparison of the target motion and
the simulated motion.
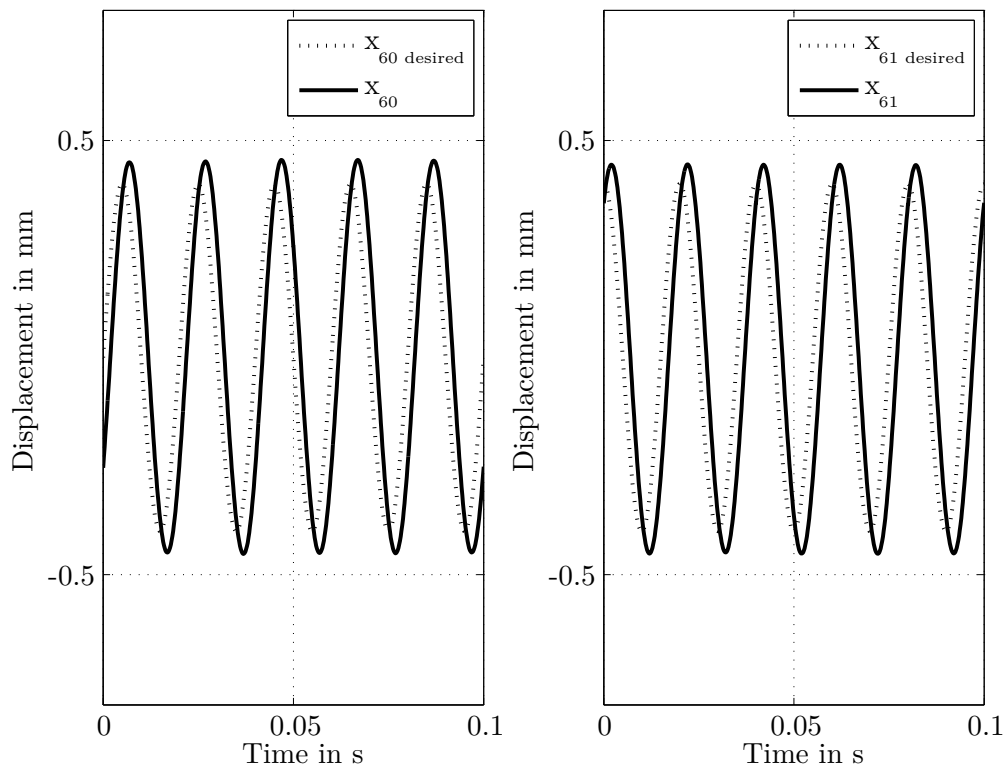
Figure 2.17: Simulation, feedback linearization controller, position

Feedback Linearization Controller with Disturbance

Now the additional disturbance forces are applied as described above. Figure 2.18 shows the comparison of the movement of the auxiliary bearing, Figure 2.19 shows the applied disturbance forces and Figure 2.20 the actuator forces. There is a significant improvement of the control quality compared to the PID controller. The controller is stable despite of the disturbance forces and the actuator forces stay in the operational range.
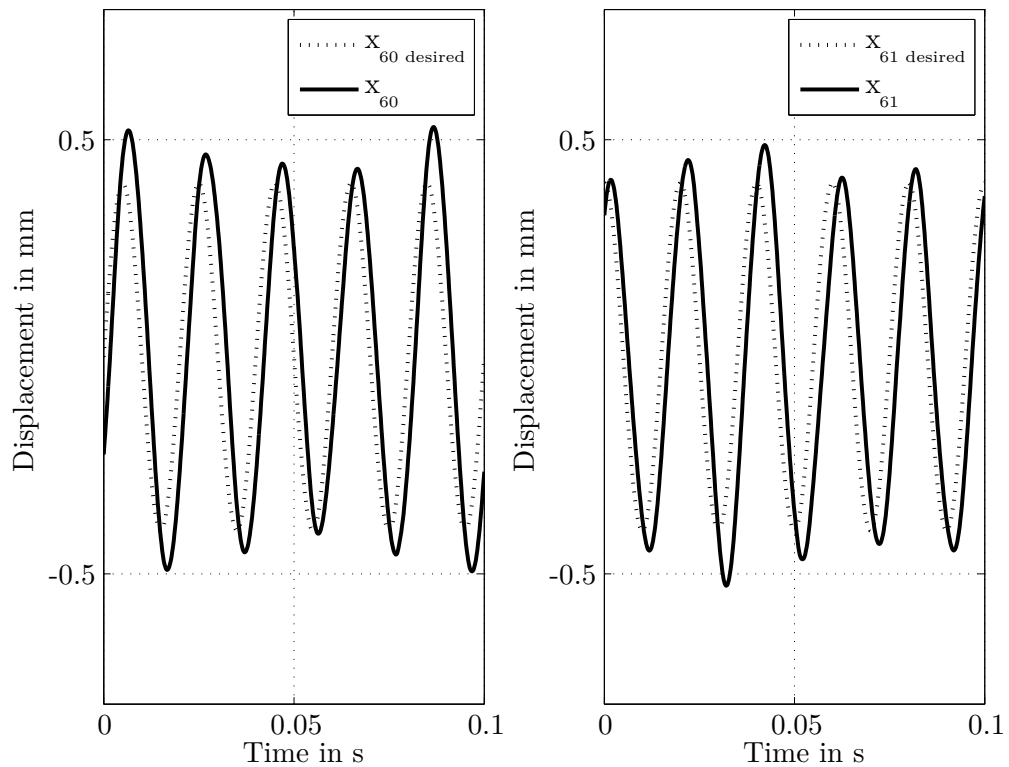
Figure 2.18: Simulation, feedback linearization controller with disturbance, position
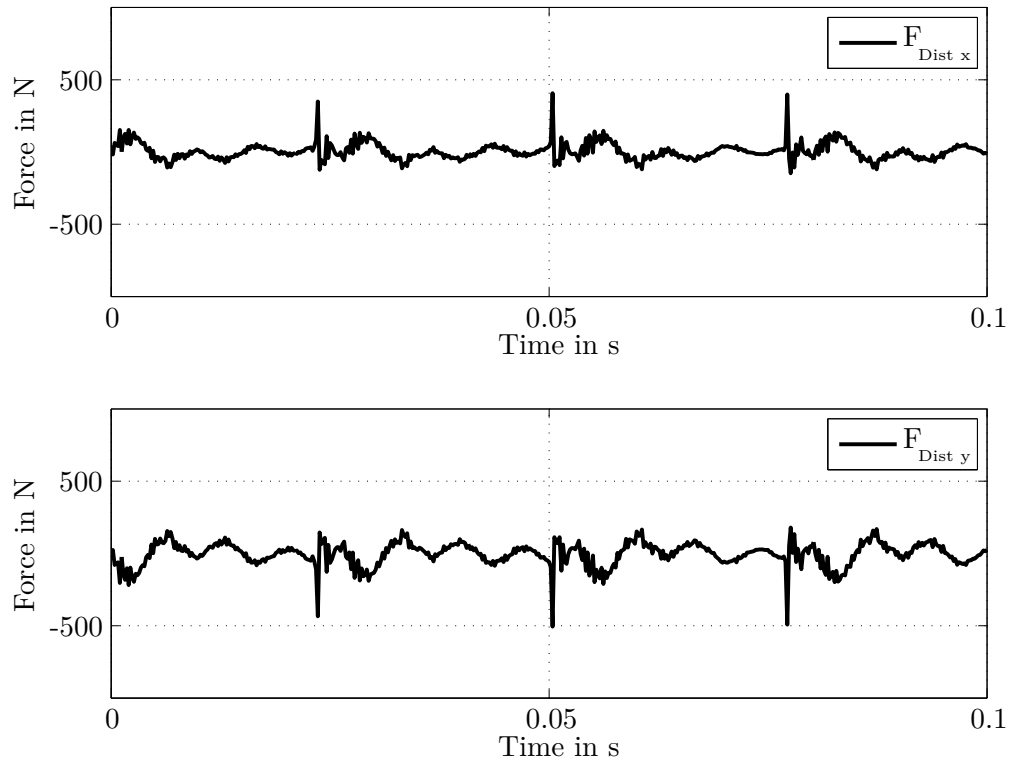
Figure 2.19: Simulation, feedback linearization controller with disturbance, disturbance forces
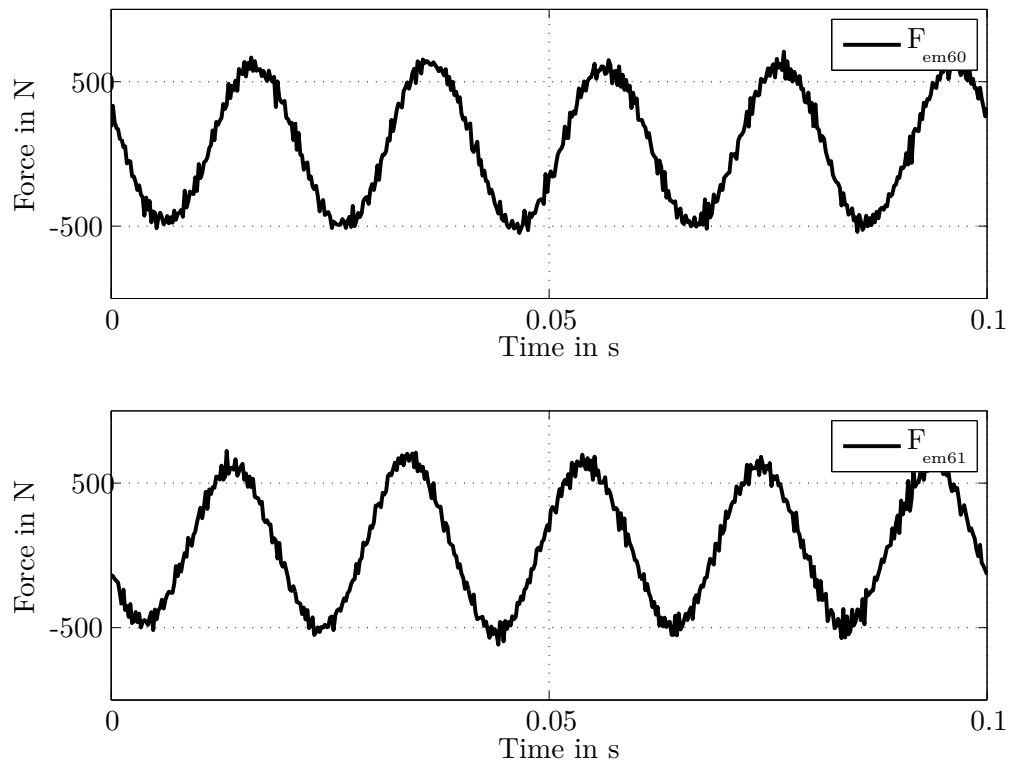
Figure 2.20: Simulation, feedback linearization controller with disturbance, actuator forces

Determination of the Concept to be Applied

Regarding the presented simulation results, the feedback linearization control is definitely the better concept for this purpose. A disadvantage is the higher computation effort, but for the given experimental setup, as it is presented in Chapter 3, the concept is applicable, because the real-time platform is powerful enough. Therefore, all further discussed experiments and simulations use the feedback linearization controller.

2.6.2 Simulation Results with Contact

After the determination of the feedback control concept for the electromagnetic actuators, SIMULINK® simulations of the complete system including the contact between rotor and auxiliary bearing have been performed. As discussed above, the feedback linearization control has been used to control the actuators. The controller parameters can be found in Table 2.4. The parameters for the model of the rotor and the auxiliary bearing have been chosen from the test rig with the "12 mm shaft", for a detailed description, see Chapter 3.

Rubbing without Control

In the condition "without Control" the active auxiliary bearing works like a conventional auxiliary bearing, which is fixed concentric with the undeformed rotor shaft.

The rotor runs at a constant rotational frequency of about 11 Hz without contact. At a time of 1.0 s there is a short-time excitation in form of a radial force, which leads to contact between rotor and auxiliary bearing. The rubbing turns into backward whirling with a very high contact force. The orbit of the rotor shaft at the position of the active auxiliary bearing is plotted in Figure 2.21. At the beginning of the simulation - without additional excitation - the rotor moves in the middle of the plot at a very low rotor deflection. After the arise of the radial force, the rotor deflection increased suddenly, followed by an impact between rotor and auxiliary bearing. After a few further impacts a rubbing state of backward whirling is established. In Figure 2.22(a) the amount of contact force, which arises between rotor and stator is plotted versus time. After the first multiple impacts with up to 500 N, there is rubbing with forces up to 200 N arises. In Figure 2.22(b) the phase angle of the center of the rotor is plotted versus time. One can identify the beginning of the backward whirling shortly after the occurrence of the short-time excitation.
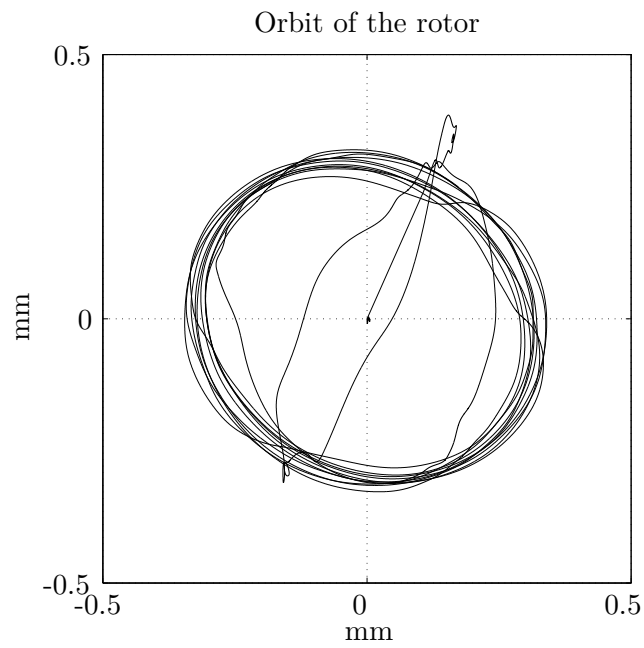
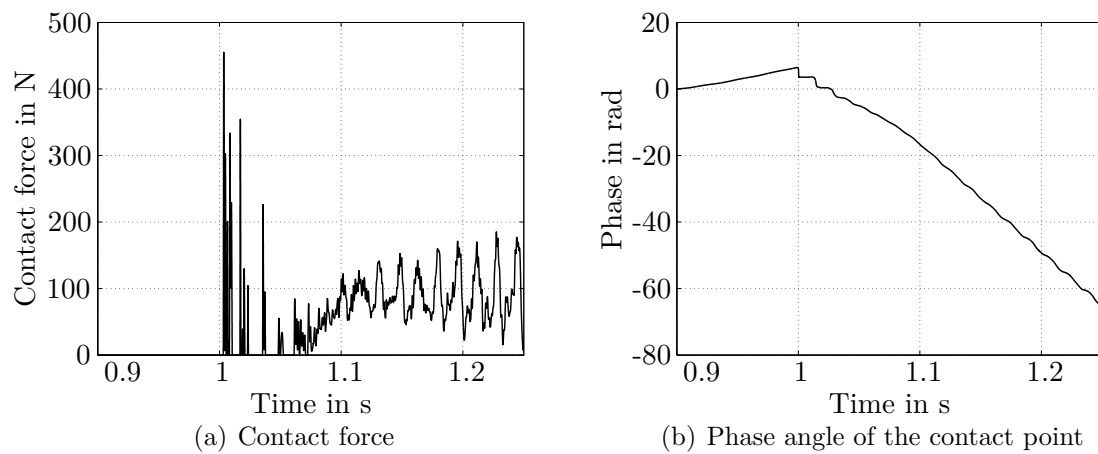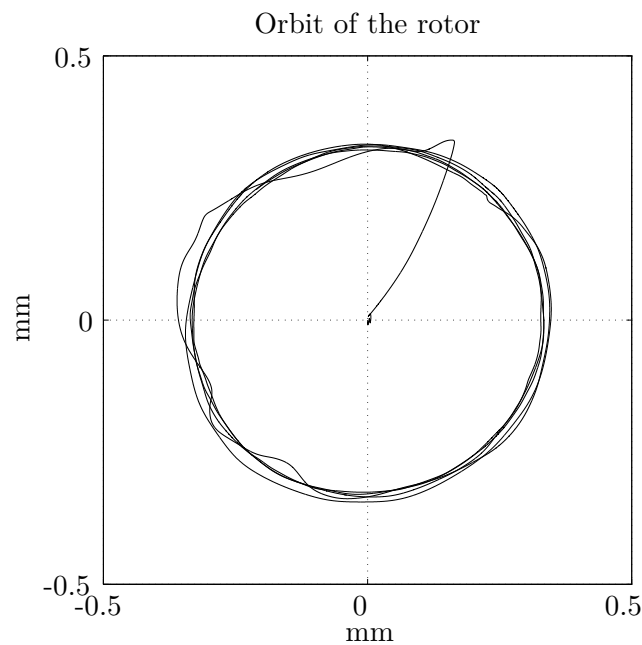**Figure 2.21:** Simulation complete system, rubbing without control, orbit

Figure 2.22: Simulation complete system, rubbing without control

Rubbing with Control

Using the SIMULINK® simulation, the overall control concept has been proven and
optimized. A simulation is presented, where the rotor is running at a constant
speed of about 11 Hz and the control system is activated. The rotor orbit is plotted
in Figure 2.23. At the beginning, the rotor is running without contact and the
control system is on stand-by and tracks the rotor deflection. At a time of 1.0 s an
excitation in form of a short-time radial force is applied on the rotor. The rotor
deflection increases suddenly and the controller is activated. The active auxiliary
bearing catches the rotor and transforms the rubbing into a smooth rubbing state of
synchronous full annular rub. The contact force, which is plotted in Figure 2.24(a),
remains under 40 N - after the first impact. In Figure 2.24(b) the phase angle of the
center of the rotor shaft is plotted, which indicates the rubbing state of synchronous
rubbing.

Figure 2.23: Simulation complete system, rubbing with feedback linearization control,
orbit

rad

(a) Contact force

(b) Phase angle of the contact point
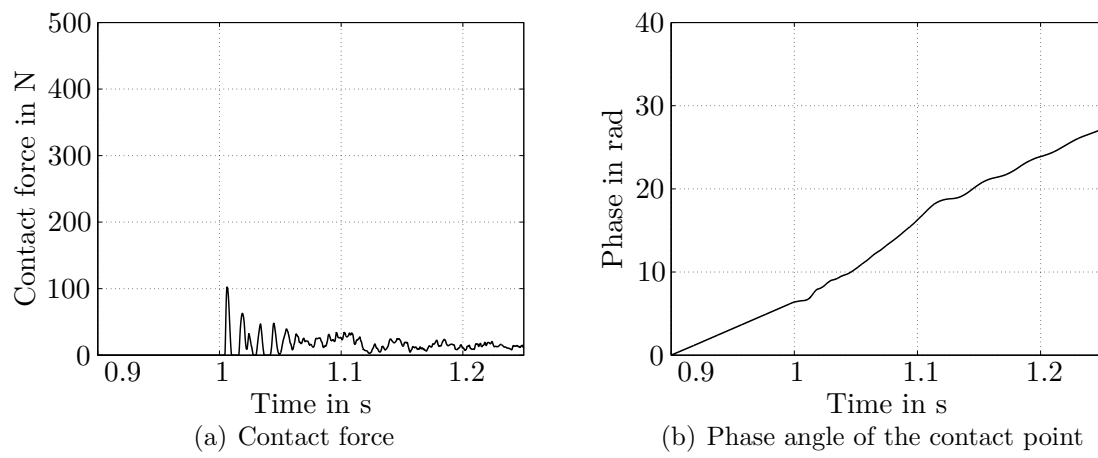
Figure 2.24: Simulation complete system, rubbing with feedback linearization control

3 Design of the Test Rig

A rotor test rig has been developed to experimentally investigate the concept of an active auxiliary bearing. In Figure 3.1 the CAD drawing of the rotor test rig is shown.
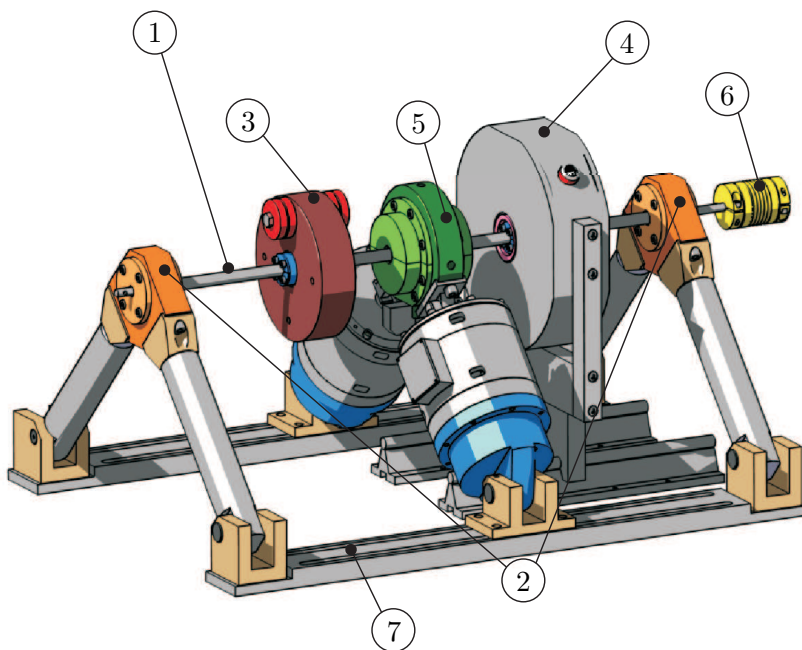

Figure 3.1: CAD drawing of the test rig

The test rig consists of the following components:

1. Rotor shaft

2. Ball bearings on isotropic mounting

3. Big disk

4. Magnetic bearing

5. Active auxiliary bearing

6. Clutch to the drive system

7. Variable mounting device for the active auxiliary bearing.

The test rig can be assembled in two modifications: a quasi rigid elastic shaft with 40 mm diameter and a flexible one with 12 mm. In both cases, the air gap between the rotor and the auxiliary bearing is 0.3 mm. A disc-servomotor allows a rotational speed up to 3500 rpm. The big disk can be moved on the rotor shaft to realize a variation of the resonant frequency. Masses can be fixed eccentrically on the disk to apply an unbalance. As shown in Figure 3.2, there is a small disk (2) running inside the magnetic bearing (1), which is made of ferromagnetic material. The magnetic bearing is only used to apply various additional excitations during the experiments and is not used by the control concept.
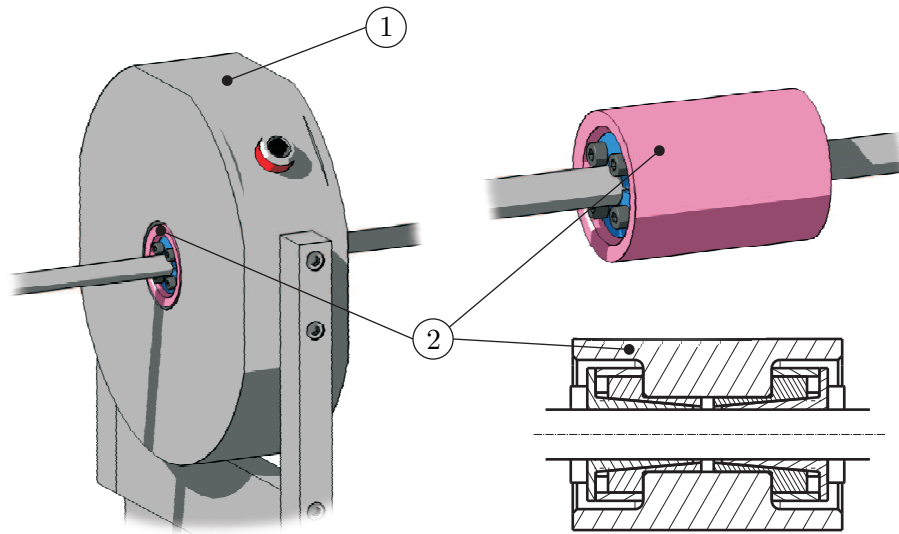
Figure 3.2: Detailed drawing of the magnetic bearing; 1: magnetic bearing; 2: ferromagnetic disk

As discussed in the previous chapters, the active auxiliary bearing consists of an auxiliary bearing (also called backup bearing or retainer bearing), which is carried out as a bushing type, and two electromagnetic actuators. A CAD drawing of the active auxiliary bearing is shown in Figure 3.3. There is a disk running inside the auxiliary bearing. The contact between rotor and active auxiliary bearing occurs between the ring of the auxiliary bearing and this disk, which is fixed on the rotor shaft. The reason for this construction is, that the contact surface of the disk is much larger than a contact surface between the thin rotor shaft and an auxiliary bearing. The larger surface results in a much higher life span of the test rig and a high temperature resistance, to allow widespread experiments.

Every component on the rotor shaft is fixed using clamping sets. Therefore, variable positions of the disks are possible.
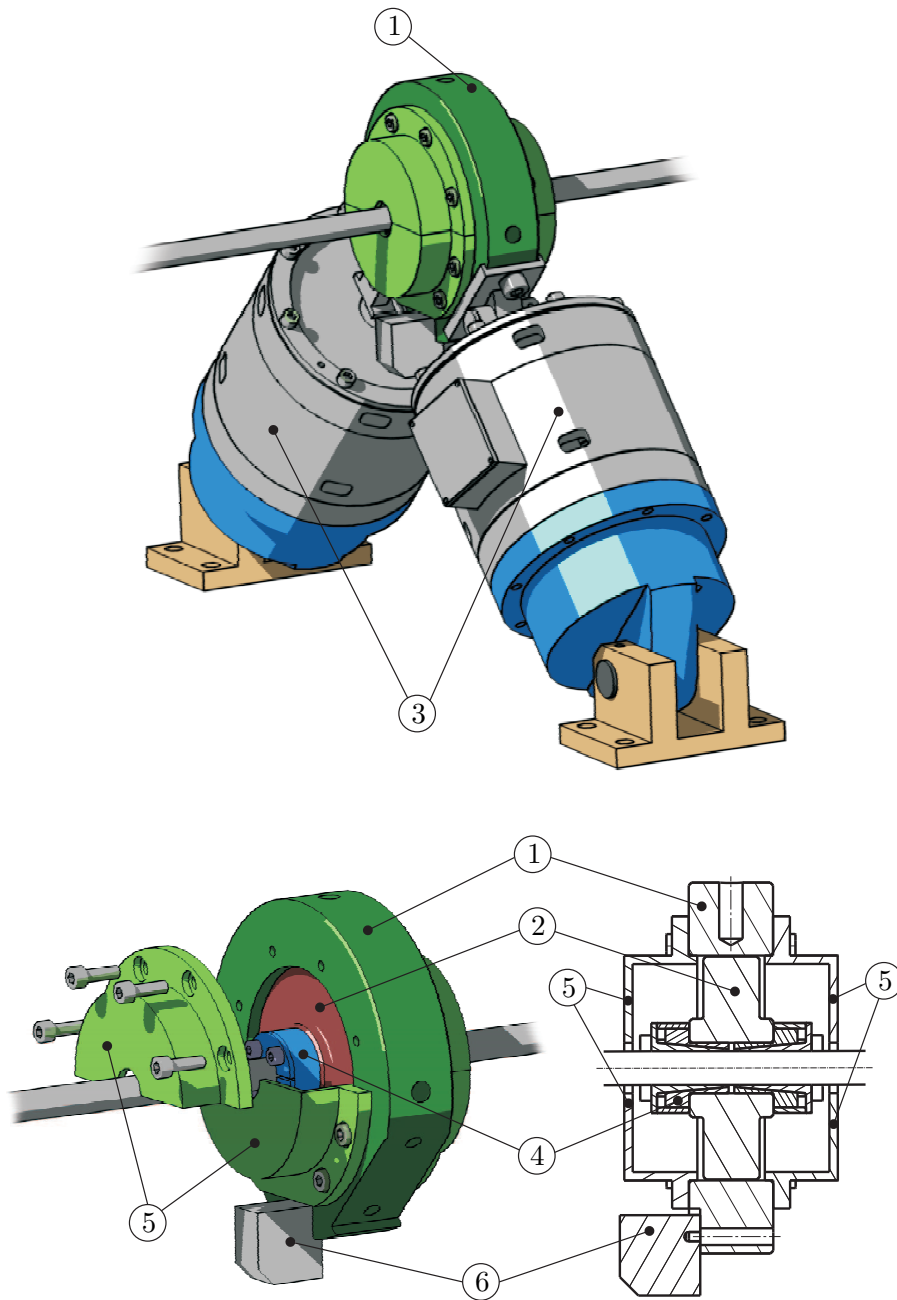
Figure 3.3: Detailed drawing of the active auxiliary bearing; 1: auxiliary bearing (ring); 2: disk, which is fixed on the rotor shaft; 3: electromagnetic actuators; 4: clamping set; 5: housing, which allows to fill the auxiliary bearing with a lubricant; 6: accelerometer

Several sensors are applied on the test rig. As shown in Figure 3.4, information is gathered in three planes, which are perpendicular to the rotor shaft:

- At the ball bearing / mounting at the open end of the rotor shaft: measurement of the acceleration of the bearing housing.

- At the active auxiliary bearing: measurement of the displacement of the rotor and the auxiliary bearing, measurement of the actuator forces.

- At the ball bearing / mounting beside the clutch: measurement of the acceleration of the bearing housing.

The measurement of the accelerations at the ball bearings is only used to determine the performance of the control system. The signals which are used by the cascade control are the displacements and forces measured at the position of the active auxiliary bearing.

Two eddy current displacement sensors are used to measure the displacement of the rotor and auxiliary bearing. Load washers in each actuator are measuring the actuator forces, from which the contact force is determined indirectly.
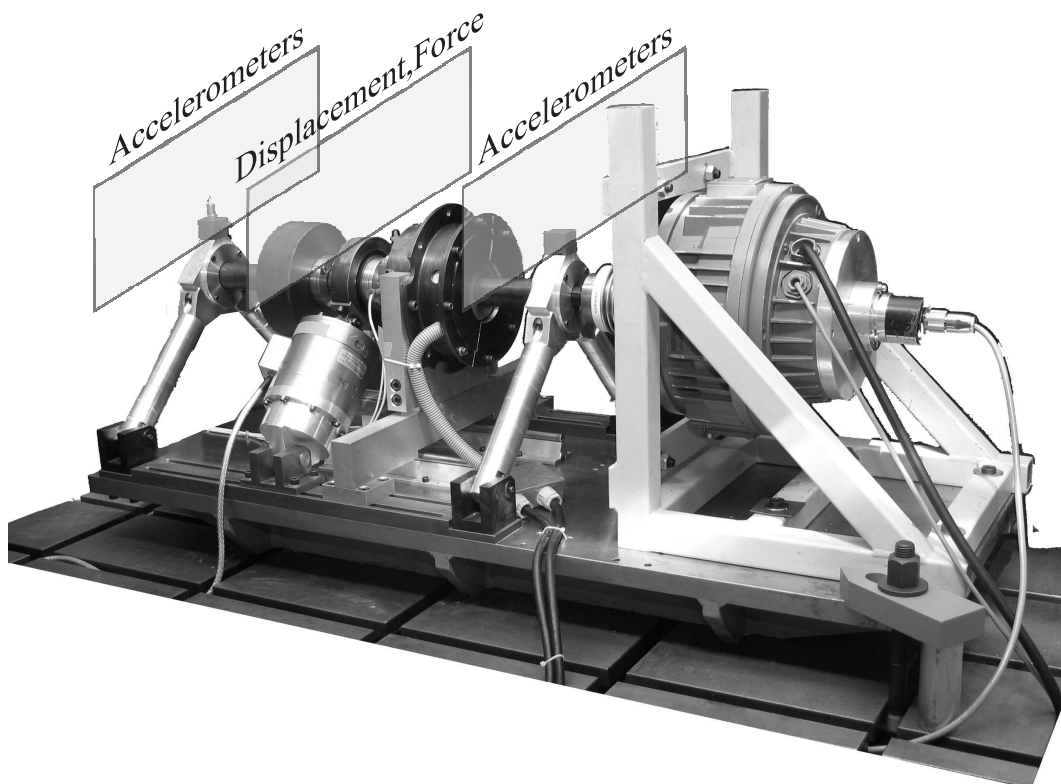

Figure 3.4: Photo of the assembled test rig

3.1 Configuration "40 mm Shaft"

At first the assembly with the quasi-rigid rotor shaft with a diameter of 40 mm is examined. The test rig in this configuration is shown in Figure 3.5. The main components are marked by numbers and explained in the caption of the figure. A more powerful magnetic bearing is used in comparison to the configuration with the 12 mm shaft. The main dimensions and parameters are given in the appendix.
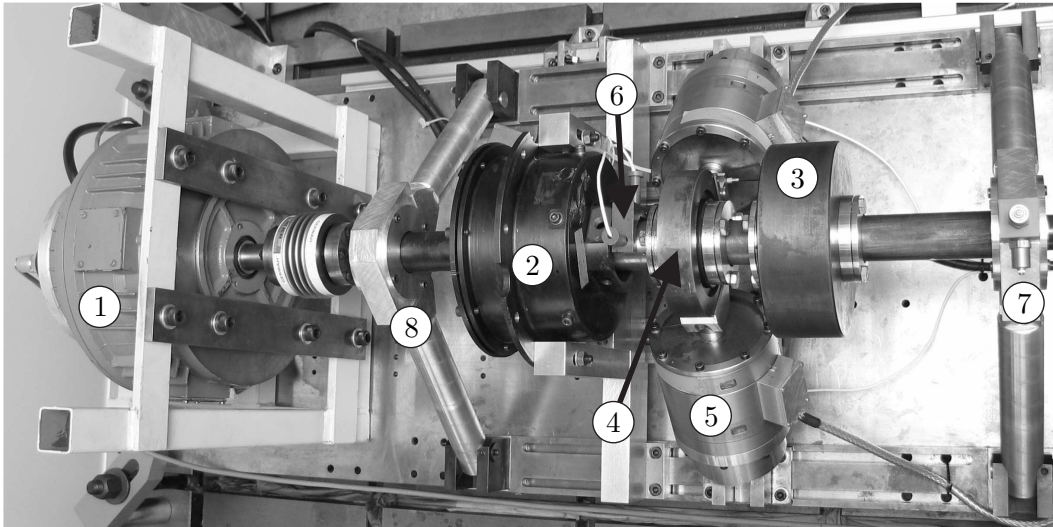

Figure 3.5: Test Rig (1: drive system, 2: magnetic bearing, 3: rotor disk, 4: auxiliary bearing, 5: electromagnetic actuators, 6: displacement sensors, 7: accelerometer, ball bearing, 8: ball bearing)

3.1.1 Frequency Analysis

To get more information about the frequencies of interest of the rotor, considering the whole system, a modal analysis has been made with the non-rotating rotor shaft. The positions of the disks on the rotor shaft of this configuration are given in the appendix. The first and second resonance frequency, which has been determined by this dynamic analysis, is given in Table 3.1.

Table 3.1: Resonance frequencies of the configuration "40 mm shaft"

No.	Type	Frequency
1st	bending	approx. 110 Hz
2nd	bending	approx. 367 Hz

3.1.2 Order Analysis

In contrast to the slander rotor shaft, the used magnetic bearing is not powerful enough to induce rubbing at every rotational speed. At certain angular velocities, the deflection of the shaft of this configuration is particularly high. To get more information about the mechanisms of excitation, an order analysis of the angular velocity and the rotor deflection has to be performed. The waterfall diagram in Figure 3.6(a) shows the FFT of the angular velocity for speeding-up from 100 rpm to 3500 rpm. Inherently, motors of this design have a rotational speed which contains parts of higher order excitations. Here, the angular velocity mainly consists of terms of the first four orders. Also the supply frequency and their harmonics are present in Figure 3.6(a).
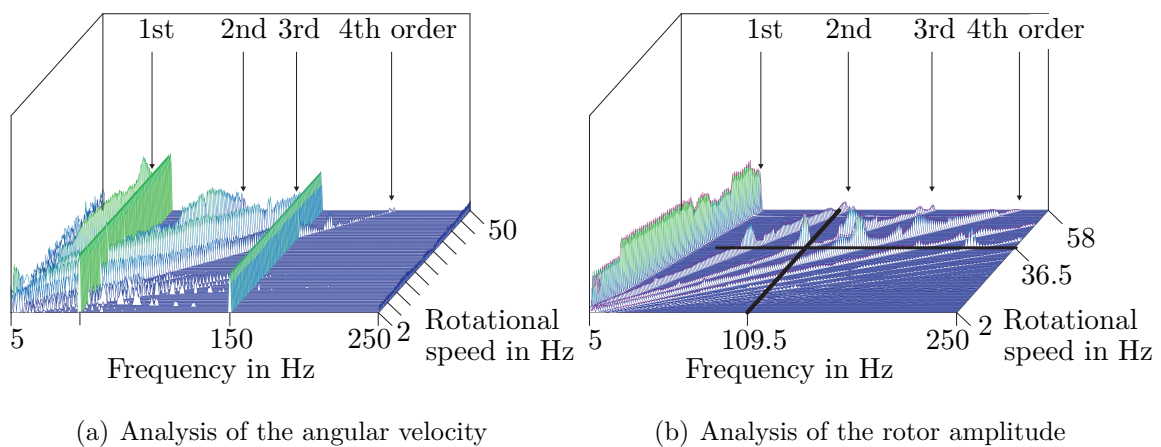

(a) Analysis of the angular velocity   (b) Analysis of the rotor amplitude

Figure 3.6: Order analysis of the configuration "40 mm Shaft"

In Figure 3.6(b) an order analysis of the bending of the rotor is shown. There is no excitation by the magnetic bearing, so there is no contact in the auxiliary bearing during the speeding-up. Only the radius of the displacement is used as input to the FFT.

At the rotational speed of about 2230 rpm to 2240 rpm, the third order of the excitation caused by the speed droop of the motor hits the first eigenfrequency. At this operation point the bending response of the elastic rotor has a significant maximum during the speeding-up from 100 rpm to 3500 rpm. As a consequence peaks appear at the first four harmonics of the excitation.

3.1.3 Electromagnetic Bearing

A further component of the test rig is the electromagnetic bearing. This conventional radial bearing is used to apply a large variety of loads on the rotor. The electromagnetic bearing, which is used in the configuration "40 mm shaft", features an air gap of 0.8 mm and forces up to 500 N.

3.2 Configuration "12 mm Shaft"

The second configuration of the test rig is the assembly with a slender rotor shaft with a diameter of 12 mm. A photo of the test rig in this configuration is shown in Figure 3.7. The main components are marked by numbers and explained in the caption of the figure. The main dimensions and parameters are given in the appendix.
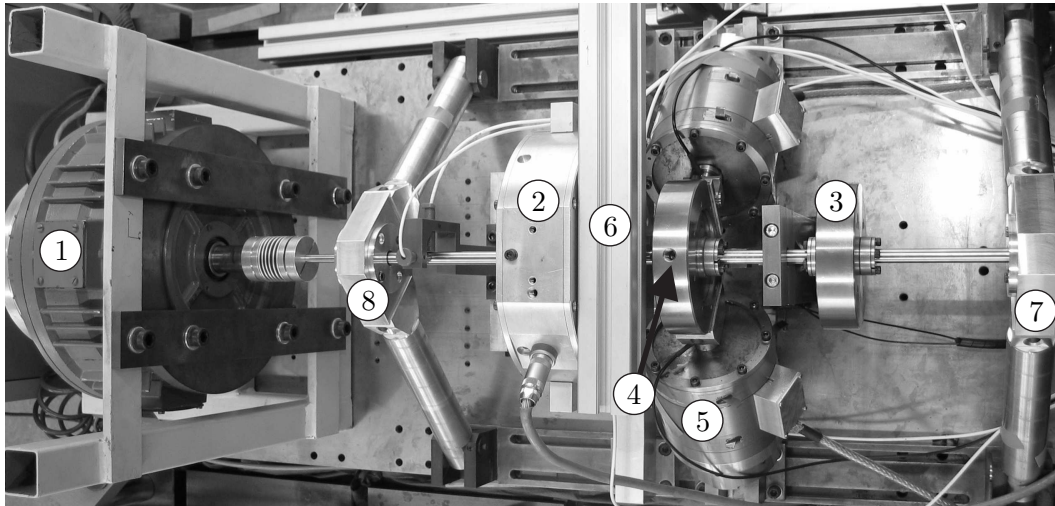
Figure 3.7: Test Rig (1: drive system, 2: magnetic bearing, 3: rotor disk, 4: auxiliary bearing, 5: electromagnetic actuators, 6: displacement sensors, 7:ball bearing, 8: ball bearing)

The used magnetic bearing in combination with the use of unbalance masses is powerful enough to cause rubbing at every rotational speed.

3.2.1 Frequency Analysis

A modal analysis has been made with the non-rotating rotor shaft. The positions of the disks on the rotor shaft of this configuration are given in the appendix. The first, second and third resonance frequency, which has been determined by this dynamic analysis is given in Table 3.2.

Table 3.2: Resonance frequencies of the configuration "12 mm shaft"

No.	Type	Frequency
1st	bending	approx. 24 Hz
2nd	bending	approx. 97 Hz
3rd	bending	approx. 231 Hz

For a detailed discussion of the modal analysis of the presented system, please refer to [36].

3.2.2 Electromagnetic Bearing

Another electromagnetic bearing has been applied in this assembly. The electromagnetic bearing features an air gap of 0.8 mm and it is possible to generate forces up to 55 N.

3.3 Electromagnetic Actuators

The electromagnetic actuators have been developed at the Institute for Applied Mechanics, TU Munich, see also [41]. The main components are shown in Figure 3.8. The actuator consists of two pull-disks (the armatures of the magnetic system), fixed on a shaft and positioned at the ends of a pot-shaped magnet. For a frictionless support of the shaft, two annular membranes with a high axial flexibility and a high stiffness in radial direction are used. To realize tensile as well as compressive forces, two control coils are integrated in the pot-shaped magnet and they are working in a differential mode.
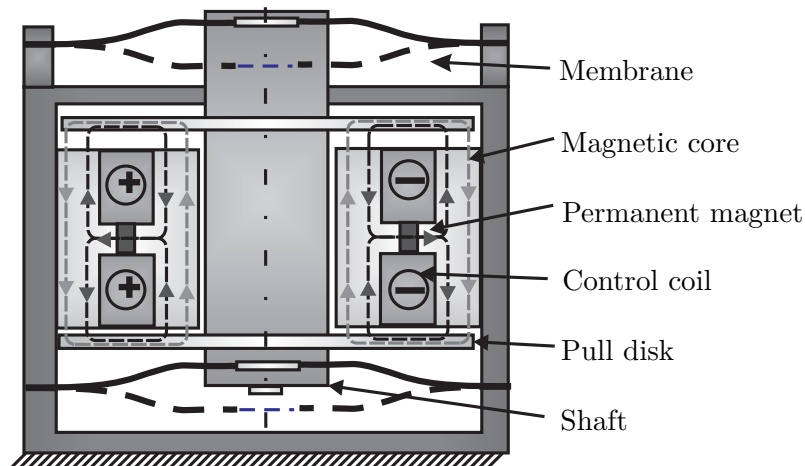

Figure 3.8: Design of the actuator

The main advantage of this type of electromagnetic actuator is a large stroke up to 1 mm at frequencies up to 250 Hz. Forces up to 1000 N are available. Figure 3.9 shows the characteristic curve (force-field), obtained by variations of the control current and the displacement. The actuator shows a nonlinear force behavior in relation to the control current and the axial position of the pull-disk.

Depending on the application of an active auxiliary bearing, the requirements for the actuators vary strongly. The selection of suitable actuators depends on various parameters, such as the size of the air gap in the auxiliary bearing and the rotational speed of the rotor system. Simulations of the presented test rig showed that actuators with a minimum stroke of ±0.3 mm are required, so piezo-electric ones have
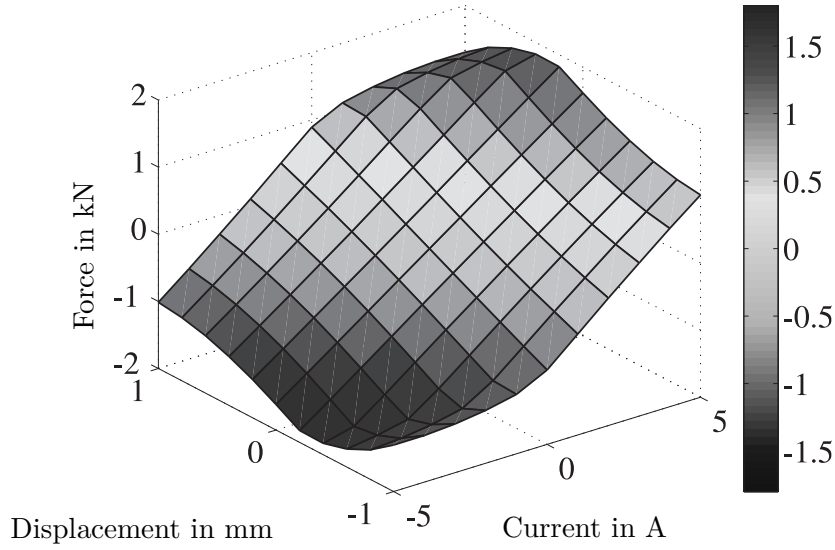
Figure 3.9: Force-field of the actuator

been classified as unsuitable for this application. But, especially for a short-time application after an impact load, commercially available piezoelectric actuators seem to be suitable.

The dynamics and the optimization of the electromagnetic actuator have been investigated using simulation and experiment in detail in [28] and [42]. OBERBECK [42] has derived a relation between force, current and displacement as follows:

$$F_{Actuator}\left(i, x\right) = k_i\left(i,x\right) \, i + k_x\left(i,x\right) \, x \tag{3.1}$$

with

$$k_i\left(i,x\right) = k_\mu^2\left(i,x\right) \, \frac{4 \, k_1 \, w \, \Theta_{PM} \left[(2 \, R_{PM} + k_2 \, x_0) \, x_0 + k_2 \, x^2\right]}{k_2 \left[(2 \, R_{PM} + k_2 \, x_0) \, x_0 - k_2 \, x^2\right]^2} \tag{3.2a}$$

as force-current-coefficient and the coefficient

$$k_x\left(i,x\right) = k_\mu^2\left(i,x\right) \, \frac{4 \, k_1 \left[\Theta_{PM}^2 \, k_2 \, x_0 + w^2 \, i^2 \, (2 \, R_{PM} + k_2 \, x_0)\right]}{k_2 \left[(2 \, R_{PM} + k_2 \, x_0) \, x_0 - k_2 \, x^2\right]^2} \tag{3.2b}$$

which describes the negative stiffness of the magnetic field. In this coefficient, the following nomenclature has been used:

- $k_\mu\left(i,x\right)$: a saturation factor, which describes the ratio of the magnetic flux and the linear approximated induction

- k_1 and k_2: constant coefficients, which consist of geometric and magnetic parameters and are used for the description of the magnetic forces

- w: the number of coil windings

- Θ_{PM}: the magnetomotive force caused by the permanent magnets

- R_{PM}: the reluctance of the permanent magnets

- x_0: the initial air gap

- x: the displacement of the actuator.

The ongoing discussion on the electromagnetic actuator will be neglected, for details please refer to the literature [42]. In the following, the force field shown in Figure 3.9, is used. This map describes the complex relation of force, current and displacement of the actuator.

The output of the control system is the desired force, which should be applied to the auxiliary bearing. Because of the inherent nonlinearity of the actuator, the ratio of the force and the control current can not only be explained by a proportional factor. Therefore, the relation is split in a proportional part using a coefficient and a nonlinear part as follows:

$$i_{Actuator} = \frac{1}{k_{i,lin}} F_{Actuator} + i_c \left(F_{Actuator}, x \right), \tag{3.3}$$

where $k_{i,lin}$ is a proportionality factor, being composed of the maximum force of the actuator $|F_{Actuator}|_{max} = 950\,\text{N}$ and the maximum allowable current of the control coils $|i_{Actuator}|_{max} = 5\,\text{A}$. This coefficient, which is constant and consequently independent from the displacement of the actuator, is given by

$$k_{i,lin} = \frac{|F_{Actuator}|_{max}}{|i_{Actuator}|_{max}} = 190\,\text{N/A}. \tag{3.4}$$

In equation (3.3) $i_c \left(F_{Actuator}, x \right)$ is the compensating current, which eliminates the nonlinearity of the actuator. This compensating current is given by a map which has been determined experimentally.

3.4 Real-Time Hardware

For the experiments, two dSPACE real-time hardware boards have been used. The main advantage of these single-board hardware is its high flexibility and its high processing power. With a variety of I/O components and the real-time interface, which enables a very fast programmability from the SIMULINK® block diagram environment, the boards are optimally suitable for rapid control development. The feedback controller for the actuators is executed on the DS1103 board and the trajectory computation is done on the DS1104 board:

- DS1103 PPC Controller Board, Sample rate: 5000 Hz, Feedback control of the actuators;

- DS1104 PPC Controller Board, Sample rate: 5000 Hz, Trajectory computation.

For testing purposes, the feedback controller has also been implemented on a Motorola MPC 555 microcontroller and tested successfully, but because of the clearly worse ease of use, the microcontroller is unsuitable for the experimental investigations, which demands a high amount of flexibility.

4 Experimental Investigation

In this chapter, the experimental investigation of the control concept is presented. For the experimental investigation of the designed control concept, only the feedback linearization control (see Section 2.4.2) has been used to control the actuator. This decision is based on the results of the SIMULINK® simulation presented in Section 2.6.

Parameter Identification After the assembly of both configurations of the test rig, the unknown parameters have been determined experimentally. Free vibration decay tests have been performed to determine stiffness and damping of the mounting of the ball bearing and of the rotor shaft. For both - shaft and mounting - the tests have been carried out in the two dimensions perpendicular to the undeformed rotor shaft. The resonances have also been determined, using these tests. The magnetic bearings, which are used in both configurations, have been investigated to determine the force parameters. The parameters of the two assemblies - the 12 mm configuration, i.e. the shaft has a diameter of 12 mm, and the 40 mm configuration, i.e. the shaft has a diameter of 12 mm - of the test rig are given in the appendix.

Online Determination of the Contact Force For the analysis of the controller, it is important to record the contact force between rotor and the auxiliary bearing during rubbing. It is hardly possible to measure these force directly without interfering the whole system. Therefore the forces of the actuators are measured. The contact force is determined using the linearized equations of motion of the active auxiliary bearing (2.67):

$$\boldsymbol{Q}_{NC,Contact} = \boldsymbol{M}_{AB,lin}\,\ddot{\boldsymbol{q}} + \boldsymbol{D}_{AB,lin}\,\dot{\boldsymbol{q}} + \boldsymbol{C}_{AB,lin}\,\boldsymbol{q} - \boldsymbol{F}_{Act}. \tag{4.1}$$

For a detailed discussion of the indirect determination of the contact force refer to [27].

4.1 Configuration "40 mm Shaft"

The experimental investigations of the configuration "40 mm Shaft", i.e. the shaft of the assembly has a diameter of 40 mm, are presented. Some presented experimental results are comparisons between various states of rotor rubbing with and without controlled auxiliary bearing. For the condition "without control", the actuators positioned the auxiliary bearing concentrically with the undeformed rotor shaft and the controller is switched to a mode with high stiffness and damping. Therefore, a passive auxiliary bearing is simulated. Measurements of the rotor deflection and of the rotor orbit are presented. These measurements have been performed beside the auxiliary bearing.

4.1.1 General Comparison

The first experiments deal with a general investigation of rubbing without control and rubbing with control. For both cases the rotor is running at a constant speed of 2233 rpm and the magnetic bearing applies an excitation which leads to a contact between rotor and auxiliary bearing. This rotational speed is within a critical range, as discussed in Section 3.1.2. The excitation for the presented measurements is a radial force which rotates synchronously with the angular velocity of the rotor shaft like an unbalance force.
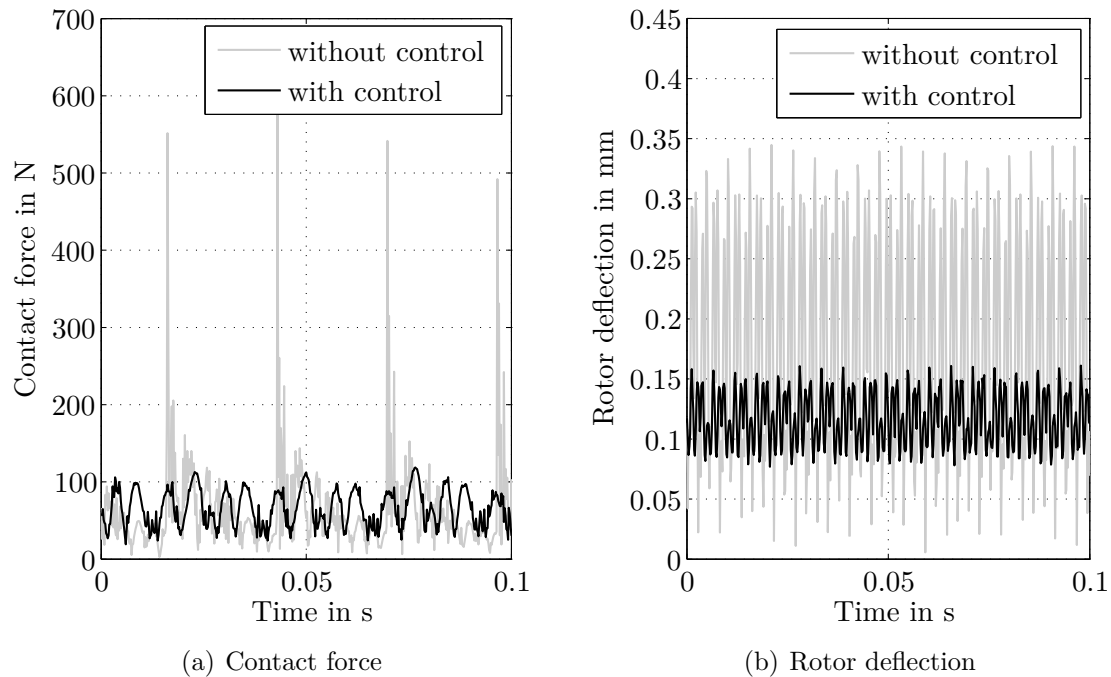

(a) Contact force   (b) Rotor deflection

Figure 4.1: General comparison: rubbing without and with control, constant speed 2233 rpm

Figure 4.1(a) shows the contact force which occur between the rotor and the auxiliary bearing versus time, one measurement without control (gray line) and another with control (black line). Without control the established rubbing state is partial rub with multiple impacts. The contact force is very high with magnitudes up to 600 N.

Using the actively controlled auxiliary bearing the rotor has a permanent contact with the auxiliary bearing and is in the desired rubbing state of "synchronous full annular rub". The contact force is reduced by 80 percent and remains below 120 N. There is still an oscillation of the contact force between 20 N and 120 N, which is caused by periodical errors of the displacement measurement and small control errors. Therefore, the control target for the contact force - cf. equation (2.103) - has to be large enough to avoid a loss of contact, which would lead to impacts.
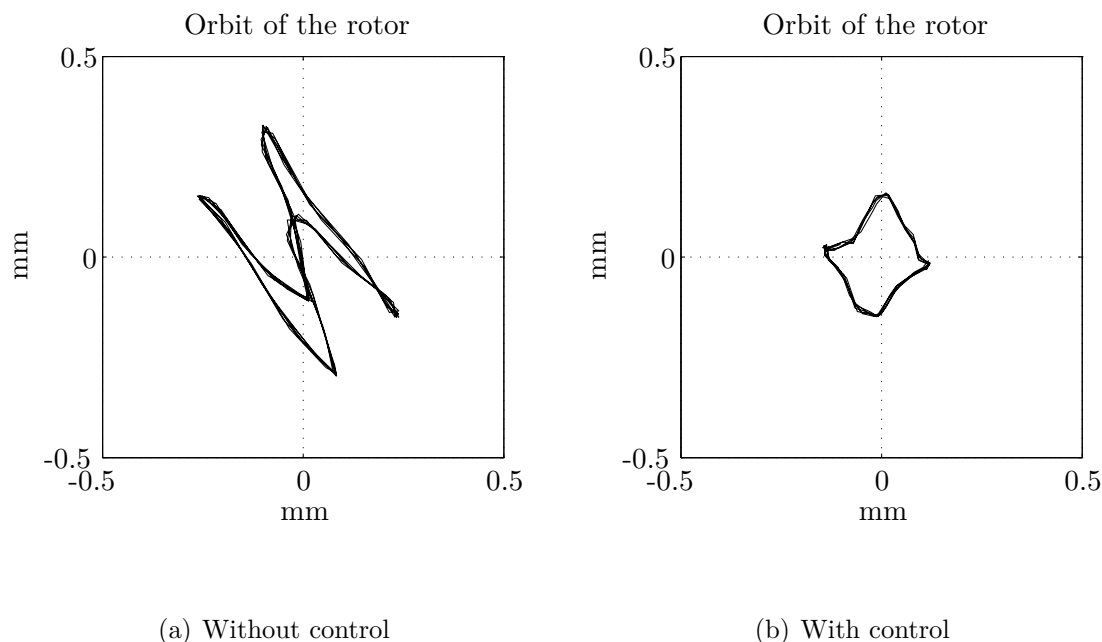

(a) Without control

(b) With control

Figure 4.2: General comparison, constant speed 2233 rpm, orbit of the rotor

In Figure 4.1(b) the rotor deflection versus time for the same experiment is plotted. Without control the auxiliary bearing limits the rotor deflection to the size of the air gap - about 0.3 mm - which is the primary purpose of the auxiliary bearing. Using the developed control system the rotor deflection is reduced by the half and remains below 0.16 mm. There is a reduced contact force at a reduced rotor deflection. Therefore, the target of the feedback controller - the reduction of the contact force at the desired rubbing state of "synchronous full annular rub" - as well as the primary purpose of an auxiliary bearing in general - the limitation of the rotor deflection - is fulfilled.

For a detailed investigation of the rubbing process the orbit of the rotor and the one of the active auxiliary bearing is discussed. Without control, there are multiple
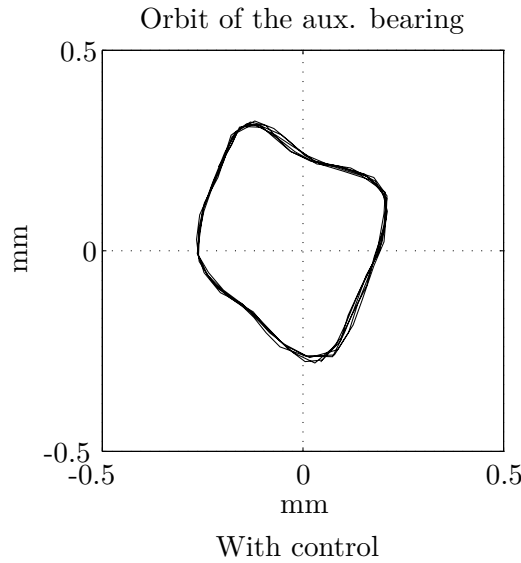
Figure 4.3: General comparison, constant speed 2233 rpm, orbit of the auxiliary bearing

impacts as one can see in Figure 4.2(a), on which the orbit of the rotor displacement of 5 rotations is plotted.

By using the proposed control system, a stabilized state of "synchronous full annular rub" is assured. The orbit of the rotor of this experiment is shown in Figure 4.2(b). Due to measurement errors and imprecision of the control system the measured orbit differs a little bit from the desired one, which is a plain circle. But also despite of this imprecision the control system is able to ensure the desired rubbing state, a permanent contact and a low rubbing force. The plot shows the measurement of 5 rotations of the test rig.

Figure 4.3 shows the orbit of the active auxiliary bearing with control. The deviation of the nominal desired orbit - which is a plain circle - shows how the active auxiliary bearing compensates the imprecision discussed above. The plot shows the measurement of 5 rotations.

4.1.2 Sudden Excitation

For the second presented experiment, the rotor is running at a constant speed without rotor to stator contact. At a time of t=1.0 s the magnetic bearing applies a suddenly arising excitation. The excitation is a radial force, which rotates synchronously with the angular velocity of the rotor shaft. Therefore, a suddenly arising unbalance is simulated. This excitation leads to rubbing. The measurement in Figure 4.4(a) shows the contact force versus time without control. The active auxiliary bearing acts as a conventional auxiliary bearing and the simulated unbalance leads to a state of partial rub with a high contact force up to 700 N. The same experiment has been
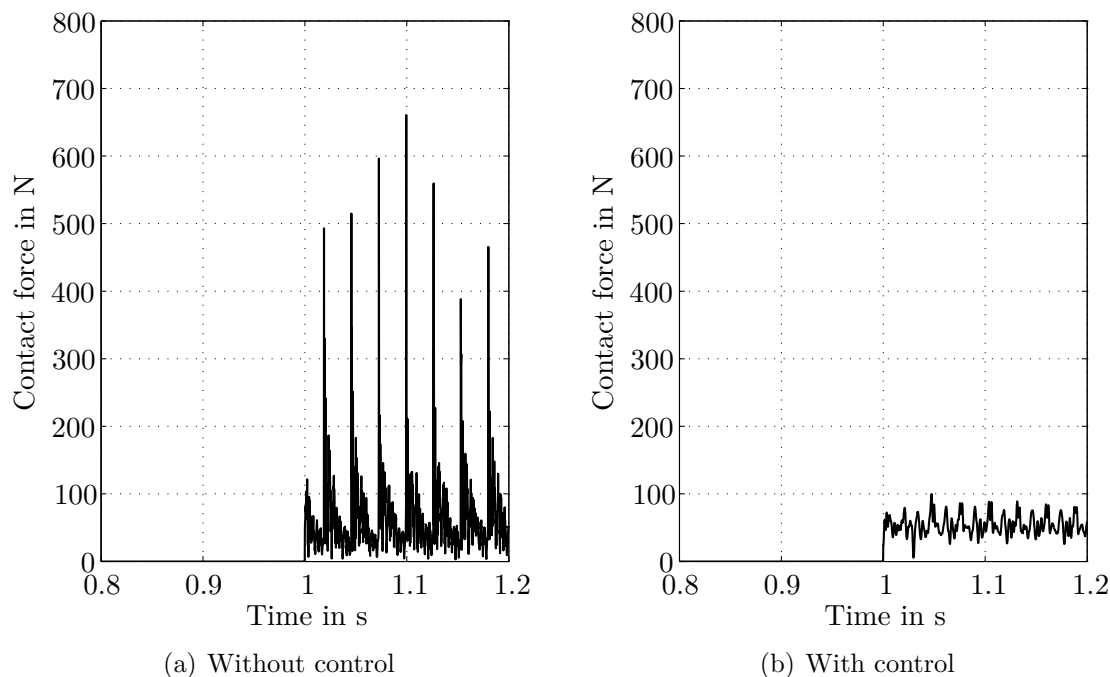
(a) Without control

(b) With control

Figure 4.4: Suddenly arising excitation, constant speed 2235 rpm, contact force

repeated using the feedback control. This measurement is shown in Figure 4.4(b). The contact force versus time is plotted. The automatic activation system tracks the position of the rotor and activates the control system just a few milliseconds after the arising of the unbalance at a time of t=1.0 s. The control system is able to assure a permanent contact in the desired state of "synchronous full annular rub" with a very low contact force. In this case the contact force is reduced by 87 percent. The reduction of the contact force is reflected in the same way in the load on the bearings and in amplitude of the noise. At the same time, the rotor deflection is reduced.

4.1.3 Speeding-Up

In Figure 4.5(a) an extract of a speeding-up of the rotor system is shown. The presented part of the speeding-up ranges from about 2080 rpm to 2350 rpm, in which the third order of the excitation caused by the speed droop of the motor hits the first eigenfrequency, as discussed in Section 3.1.2. In this part, the rotor deflection becomes larger than the nominal air gap, and rubbing occurs. The experiment has been performed twice, first without control and a second time using the control system, which is activated and deactivated automatically. For each experiment the main peaks of the contact force are plotted on the left side and the main peaks of the acceleration of the ball bearing / mounting on the right side, both versus the rotational speed. There is a significant reduction of the load by 65 percent, when using the proposed control system which assures a permanent contact during
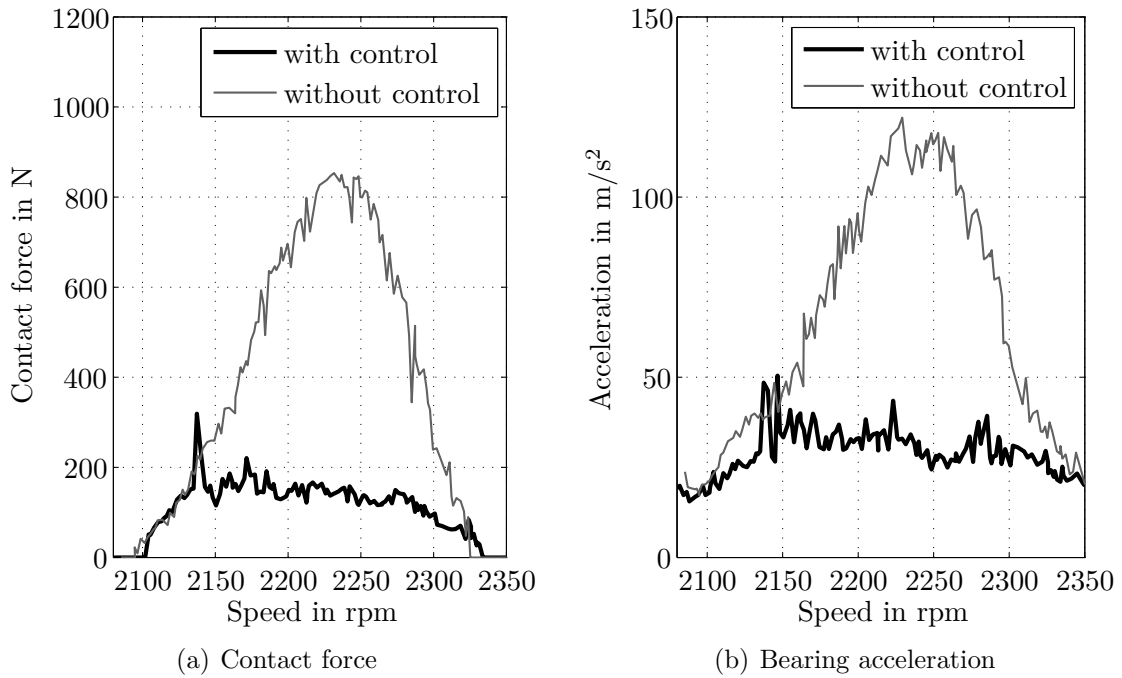
(a) Contact force

(b) Bearing acceleration

Figure 4.5: Speeding-up, with and without control

rubbing in the state "synchronous full annular rub". Also the acceleration of the mounting is reduced drastically, which goes along with a reduction of the load on the whole system. As soon as the critical speed range is crossed, the controller is deactivated automatically, and the auxiliary bearing separates from the rotor. Also the non-controller auxiliary bearing separates autonomously in the presented experiment.

4.2 Configuration "12 mm Shaft"

In the following the experiments, which have been performed using the assembly with the "12 mm Shaft", are presented. For the case "without control" the auxiliary bearing is fixed mechanically to be concentric with the undeformed rotor and is working as a conventional passive auxiliary bearing. Measurements of the rotor deflection and of the rotor orbit are presented. These measurements have been performed next to the auxiliary bearing.

Due to the slender shaft and the configuration of the masses, the possibility of a state of backward whirling is extremely high. In all experiments without control, a state of backward whirling has occurred.

4.2.1 General Comparison
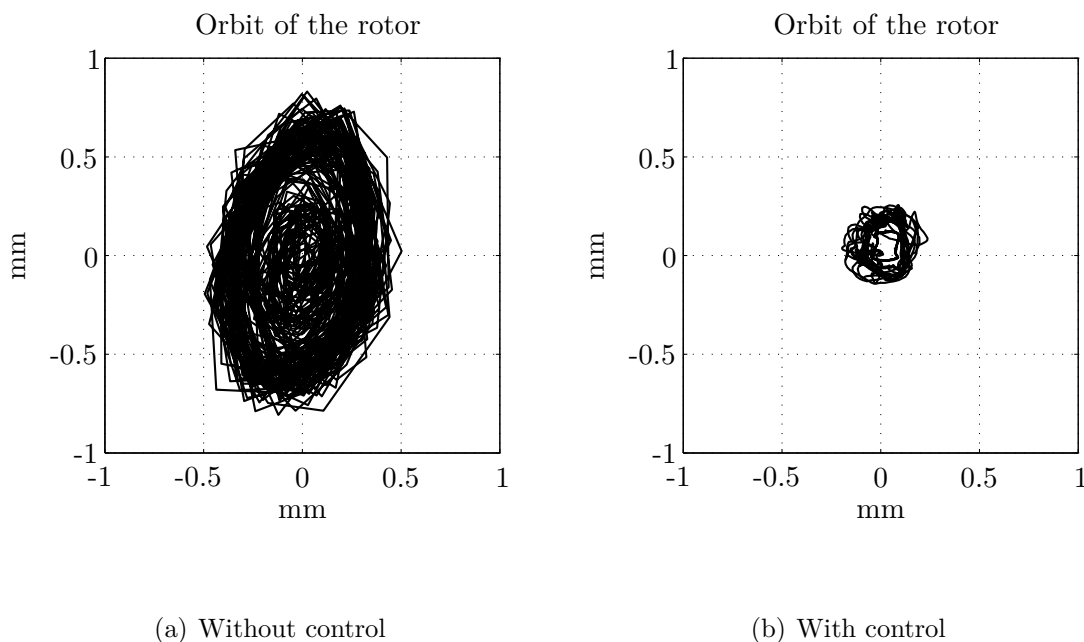

(a) Without control

(b) With control

Figure 4.6: General comparison: constant speed of 500 rpm, orbit of the rotor

This measurements show a comparison of rubbing with and without control at a very high friction coefficient, Figure 4.6(a) and 4.6(b). The rotor with a diameter of 12 mm is running at a constant speed of 500 rpm. At a time of t=1.0 s an additional excitation in form of a synchronous rotating radial force arises suddenly. This simulated arise of an unbalance leads to rubbing. The high friction coefficient is achieved by applying no lubrication at all inside the auxiliary bearing. Figure 4.6(a) shows the rotor orbit of the experiment without activated control system. A few revolutions after the first contact the rubbing state turns into "backward whirling"

with a very high rubbing force and a large deflection. Figure 4.6(b) shows the rotor orbit of the experiment with control. At the beginning of the experiment - without the additional unbalance - the rotor is running with a low deflection (inner circle). When the unbalance arises, the rotor deflection exceeds the normal range and the controller is activated, catches the rotor and assures a permanent contact (outer circle) at a low rotor deflection.

4.2.2 Sudden Excitation

In the course of this experiment, the rotor is running at a constant speed without rotor to stator contact. At a time of t=1.0 s, the magnetic bearing applies a suddenly arising excitation. The excitation is a radial force, which rotates synchronously with the angular velocity of the rotor shaft. Therefore, a suddenly arising unbalance is simulated. This excitation leads to rubbing.
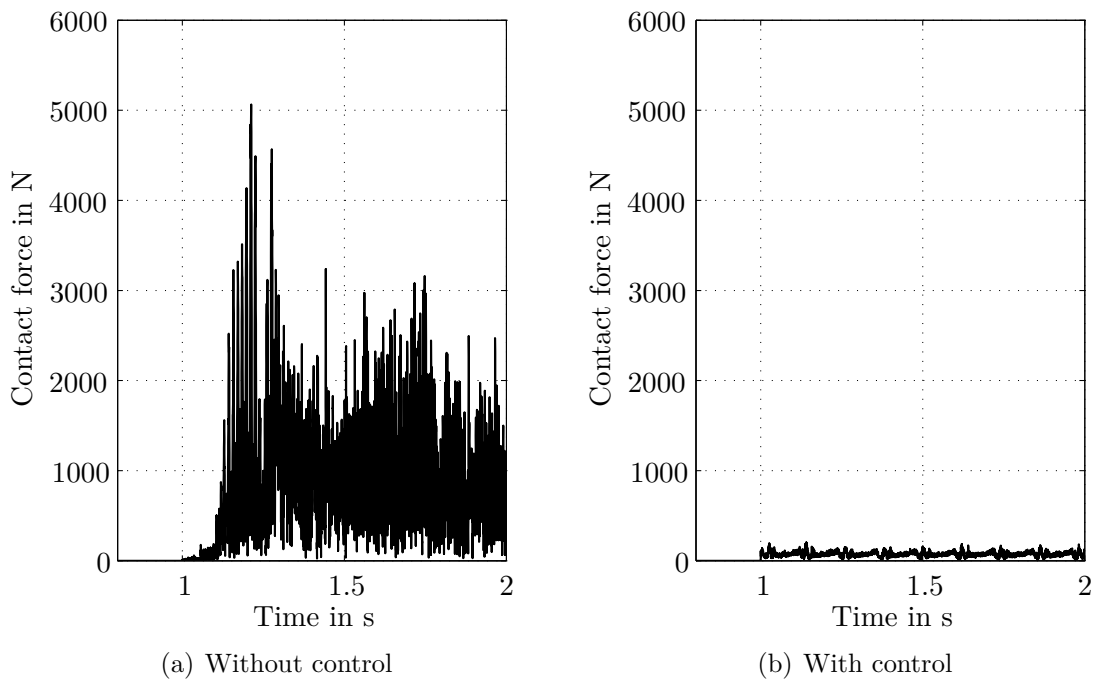

(a) Without control   (b) With control

Figure 4.7: Suddenly arising excitation, constant speed of 500 rpm, contact force

In Figure 4.7(a) the contact force versus time of the experiment without control is displayed. The active auxiliary bearing acts like a conventional auxiliary bearing. The simulated unbalance leads to rubbing in the very destructive state of "backward whirling". The contact force is very high, up to 5000 N. The same experiment has been repeated using the control system. This measurement is shown in Figure 4.7(b). The contact force versus time is plotted. The automatic activation system tracks the position of the rotor and activates the control system just a few milliseconds after the arising of the unbalance at a time of t=1.0 s. The control system is able to assure
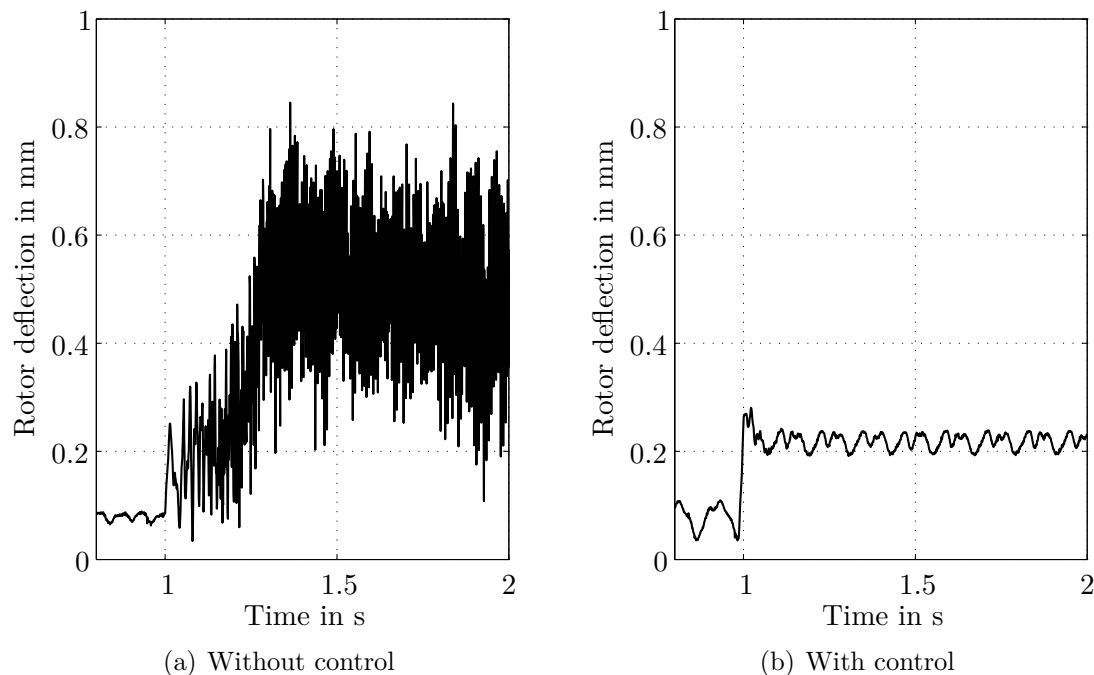
(a) Without control   (b) With control

Figure 4.8: Suddenly arising excitation, constant speed of 500 rpm, rotor deflection

a permanent contact in the desired state of "synchronous full annular rub" with a very low contact force. We achieve a reduction of the contact force of 96 percent.

For both experiments, the rotor deflection is shown in Figures 4.8(a) and 4.8(b). Without control, the rotor deflection is extraordinary high because of the high contact force compared to the stiffness of the auxiliary bearing in this assembly. By using the control system, the rotor deflection is reduced by 70 percent, below the amount of the nominal air gap.

4.2.3 Variation of Friction

Next a variation of the friction between rotor and auxiliary bearing is investigated.

The experimental results deal with two different friction coefficients. It is very difficult to establish a certain friction coefficient at the experimental setup. For this reason, two extreme conditions are compared - high friction and low friction. For achieving the high friction, we performed the experiment without any lubrication inside the auxiliary bearing. The low friction condition is achieved by lubricating the auxiliary bearing. The procedure of the experiment is the same as in the experiment presented in Section 4.2.2. The 12 mm rotor is running at a constant speed of 500 rpm without contact. At t=1.0 s an additional excitation, which simulates an unbalance, arises and leads to rubbing. The control system is activated at all experiments. Figure 4.9(a), 4.10(a) and 4.11(a) show the measurements with a low friction coefficient. Figure 4.9(a) shows the contact force vs. time, Figure 4.10(a)
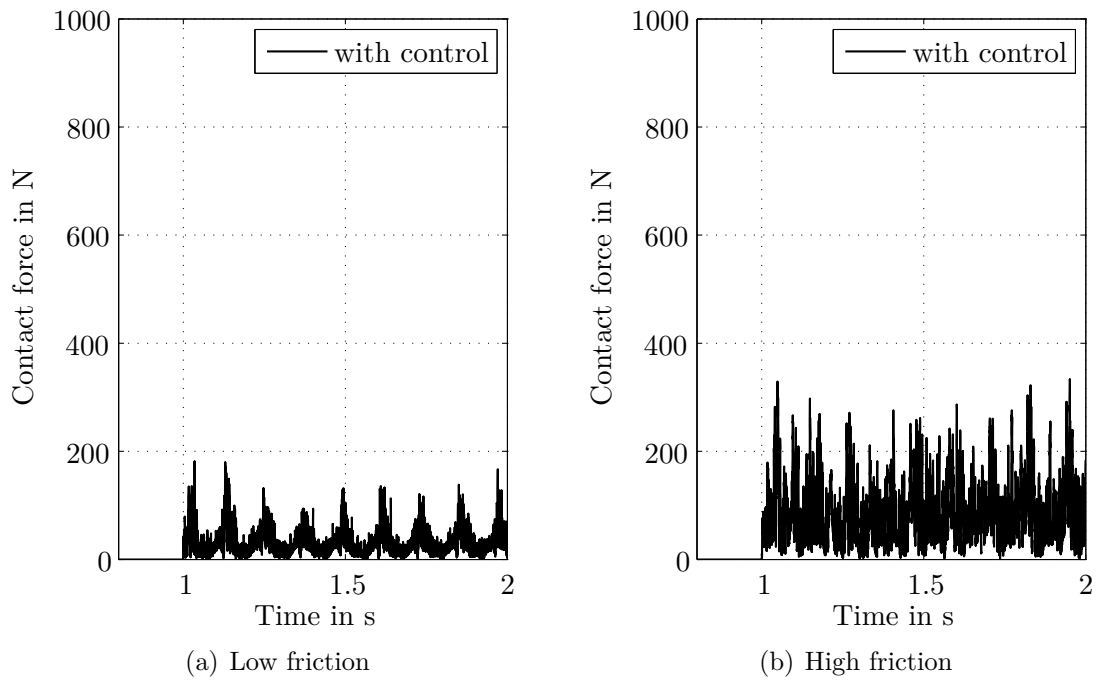
Figure 4.9: Variation of friction: constant speed of 500 rpm, with control, contact force
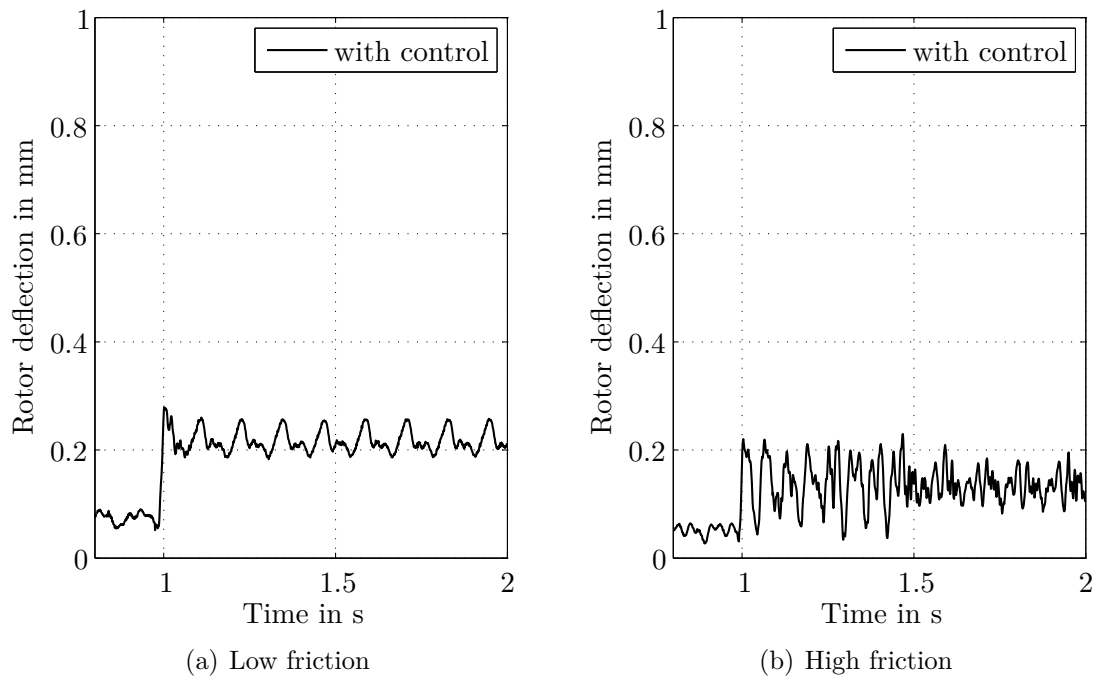

Figure 4.10: Variation of friction: constant speed of 500 rpm, with control, rotor deflection

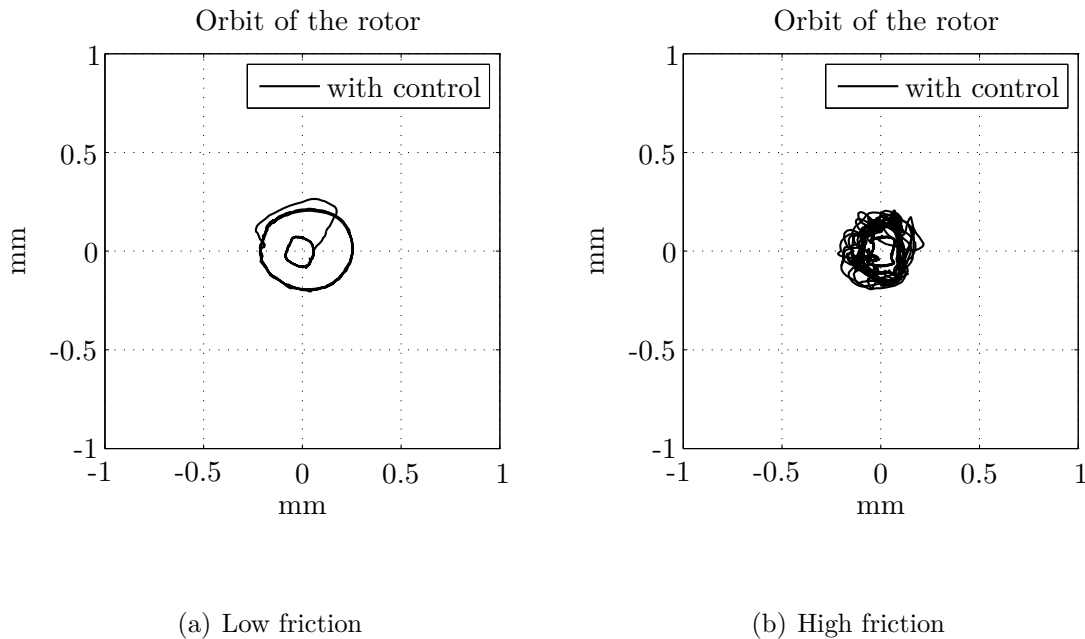(a) Low friction   (b) High friction

Figure 4.11: Variation of friction: constant speed of 500 rpm, with control, orbit of the rotor

the rotor deflection versus time. In Figure 4.11(a) the rotor orbit is plotted. The deflection of the rotor is tracked and when it exceeds a normal range the controller starts the first phase. In the first phase the auxiliary bearing catches the rotor with an impact which is as small as possible. After this, the controller assures a permanent contact with a low contact force and a rubbing state of "synchronous full annular rub". This whole process can be seen in the plot of the orbit, Figure 4.11(a). The inner circle is the orbit of the rotor without unbalance and contact. The outer one is the orbit during the second control phase. Figure 4.10(a) shows the rotor deflection at a low friction. One can see that the deflection is small and it has only a little fluctuation during the controlled rubbing state. This oscillation is caused by measurement imprecision. In Figure 4.9(a) we can see that the contact force is kept very low from the beginning of the arising unbalance.

Figure 4.9(b), 4.10(b) and 4.11(b) show the measurement with the high friction coefficient. Even under this condition the controlled auxiliary bearing keeps the contact force very low (Figure 4.9(b)). The force is a little higher compared to the experiment with low friction. Due to higher peaks of the contact force there is more oscillation of the rotor deflection, as shown in Figure 4.10(b). The higher contact force also results in a smaller rotor-orbit, Figure 4.11(b). The orbit is not as smooth as the orbit of the experiment with low friction. But the controller assures a permanent contact and avoids a destructive rubbing state, so that the contact force is kept very low.

4.2.4 Variation of Rotational Speed

The next experimental results deal with a comparison of various rotational speeds during controlled rubbing of the 12 mm rotor. The procedure of the experiment is the same as in the experiment presented in Section 4.2.2.

The control system is activated. Figure 4.12(a) and 4.12(b) show the experiment with a rotational speed of 200 rpm. Figure 4.13(a) and 4.13(b) show the same experiment at a rotational speed of 400 rpm and Figure 4.14(a) and 4.14(b) for a rotational speed of 600 rpm.

With an increasing speed it takes longer to stabilize the rotor in the controlled rubbing state after the arising of the unbalance. This effect can be also identified in the plots of the orbits (Figure 4.12(b), 4.13(b) and 4.14(b)). At higher rotational speeds there is more oscillation around the desired controlled orbit (outer circle). But in all cases the control system stabilizes the rotor after a few revolutions.
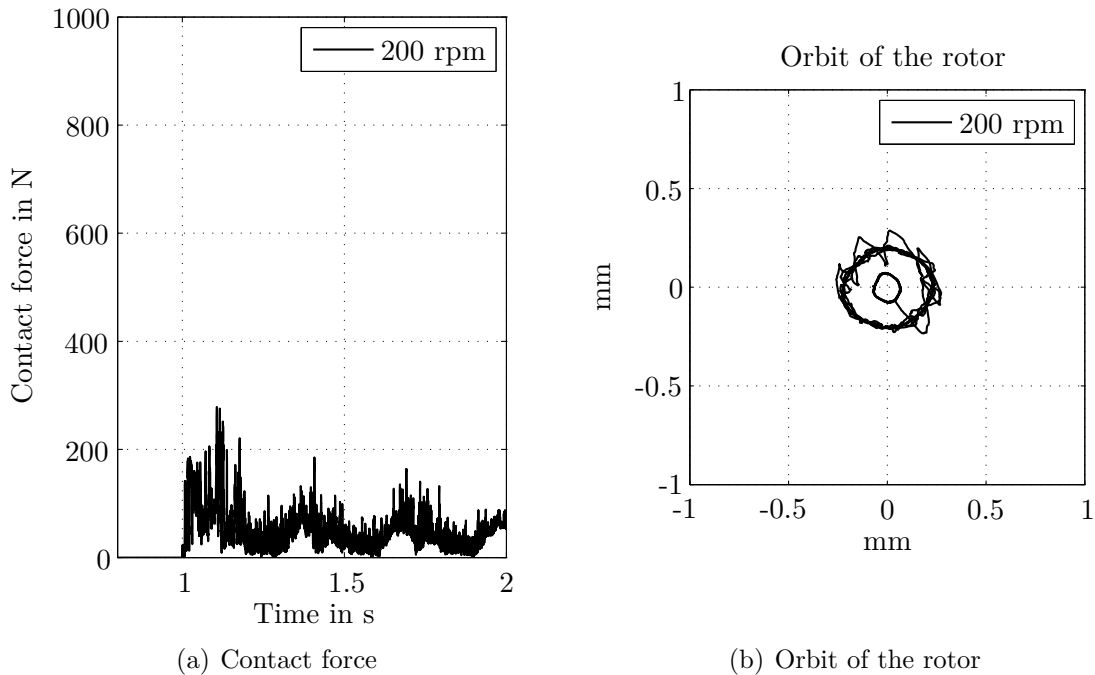

(a) Contact force   (b) Orbit of the rotor

Figure 4.12: Variation of rotational speed: constant speed of 200 rpm, with control

(a) Contact force

(b) Orbit of the rotor
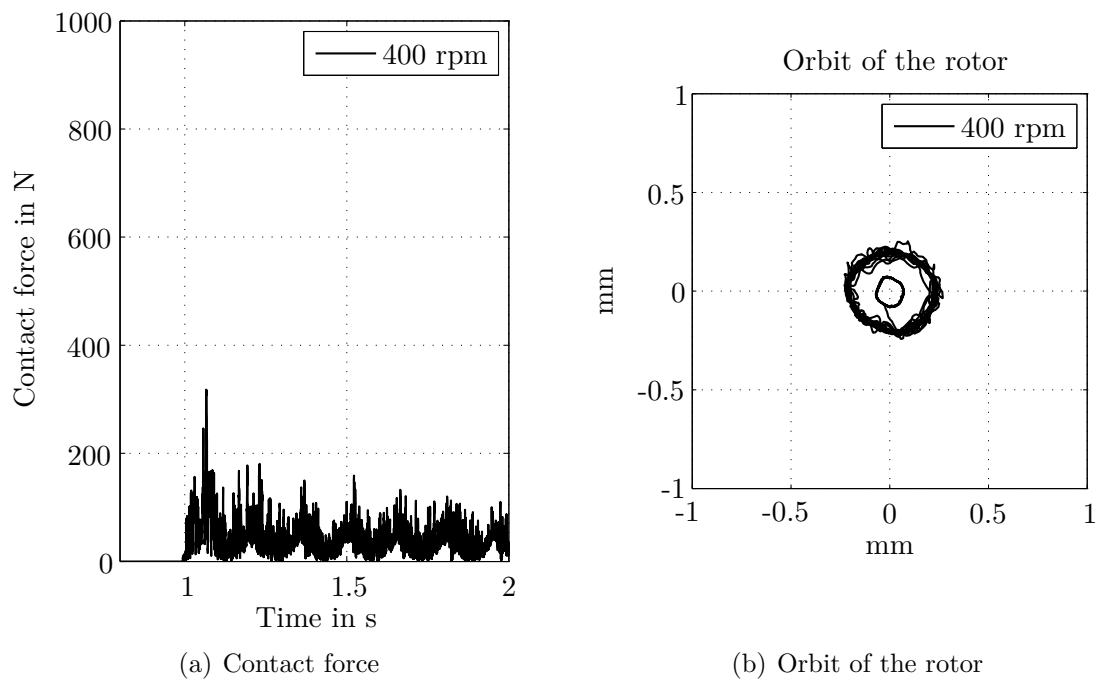
Figure 4.13: Variation of rotational speed: constant speed of 400 rpm, with control

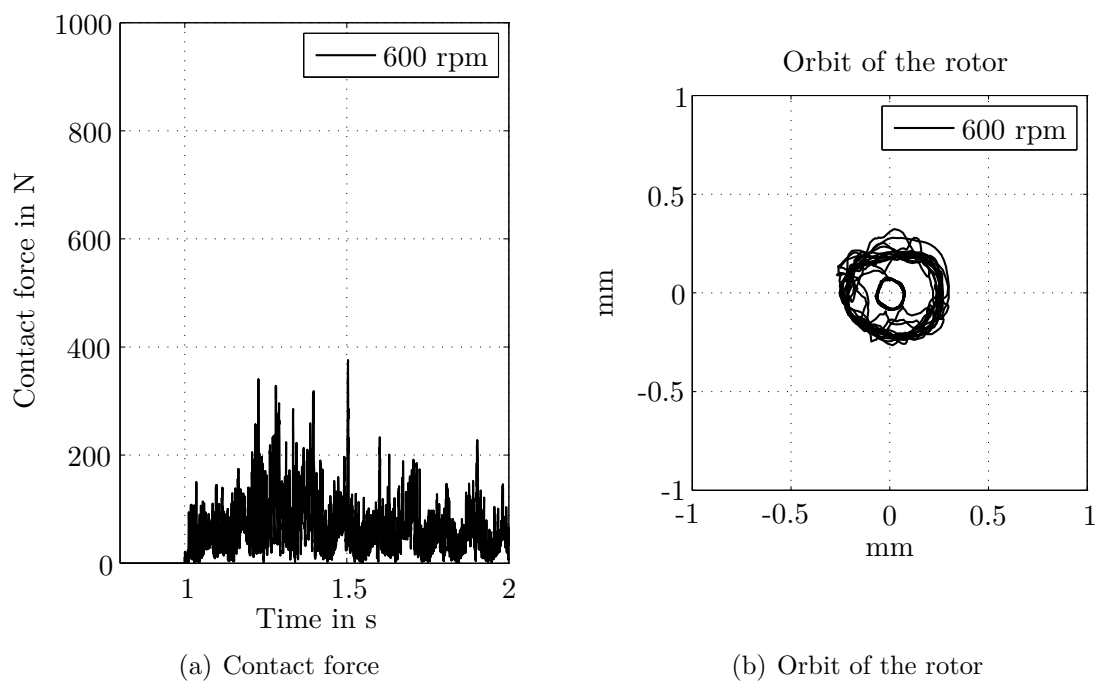(a) Contact force

(b) Orbit of the rotor

Figure 4.14: Variation of rotational speed: constant speed of 600 rpm, with control

4.2.5 Impact Load

Finally, the quality of the control system after an impact load is discussed. At first, results without using the control system are presented. The rotor system is running at a constant speed of 600 rpm. At a time of t=1.0 s a sudden impact is applied on the big disc using a hammer.
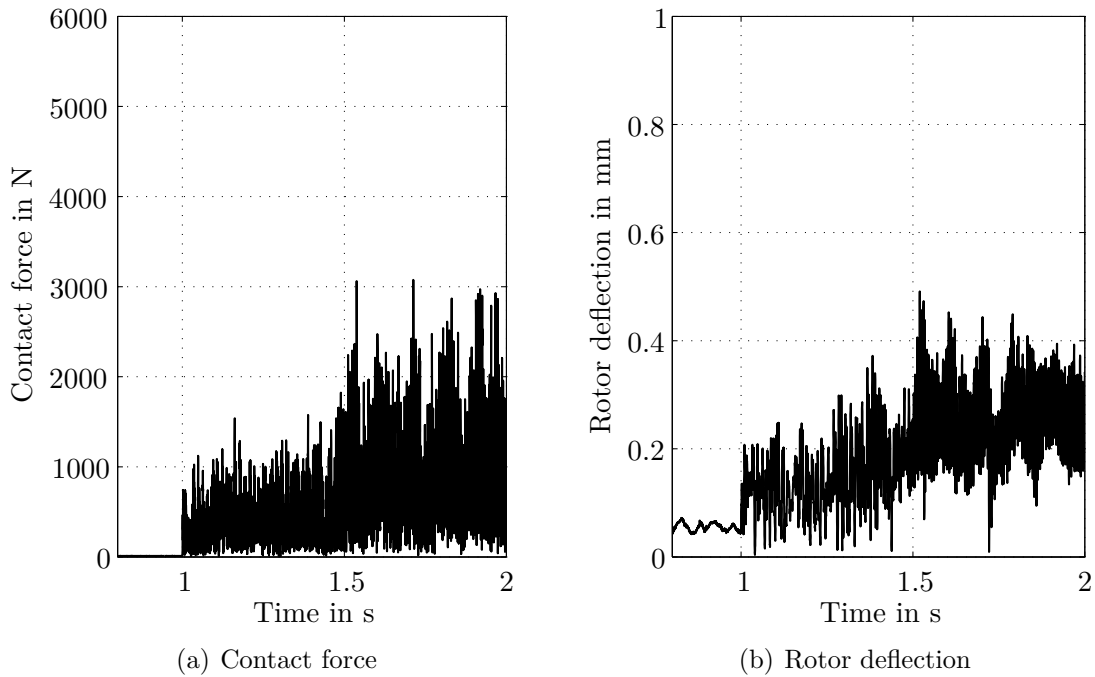

(a) Contact force   (b) Rotor deflection

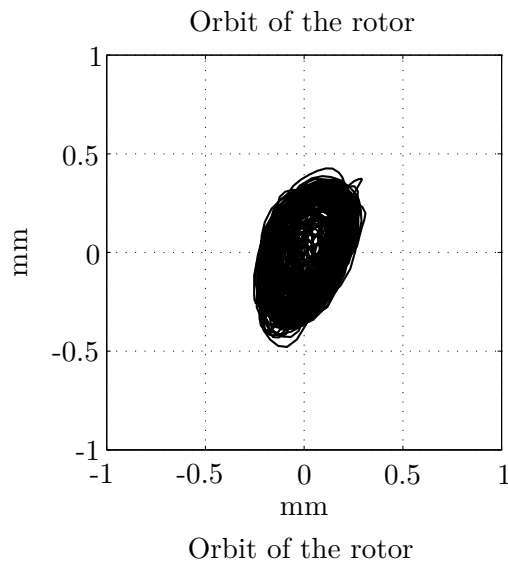**Figure 4.15:** Impact load: constant speed of 600 rpm, without control

Figure 4.16: Impact load: constant speed of 600 rpm, without control

Figure 4.15(a) shows the contact force versus time, Figure 4.15(b) the rotor deflection versus time and Figure 4.16 the rotor orbit. At the beginning of the experiment t<1.0 s the rotor is running in a normal operation mode without contact. The rotor deflection is below 0.1 mm. Shortly after the impact at t=1.0 s the rotor comes into contact with the auxiliary bearing and the destructive "backward whirling" with a very high contact force occurs. The contact force is very high - up to 3200 N. The deflection of the rotor goes up to 0.5 mm. The high number of revolutions on the plot of the rotor orbit originates from the high backward whirling speed.

The same experiment (600 rpm, sudden impact at t=1.0 s) has been repeated with the activated control system. The Figures 4.17(a), 4.17(b), 4.18(a) and 4.18(b) show the measurements using the active auxiliary bearing. The automatic activation system tracks the position of the rotor and activates the control system after the arising of the rotor deflection at a time of t=1.0 s just before the occurrence of the first contact. The control system is able to avoid "backward whirling" and separates the auxiliary bearing from the rotor after the impact. The contact force is reduced by 95 percent. At the same time, the rotor deflection is reduced by 40 percent. Figure 4.18(a) shows the rotor orbit during the experiment and Figure 4.18(b) the orbit of the auxiliary bearing. It should be denoted, that there is no lubrication inside the auxiliary bearing in both experiments. This results in a very high friction, which is the "worst case".

(a) Contact force

(b) Rotor deflection
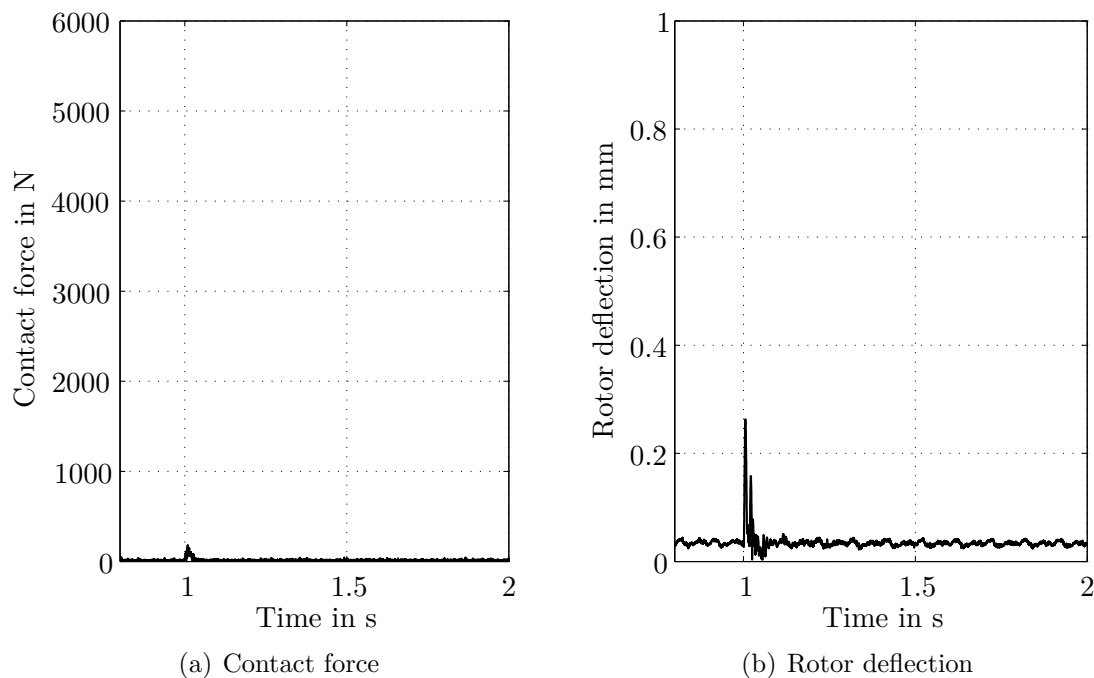
Figure 4.17: Impact load: constant speed of 600 rpm, with control

Orbit of the rotor

Orbit of the aux. bearing
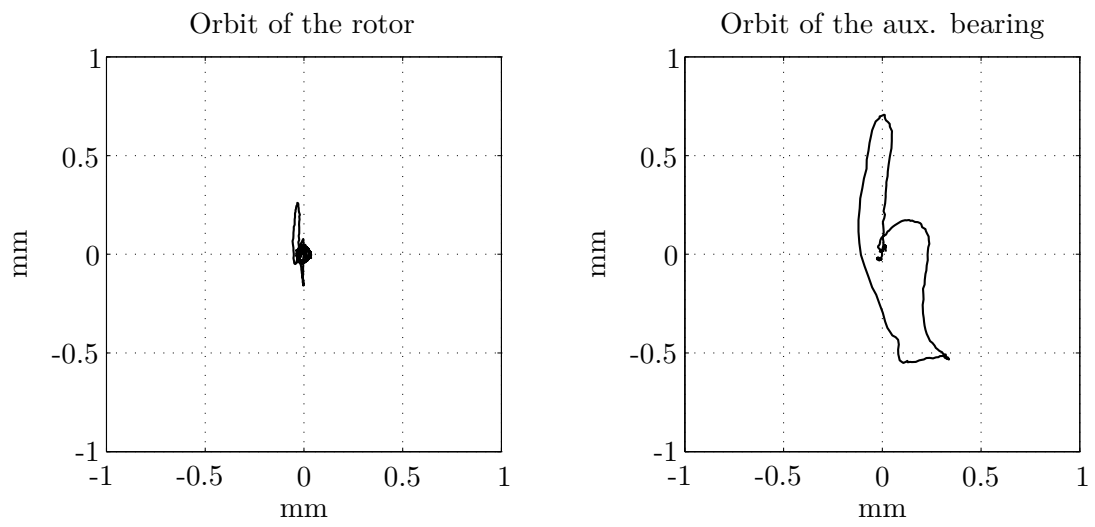
(a) Orbit of the rotor

(b) Orbit of the auxiliary bearing

Figure 4.18: Impact load: constant speed of 600 rpm, with control

5 Advanced Simulation

For a practical realization of the proposed control system, the question for a realistic simulation environment arises. The main requirements to the simulation are:

- Capability to model a full 3D rotor

- Capability to model a general multibody system with standard components

- Interface to import FE data

- Implementation of unilateral contacts

- Cosimulation with SIMULINK® to integrate feedback controller

- High efficiency to be suitable for optimization

Various simulation environments have been investigated concerning the suitability for the given simulation task. SIMPACK as well as other proprietary software turned out to be unsuitable. The major problem has been the unilateral contact in the given dimensions, for a detailed discussion of this topic see [70]. The developed basic rotor simulation, which has been discussed in Section 2.6, does not meet the demands above - even if it was successfully used for the controller development of the presented system.

Finally, for the simulation of a controlled rubbing rotor system and the optimization, the simulation environment MBSim (http://mbsim.berlios.de), which was developed at the Institute of Applied Mechanics, has been chosen. This simulation library is licensed under *GNU Lesser General Public License (LGPL)*. The modeling of the rotor system with the active auxiliary bearing is presented, following by a comparison between experimental results and simulation.

5.1 Simulation Environment

MBSim is based on a framework for the efficient simulation of multibody systems with unilateral contacts and elastic elements. The framework comprises of the description of the system dynamics as well as numerical methods as provided in [20], [21], [73]. A brief overview will be given in the following. For a more comprehensive introduction to the formulation and numerics of non-smooth dynamics see [10], [57].

The non-smooth dynamics of the system is described in terms of a measure differential equation. The dynamics of a bi- and unilateral constrained system can be expressed by

$$\mathbf{M}d\mathbf{u} = \mathbf{h}dt + \mathbf{W}d\mathbf{\Lambda}. \tag{5.1}$$

The matrix $\mathbf{M} = \mathbf{M}(\mathbf{q})$ denotes the symmetric, positive definite mass matrix and depends on the f-dimensional vector of generalized coordinates $\mathbf{q} \in \mathbb{R}^f$. The vector $\mathbf{u} = \dot{\mathbf{q}}$ denotes the velocity vector. The acceleration measure

$$d\mathbf{u} = \dot{\mathbf{u}}dt + (\mathbf{u}^+ - \mathbf{u}^-)d\eta \tag{5.2}$$

is the sum of the continuous part $\dot{\mathbf{u}}dt$ and the discrete parts $(\mathbf{u}^+ - \mathbf{u}^-)d\eta$. The second term is the difference of the left and the right limit of the velocities weighted by the sum of the DIRAC delta functions $d\delta_i$ at the discontinuities t_i:

$$d\eta = \sum_i d\delta_i, \qquad d\delta_i = d\delta(t - t_i) = \begin{cases} \infty \text{ if } t = t_i \\ 0 \text{ if } t \neq t_i \end{cases}. \tag{5.3}$$

On the right hand side of equation (5.1) the vector $\mathbf{h} = \mathbf{h}(\mathbf{u},\mathbf{q},t)$ contains all smooth external, internal and gyroscopic forces. The reaction measure in the contacts $\mathbf{W}d\mathbf{\Lambda}$ is decomposed by the generalized force directions $\mathbf{W} = \mathbf{W}(\mathbf{q})$ and the magnitudes $d\mathbf{\Lambda}$. In analogy to the acceleration measure, the reaction measure $d\mathbf{\Lambda}$ contains forces $\mathbf{\lambda}$ due to persisting contacts as well as impulses $\mathbf{\Lambda}$ due to collisions of bodies at the impact times t_i:

$$d\mathbf{\Lambda} = \mathbf{\lambda}dt + \mathbf{\Lambda}d\eta. \tag{5.4}$$

Integrating (5.1) under consideration of the DIRAC delta (5.3) yields the classical equations of motion for a constrained system and the impact equations.

The computation of the accelerations $\dot{\mathbf{u}}$ as well as the post-impact velocities $\mathbf{u}_i^+$ in equation (5.1) requires the knowledge of the unknown contact reactions $\mathbf{\lambda}$ and $\mathbf{\Lambda}_i$, respectively. Thus, additional contact laws must be constituted. Contacts between bodies in the system are modeled as discrete point contacts whereby the contact zone is assumed to be totally rigid. Deformations of elastic components are only regarded in form of the overall discretization, no local deformation e.g. of a beam cross-section is modeled. Consequently, a contact corresponds to a constraint. In this context two different types of contacts are considered, for which different contact laws hold: persisting contacts which are always closed and contacts that may be open or closed. In the following, the force laws of the two contact types are explained for smooth and non-smooth motion. For this, the contact reactions

$$\mathbf{W}d\mathbf{\Lambda} = \begin{pmatrix} \mathbf{W}_N & \mathbf{W}_T \end{pmatrix} \begin{pmatrix} d\mathbf{\Lambda}_N \\ d\mathbf{\Lambda}_T \end{pmatrix} = \begin{pmatrix} \mathbf{W}_B & \mathbf{W}_U & \mathbf{W}_T \end{pmatrix} \begin{pmatrix} d\mathbf{\Lambda}_B \\ d\mathbf{\Lambda}_U \\ d\mathbf{\Lambda}_T \end{pmatrix} \tag{5.5}$$

are decomposed into components, which are the normal (index N) - split up in bilateral (B) and unilateral (U) - and tangential component (T) to the contact plane.

5.2 Dynamics between Impacts

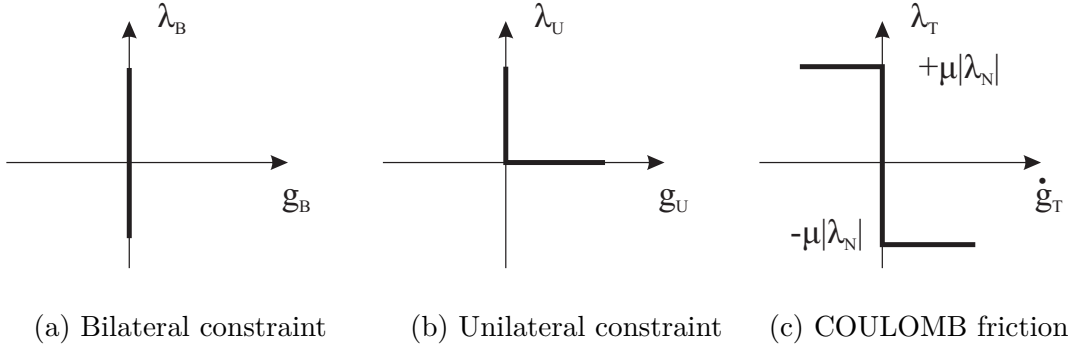(a) Bilateral constraint   (b) Unilateral constraint   (c) COULOMB friction

Figure 5.1: Force laws for bi- and unilateral contacts and friction

First of all, only smooth motion is considered, i.e. no impacts occur. Then a bilateral contact implies a bilateral constraint of the form

$$g_B = 0, \lambda_B \in \mathbb{R}, \tag{5.6}$$

where g_B denotes the normal distance of the interacting bodies in the contact point. The second type of contact also allows for detachment. The associated unilateral constraint is given by the SIGNORINI-FICHERA-condition

$$g_U \geq 0, \quad \lambda_U \geq 0, \quad g_U \lambda_U = 0. \tag{5.7}$$

The respective force laws are shown in the Figures 5.1(a) and 5.1(b).

For both bi- and unilateral constraints dry friction is considered. In order to establish COULOMB's law, the force of a single contact is decomposed in a component $\lambda_N \in \{\lambda_B, \lambda_U\}$ normal to the contact plane and – in case of three dimensional dynamics – tangential components λ_T in friction direction. Using the relative tangential velocity $\dot{g}_T$, COULOMB's friction law is given by

$$\dot{g}_T = 0 \Rightarrow |\lambda_T| \leq \mu_0 |\lambda_N| \tag{5.8}$$

$$\dot{g}_T \neq 0 \Rightarrow \lambda_T = -\frac{\dot{g}_T}{|\dot{g}_T|} \mu |\lambda_N|. \tag{5.9}$$

For the planar case, the force law of a tangential frictional contact is shown in Figure 5.1(c).

5.3 Impact Dynamics

In contrast to persisting and detaching contacts, a closing contact implies a discontinuity in the relative velocities and therewith possibly all generalized velocities. Therefore impacts must be treated separately. The effect of an impact of a specific contact may concern all other constraints, the bilateral as well as the unilateral ones.

The impact law for a bilateral contact is given by

$$\dot{g}_B^+ = 0, \Lambda_B \in \mathbb{R} \tag{5.10}$$

and ensures that relation 5.6 is not violated after collisions. Given on impulsive level, NEWTON's impact law in the formulation of MOREAU

$$\dot{g}_U^+ \geq 0, \Lambda_U \geq 0, \dot{g}_U^+ \Lambda_U = 0 \tag{5.11}$$

and COULOMB's friction law with the normal reaction $\Lambda_N \in \{\Lambda_B, \Lambda_U\}$

$$\dot{g}_T^+ = 0 \Rightarrow |\Lambda_T| \leq \mu |\Lambda_N| \tag{5.12}$$

$$\dot{g}_T^+ \neq 0 \Rightarrow \Lambda_T = -\frac{\dot{g}_T^+}{|\dot{g}_T^+|} \mu |\Lambda_N| \tag{5.13}$$

hold for active contacts with $g_N = 0$ only.

5.4 Elastic Components

The rotor shaft is modeled by a spatial bending-torsional beam using a polynomial finite-element formulation for slender structures [74]. Based on the EULER-BERNOULLI theory with superposed torsion and small deflections, all deformations are described in rotating reference systems individually attached to each node. The formulation allows for arbitrary dynamic contact situations as introduced in the previous section, especially non-smooth dynamics including unilateral contacts and dry friction. For the present case, rigid disks are bilaterally bound to the shaft; the two unilateral contacts to the top and bottom circles of auxiliary bearing are modeled rigid including COULOMB friction.

5.5 Numerical Framework

Two different groups of numerical schemes can be used to integrate unilateral constrained equations of motion: event-driven and time-stepping schemes [21]. The event-driven detects events like detachments or impacts and resolves the exact transition times. Between these events the motion of the system is smooth and all

contact laws are reduced to bilateral constraints. Thus the equations of motion can be integrated by a standard ODE/DAE-integrator with root-finding.

In contrast, time-stepping methods are based on a time-discretization of the system dynamics including the constraints. A detection of events is not needed and the discretization can be chosen such that the constraints are fulfilled either on position or on velocity level. Moreover, a time-stepping algorithm turns out to be very robust in terms of numerical errors.

The presented multibody simulation uses a time-stepping method on position level. A detailed description of the numerical framework can be found in [20]. A comprehensive review on time integration of non-smooth systems is provided in [57].

5.6 Cosimulation with SIMULINK®

A cosimulation between MBSim and MATLAB®/SIMULINK® is used to integrate the feedback controller. MATLAB® provides an Application Program Interface (API) called "the MATLAB® engine" which allows a C program to call MATLAB® as a computation engine. MATLAB® engine programs communicate with a separate MATLAB® process via pipes (in UNIX) and through ActiveX on MICROSOFT WINDOWS®. There exists a library of functions, that allows the program to start and end a process, send data to and from MATLAB®, and send commands to be processed. Figure 5.2 shows the synchronization of the cosimulation. The feedback controller
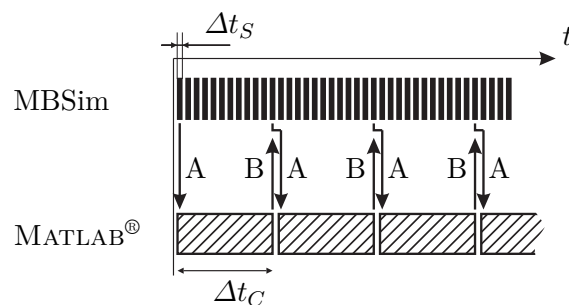

Figure 5.2: Cosimulation

is calculated in MATLAB®/SIMULINK® with a fixed time step size of Δt_C using an EULER discretization as it is used at the experimental test rig. The simulation is calculated with the much lower fixed time step size Δt_S of the time stepping integrator. The synchronization starts with "A". The positions and velocities, which are used by the feedback controller, are transferred to MATLAB® and one calculation step of the controller is started in MATLAB®. In the meanwhile the multibody simulation MBSim is performed until the end of the controller time step Δt_C is reached. With the synchronization "B" the calculated control force for the actuators is transferred to MBSim and the actuator force in the multibody simulation is updated.

The advantages of the cosimulation are the following. Since the dSPACE real-time hardware uses SIMULINK® for the code generation of the controller, a single

Simulink® model of the controller can be used for both - simulation and experiment. So a very rapid controller development and optimization can be achieved. There exists no error source caused by modeling the test rig controller in another simulation software. Furthermore, the cosimulation takes advantage of recent multi-core-processors, because between the synchronization steps MBSim and Matlab® are two independent processes. A detailed discussion about the implementation of the cosimulation can be found in [34].

5.7 Modeling

The simulation model of the rotor system represents the test rig and comprises of the flexible rotor, a unilateral contact with friction between the rotor and the auxiliary bearing and a cosimulation between MBSim and Matlab® /Simulink® to integrate the feedback controller. There are three rigid disks - the big disk, one small disk which is running inside the auxiliary bearing and a disk which is running inside the magnetic bearing. The disks are rigidly coupled on the elastic rotor. The rotor is attached to the environment via two spring-damper elements, which represent the ball bearings and bearing housings. The modeling of the auxiliary bearing is shown in Figure 5.3 and includes the actuators, the three joints and the joint friction. The contact between the rotor and the auxiliary bearing is modeled as a rigid contact as described above. The overall model is a full 3D model of the presented rotor system. So, one simulation model is able to cover totally free motion, impacts and a state of permanent contact.
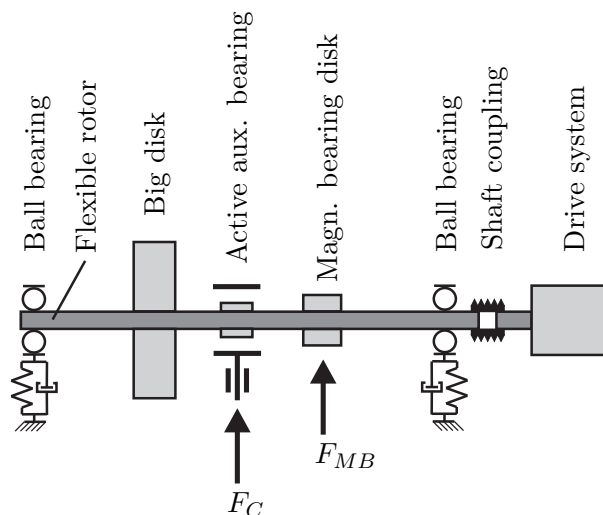

Figure 5.3: Model of the test rig

5.8 Experiment vs. Simulation

The 12 mm configuration of the test rig has been taken to compare experiment and simulation. A measurement with a suddenly arising unbalance, as described in Chapter 4, is used. The rotor is running at a constant speed of 500 rpm.

After the parametrization of the simulation, several experiments have been compared to the simulation to determine the unknown parameters (e.g. free vibration decay tests of bending and torsion). Experiments at various rotational speed with varying excitations, with and without contact, have been performed. Therefore, the dynamics of the rotor simulation has been aligned with reality in a broad operational range.

For the analysis of the dynamics of the system, the contact force between rotor and the auxiliary bearing during rubbing is highly important, because it reflects the severity of the rubbing. For this reason this force has been taken into account for the comparison between experiment and simulation. It is nearly impossible to measure the contact force directly without manipulating the whole system. Therefore it has been determined indirectly via measurements of the forces of the actuators using the mechanical model.

The presented results deal with the state "without control" and "with control". For the case "without control" the auxiliary bearing is fixed mechanically and is working as a conventional passive auxiliary bearing. The Figures 5.4 and 5.5 show a comparison between experiment and simulation in the case of a deactivated as well as an activated control system. The contact force versus time is plotted in Figure 5.4. The experimental results are plotted on the left (Figures 5.4(a), 5.4(c)), the simulation results on the right (Figures 5.4(b), 5.4(d)). For this experiment the rotor is running at a constant speed without rotor to stator contact. At a time of t=1.0 s the magnetic bearing applies a suddenly arising unbalance. At first the experiment has been performed without using the control system. Then the experiment has been repeated with an activated controller. In the case of "without control" (Figures 5.4(a), 5.4(b)) rubbing in a state of backward whirling occurs with a very high contact force up to 5500 N. The simulation shows an excellent agreement with the experiment.

By using the control system a rubbing state of synchronous full annular rub with a very low contact force (below 200 N) is assured in the simulation as well as in reality. The simulation shows a very good agreement. The oscillation of the contact force of the experiment is caused by measurement errors, which are not covered by the simulation. As a result the plot of the simulation is smoother than the experimental measurement. In Figure 5.5 the rotor orbit beside the auxiliary bearing of each discussed experiment is plotted. Also regarding the orbit plots, there is a very good agreement between experiment and simulation in case of "without control" as well as in case of "with control".
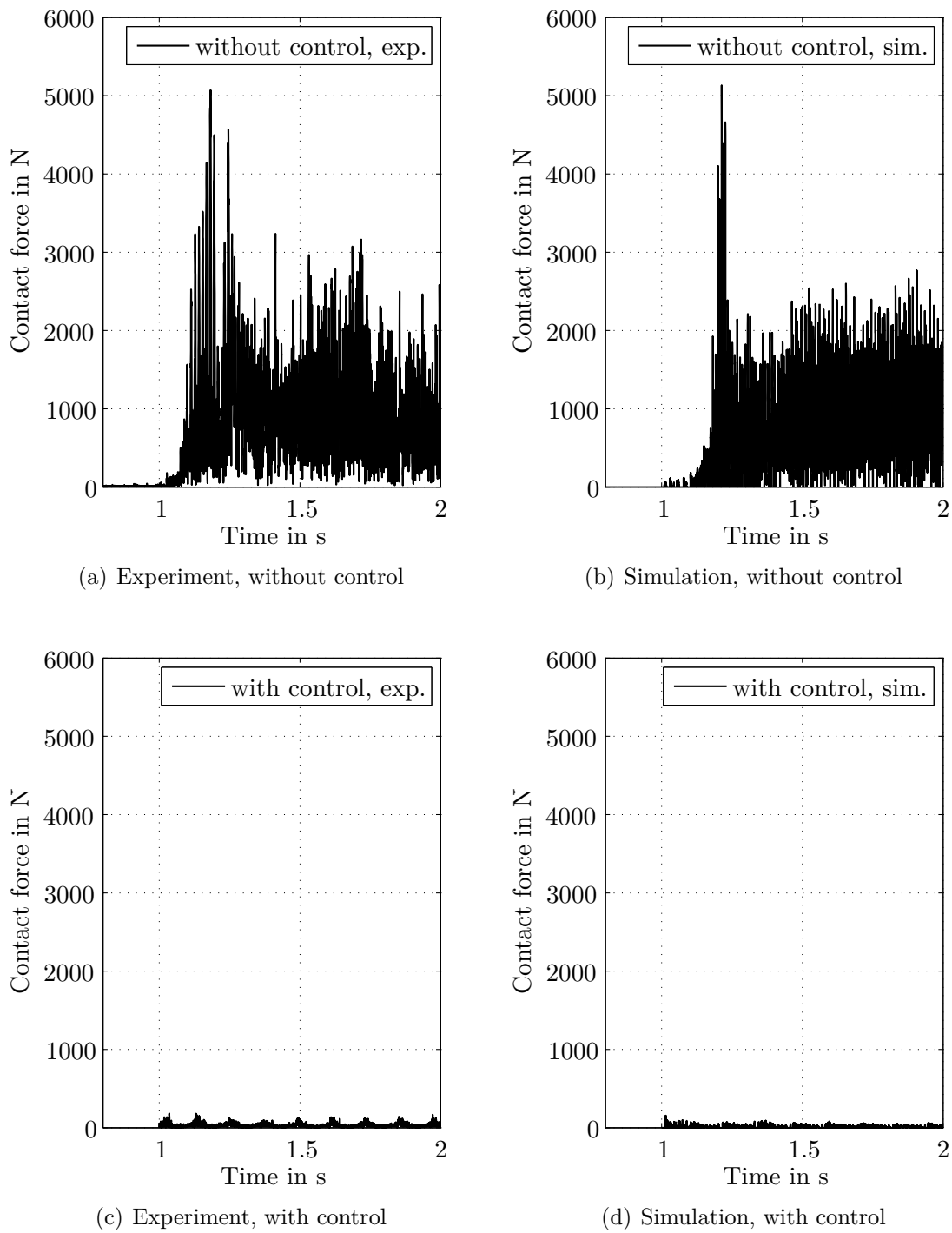
(a) Experiment, without control

(b) Simulation, without control

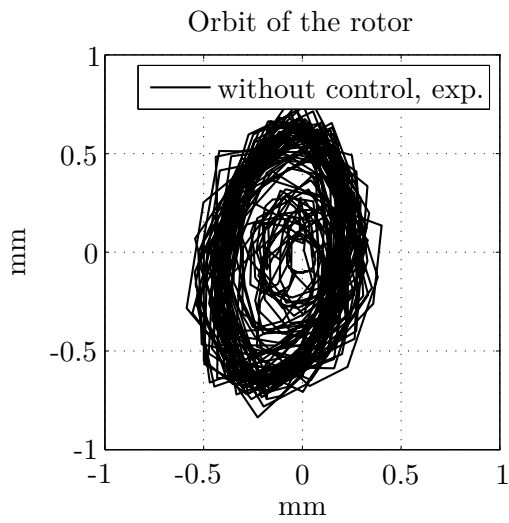(c) Experiment, with control

(d) Simulation, with control
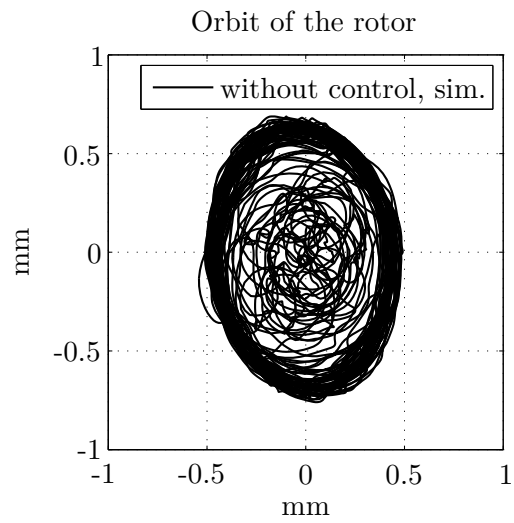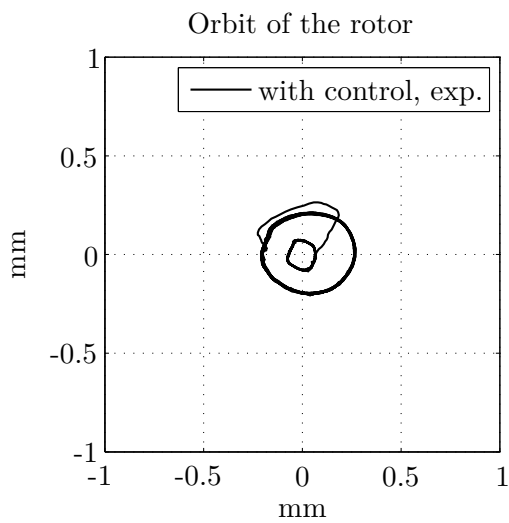
Figure 5.4: Contact force: the 12 mm rotor runs at a constant speed of 500 rpm, at t=1.0 s there is a suddenly arising unbalance
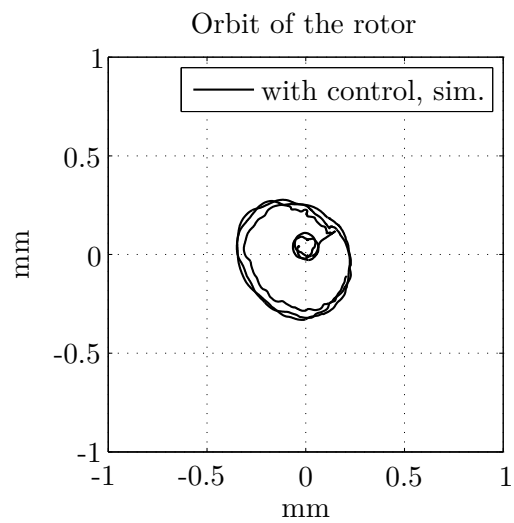
(a) Experiment, without control

(b) Simulation, without control

(c) Experiment, with control

(d) Simulation, with control

Figure 5.5: Rotor orbit: the 12 mm rotor runs at a constant speed of 500 rpm, at t=1.0 s there is a suddenly arising unbalance

6 Summary and Conclusion

A new approach to control a rubbing rotor by applying an active auxiliary bearing has been developed. The control force is applied indirectly using an auxiliary bearing, in case of rotor rubbing only. The auxiliary bearing is designed as a dry bushing type bearing and actuated using two unidirectional actuators. During the normal operation state, the feedback control does not interfere with the rotor system at all.

A three-phase control strategy has been developed, which stabilizes the rotor system in case of rubbing and effectively avoids the destructive *backward whirling*. The model-based cascade-control consists of a feedback control of the actuators, the computation of the target trajectory and an activation routine which tracks the orbit of the rotor. The control system is activated shortly before each occurrence of an impact, if a contact between rotor and the auxiliary bearing is inevitable. In the first phase, when the contact is still open, a target trajectory for the movement of the auxiliary bearing is determined, which synchronizes the auxiliary bearing with the orbit of the rotor. The synchronization is followed by a smooth transition to a contact. Thereby, the relative velocity is minimized, depending on the deflection of the rotor. In the second control phase (during contact) a target trajectory is determined, which keeps a permanent contact with a low contact force and ensures a state of *synchronous full annular rub*. The third phase opens the contact in case of a short-time load. As soon as the excitation has disappeared, the auxiliary bearing is separated from the rotor again and the normal operation mode continued.

Furthermore, the controller ensures that the rotor deflection does not exceed the initial air gap of the auxiliary bearing, to keep its general purpose in mind. The feedback control of the actuators is based on a feedback linearization and assures an accurate and robust motion control of the auxiliary bearing throughout the full range of possible contact forces and impacts.

Only a few signals are required by the control system. The displacement of the auxiliary bearing and the rotor in the plane perpendicular to the rotor at the location of the auxiliary bearing are used as input to the controller.

A test rig has been developed to experimentally verify the control system. Various experiments show the success of the control strategy. In the case of controlled rubbing, the reduction of the contact force ranges from 74 percent to 96 percent. At the same time, the rotor deflection is decreased too. The activation and deactivation of the control system is operated automatically.

Using the equations of motion, which have been required for the feedback controller development, a basic simulation has been designed. This simulation has been successfully used during the controller design process. However, as the experimental results show, this simulation is not able to represent the dynamics of a real rotor system. Therefore, a sophisticated and at the same time highly efficient simulation framework has been developed, which can be used to configure active auxiliary bearings for future applications. The advanced simulation is based on a framework for the efficient simulation of multibody systems with unilateral contacts and elastic elements. The simulation comprises of the modeling of a 3D flexible rotor, unilateral contacts with and without friction between the rotor and stationary parts and an interface to MATLAB® /SIMULINK® to co-simulate the feedback control of active elements. The fundamentals of unilateral constraints allow a detailed simulation of processes like contact/detachment, stick/slip or impacts with and without friction. The developed simulation environment has been successfully verified using experimental data. One and the same simulation model was able to cover situations of controlled as well as uncontrolled rubbing.

An industrial application of the proposed control system primarily depends on the availability of suitable actuators. On the one hand, these actuators have to fulfill the requirement of high speed. The rotational frequency of the rotor system has to be met. On the other hand the required force capability depends on the rotor system to be controlled. Due to the additional costs of actuators and real-time hardware, the primary focus at the moment lies on applications, which are highly relevant to security.

A General Parameters

A.1 Dimensions Active Auxiliary Bearing
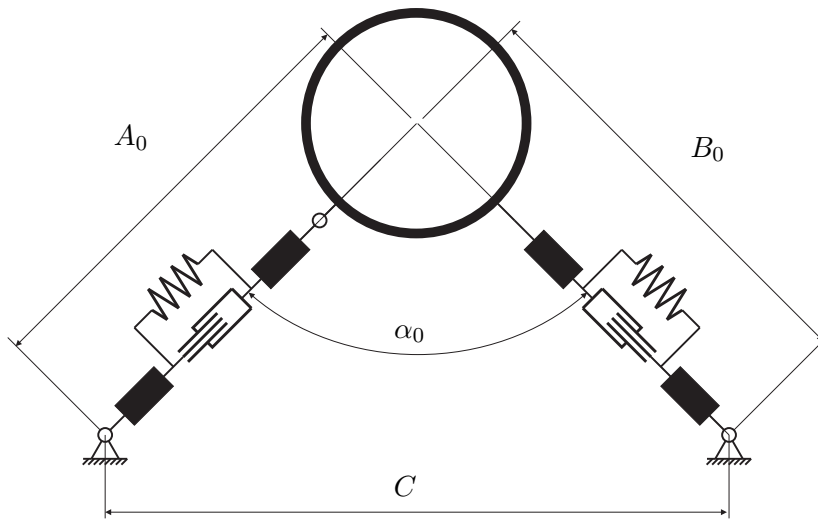
Figure A.1: Main dimensions active auxiliary bearing - drawing

A_0	appr. 283 mm
B_0	appr. 283 mm
C	406.5 mm
α_0	appr. 90 deg

Table A.1: Main dimensions active auxiliary bearing - parameters

A.2 Drive System

Parameter	Value
Manufacturer	Mattke
Type	MC27R0006
Maximum speed	3500 rpm
Nominal torque	1430 Ncm

Table A.2: Selected parameters of the drive system

A.3 Sensors

Measured quantity	Manufacturer	Type
Force (actuator)	Kistler	9021A
Displacement (actuator)	Micro-Epsilon	U3
Displacement (rotor)	Micro-Epsilon	S2

Table A.3: Sensors used by control concept

B Configuration "40 mm Shaft"

B.1 Dimensions Rotor
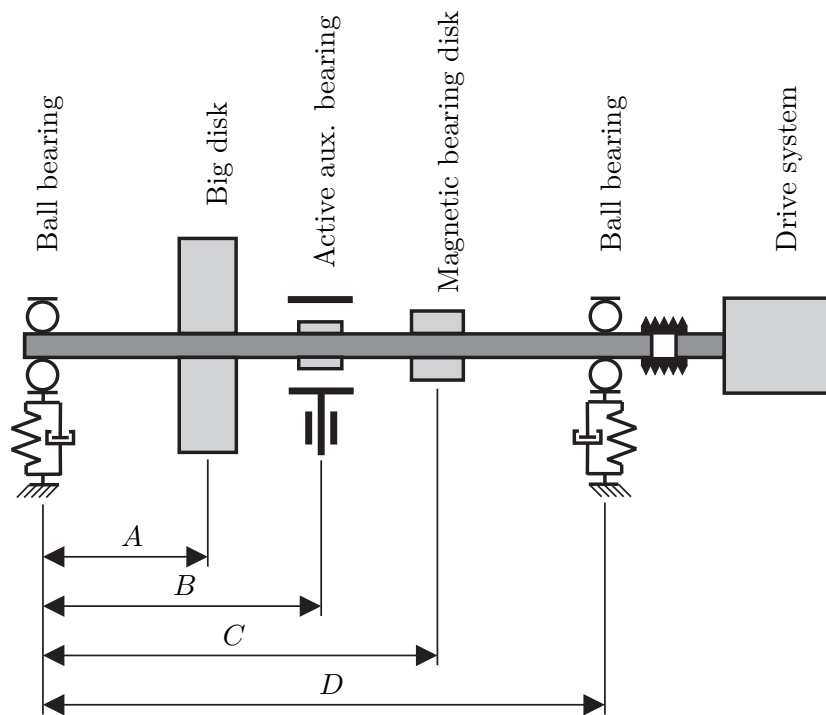
Figure B.1: Main dimensions rotor - drawing

A	175 mm
B	280 mm
C	430 mm
D	590 mm

Table B.1: Main dimensions rotor - parameters

B.2 Parameters

Parameter	Value
Diameter of the shaft	40 mm
Mass of the big disk	9.6 kg
Mass of the auxiliary bearing disk	1.4 kg
Mass of the magnetic bearing disk	2.6 kg
Stiffness of the ball bearing mounting	6000 N/mm

Table B.2: Selected parameters of the rotor

C Configuration "12 mm Shaft"

C.1 Dimensions Rotor
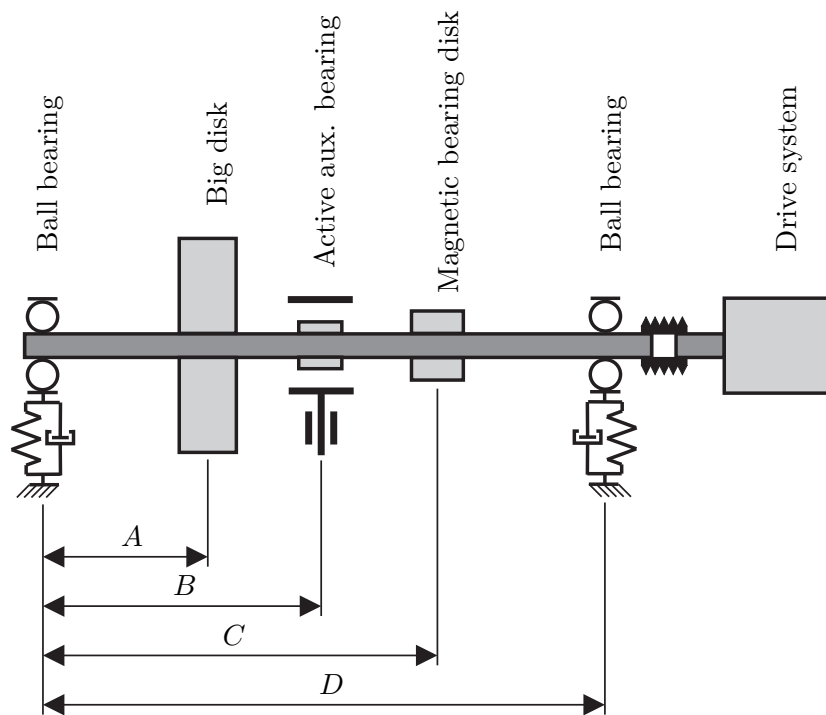
Figure C.1: Main dimensions rotor - drawing

A	$175\,\mathrm{mm}$
B	$280\,\mathrm{mm}$
C	$380\,\mathrm{mm}$
D	$590\,\mathrm{mm}$

Table C.1: Main dimensions rotor - parameters

C.2 Parameters

Parameter	Value
Diameter of the shaft	12 mm
Mass of the big disk	2.51 kg
Mass of the auxiliary bearing disk	0.791 kg
Mass of the magnetic bearing disk	0.519 kg
Stiffness of the ball bearing mounting	6000 N/mm

Table C.2: Selected parameters of the rotor

Bibliography

[1]   ABULRUB, A. G. ; SAHINKAYA, M. N. ; KEOGH, P. S. ; BURROWS, C. R.:
      Experiments on ROLAC to recover rotor position following contact. In:
      Proceedings of the 10th International Symposium on Magnetic Bearings (ISMB10),
      2006

[2]   ALLIANZ VERSICHERUNGS-AG (Editor): *Allianz-Handbuch der Schadenverhütung.*
      3.neu bearbeitete und erweiterte Auflage. VDI Verlag, 1984

[3]   ALTHAUS, J. : *Eine aktive hydraulische Lagerung für Rotorsysteme*, Technische
      Universität München, Dissertation, 1991. – Fortschr.-Ber. VDI Reihe 11 Nr. 154.
      Düsseldorf: VDI Verlag 1991.

[4]   BARTHA, A. R.: Dry Friction Induced Backward Whirl: Theory and Experiments.
      In: *Proceedings of the Fifth International Conference on Rotor Dynamics,
      IFToMM*, 1998, pp. 756–767

[5]   BLACK, H. F.: Interaction of a Whirling Rotor with a Vibrating Stator across a
      Clearance Annulus. In: *Journal of Engineering Science* 10 (1968), Nr. 1, pp. 1–12

[6]   BOOR, C. de: *A Practical Guide to Splines.* 4. Auflage. New York : Springer,
      1978

[7]   BOOR, C. de: *Splinefunktionen.* Basel; Boston; Berlin : Birkhäuser, 1990

[8]   BREMER, H. : *Dynamik und Regelung mechanischer Systeme.* Stuttgart :
      Teubner, 1988

[9]   BREMER, H. ; PFEIFFER, F. : *Elastische Mehrkörpersysteme.* Stuttgart : Teubner,
      1992

[10] BROGLIATO, B. ; TEN DAM, A. A. ; PAOLI, L. ; GÉNOT, F. ; ABADIE, M. :
      Numerical simulation of finite dimensional multibody nonsmooth mechanical
      systems. In: *ASME Applied Mechanics Reviews* Bd. 55(2), 2002, pp. 107–150

[11] CADE, I. S. ; SAHINKAYA, M. N. ; BURROWS, C. R. ; KEOGH, P. S.: On the
      Design of an Active Auxiliary Bearing for Rotor/Magnetic Bearing Systems. In:
      Proceedings of the 11th International Symposium on Magnetic Bearings (ISMB11),
      2008

[12] CHAVEZ, A. ; ULBRICH, H. ; GINZINGER, L. : Reduction of Contact Forces in a
      Rotor-Stator-System in Case of Rubbing through Active Auxiliary Bearing. In:
      Shock and Vibration 13 (2006), pp. 505–518

[13] CHAVEZ, A. : *Minimierung von Kontaktkräften bei Anstreifvorgängen durch
      Regelung*, Technische Universität München, Dissertation, 2006. – Fortschr.-Ber.
      VDI Reihe 8 Nr. 1115. Düsseldorf: VDI Verlag 2007.

[14] CHILDS, D. W.: Rub-Induced Parametric Excitation in Rotors. In: *Transactions
      of the ASME* 101 (1979), pp. 640–644

[15] CHILDS, D. W.: *Turbomachinery Rotordynamics: Phenomena, Modeling, & Analysis.* John Wiley & Sons, Inc., 1993

[16] ECKER, H. : Nonlinear Stability Analysis of a Single Mass Rotor Contacting a Rigid Auxiliary Bearing. In: *Proceedings of the Fifth International Conference on Rotor Dynamics, IFToMM*, 1998, pp. 790–801

[17] EHEHALT, U. : *Bewegungsformen elastischer Rotoren bei Statorkontakt*, Technische Universität Darmstadt, Dissertation, 2007. – Fortschr.-Ber. VDI Reihe 11 Nr. 335. Düsseldorf: VDI Verlag 2008.

[18] EHRICH, F. F. (Editor): *Handbook of Rotordynamics.* McGraw-Hill, Inc., 1992

[19] FENG, Z. ; ZHANG, X.-Z. : Rubbing phenomena in rotor-stator contact. In: *Chaos, Solitons and Fractals* 14 (2002), pp. 257–267

[20] FÖRG, M. ; ZANDER, R. ; ULBRICH, H. : A Framework for the Efficient Simulation of Spatial Contact Problems. In: *Proceedings of the ECCOMAS Conference on Multi-Body Systems.* Milano, Italy, 2007

[21] FÖRG, M. : *Mehrkörpersysteme mit mengenwertigen Kraftgesetzen - Theorie und Numerik*, Technische Universität München, Dissertation, 2007. – Fortschr.-Ber. VDI Reihe 20 Nr. 411. Düsseldorf: VDI Verlag 2007.

[22] FRANKLIN, G. F. ; POWELL, J. D. ; EMAMI-NAEINI, A. : *Feedback Control of Dynamic Systems.* Pearson Prentice Hall, 2006

[23] FUERST, S. ; ULBRICH, H. : An Active Support System for Rotors with Oil-Film Bearings. In: *IMechE Conference Transactions, Fourth International Conference on Vibrations in Rotating Machinery*, 1987, pp. 61–68

[24] GASCH, R. ; NORDMANN, R. ; PFÜTZNER, H. : *Rotordynamik.* 2. Auflage. Springer-Verlag, 2002

[25] GINZINGER, L. ; ULBRICH, H. : Control of a Rubbing Rotor - Experiments and Theory. In: *Proceedings of the 11th International Symposium on Transport Phenomena and Dynamics of Rotating Machinery (ISROMAC 11)*, 2006

[26] HALBLAUB, A. B.: *Control Strategies for a Rubbing Rotor*, Technische Universität München, Lehrstuhl für Angewandte Mechanik, Semesterarbeit, 2006

[27] HECKMANN, B. : *Entwicklung einer Real-Time Kontaktkraftberechnung bei Rotor-Anstreifvorgängen*, Technische Universität München, Lehrstuhl für Angewandte Mechanik, Semesterarbeit, 2006

[28] HERRMANN, M. : *Entwurf, Berechnung und Regelung magnetischer Reluktanz-aktoren*, Technische Universität München, Dissertation, 2008. – Verlag Dr. Hut, München.

[29] HUNT, K. ; CROSSLEY, F. : Coefficient of restitution interpreted as damping in vibroimpact. In: *Journal of Applied Mechanics* 42 (1975), pp. 440 – 445

[30] ISAKSSON, J. L.: *On the Dynamics of a Rotor Interacting with Non-Rotating Parts*, Linköping University, PhD Thesis, 1994

[31] JIANG, J. : *Investigation of Friction in Blade/Casing Rub and Its Effect on Dynamics of A Rotor with Rubs*, Universität Essen, Dissertation, 2001. – Shaker Verlag, Aachen.

[32] LAWEN, J. L. ; FLOWERS, G. T.: Interaction dynamics between a flexible rotor and an auxiliary clearance bearing. In: *Journal of Vibration and Acoustics* 121 (1999), pp. 183–189

[33] LEGRAND, M. ; PIERRE, C. ; CARTRAUD, P. : Full 3D Strategies for Rotor-Stator Contact Interaction in Turbomachinery. In: *Proceedings of the 12th International Symposium on Transport Phenomena and Dynamics of Rotating Machinery (ISROMAC 12)*, 2008

[34] LOEFFL, F. : *Entwicklung einer Co-Simulation zur Optimierung von Regelgesetzen für einen anstreifenden Rotor*, Technische Universität München, Lehrstuhl für Angewandte Mechanik, Semesterarbeit, 2007

[35] MAIA, N. M. M. ; SILVA, J. M. M.: *Theoretical and Experimental Modal Analysis.* Research Studies Press, 1997

[36] MAIER, K. : *Parameteridentifikation eines Rotorprüfstands*, Technische Universität München, Lehrstuhl für Angewandte Mechanik, Semesterarbeit, 2007

[37] MARKERT, R. ; WEGENER, G. : Transient Vibrations of Elastic Rotors in Retainer Bearings. In: *Proceedings of the 7th International Symposium on Transport Phenomena and Dynamics of Rotating Machinery (ISROMAC 7)*, 1998

[38] MOORE, J. ; LEWIS, D. ; HEINZMANN, J. : Feasibility of active instability problems in high-performance turbomachinery. In: *Proceedings of Workshop, Texas A & M University, College Station.* Texas, USA, 1980

[39] MÜHLENFELD, K. ; TADROS, R. : Numerical simulation of jet engine behaviour in case of an assumed blade loss. In: *IMechE Conference Transactions, Sixth International Conference on Vibrations in Rotating Machinery*, 1996, pp. 415–424

[40] MUSZYNSKA, A. : Rotor-To-Stationary Element Rub-Related Vibration Phenomena in Rotating Machinery – Literature Survey. In: *The Shock and Vibration Digest* 21 (1989), Nr. 3, pp. 3–11

[41] OBERBECK, C. ; ULBRICH, H. : Linear Unidirectional Electromagnetic Actuators for Active Vibration Excitation/Isolation in Mechanical Engineering. In: *Proceedings of the 6th International Symposium on Magnetic Suspension Technology.* Turin, Italy, 2001, pp. 224–449

[42] OBERBECK, C. : *Entwicklung und mechatronische Optimierung eines elektromagnetischen Aktors*, Technische Universität München, Dissertation, 2002

[43] PFAB, C. : *Implementierung einer Rotoranstreifregelung auf einem Mikrocontroller*, Technische Universität München, Lehrstuhl für Angewandte Mechanik, Semesterarbeit, 2007

[44] PFEIFFER, F. ; GLOCKER, C. : *Multibody Dynamics with Unilateral Contacts.* John Wiley and Sons, 1996

[45] PILKEY, W. D.: *Analysis and Design of Elastic Beams: Computational Methods.* John Wiley and Sons, 2002

[46] SAHINKAYA, M. N. ; ABULRUB, A. G. ; KEOGH, P. S.: On the modelling of flexible rotor/magnetic bearing systems when in contact with retainer bearings. In: *Proceedings of the 9th International Symposium on Magnetic Bearings (ISMB9)*, 2004

[47] SAWICKI, J. T. ; PADOVAN, J. ; AL-KHATIB, R. : The Dynamics of Rotor with Rubbing. In: *International Journal of Rotating Machinery* 5 (1999), pp. 295–304

[48] SCHNEIDER, M. : *Dynamisches Verhalten eines elastischen Rotors mit einseitigem Kontakt in einem aktiven Fanglager*, Technische Universität München, Lehrstuhl für Angewandte Mechanik, Diplomarbeit, 2007

[49] SCHULZ, G. : *Regelungstechnik 1*. 2. Auflage. Oldenbourg Wissenschaftsverlag, 2004

[50] SCHWEITZER, G. : Stabilization of Self-excited Rotor Vibration by an Active Damper. In: *Dynamics of Rotors - IUTAM Symposium*. Lyngby, Denmark, 1974

[51] SCHWEITZER, G. ; LANGE, R. : Characteristics of a Magnetic Rotor Bearing for Active Vibration Control. In: *IMechE Conference on Vibrations in Rotating Machinery*. Cambridge, England, 1974

[52] SHABANA, A. A.: *Dynamics of Multibody Systems*. Third Edition. Cambridge University Press, 2005

[53] SLOTINE, J.-J. E. ; LI, W. : *Applied Nonlinear Control*. Prentice Hall, 1991

[54] SOMEYA, T. : *Journal-Bearing Databook*. Springer-Verlag Berlin and Heidelberg GmbH, 1989

[55] SPRINGER, H. : Zur Berechnung hydrodynamischer Lager mit Hilfe von Tschebyscheff-Polynomen. In: *Forsch. Ing.-Wes.* 44/4 (1978), pp. 126–134

[56] STANWAY, R. ; O'REILLY, J. : State-Variable Feedback Control of Rotor-Bearing Suspension Systems. In: *IMechE Conference Transactions, Third International Conference on Vibrations in Rotating Machinery*. Heslington, England, 1984

[57] STUDER, C. : *Augmented time-stepping integration of non-smooth dynamical systems*, Eidgenössische Technische Hochschule Zürich, Dissertation, 2008. – ETH E-Collection: doi:10.3929/ethz-a-005556821

[58] SZCZYGIELSKI, W. M.: *Dynamisches Verhalten eines schnell drehenden Rotors bei Anstreifvorgängen*, Eidgenössische Technische Hochschule Zürich, Dissertation, 1986

[59] TONDL, A. : *Some Problems of Rotor Dynamics*. Chapmann & Hall, London, 1965

[60] ULBRICH, H. : *Maschinendynamik*. Stuttgart : Teubner, 1996

[61] ULBRICH, H. ; ALTHAUS, J. : Actuator Design for Rotor Control. In: *Proceedings of the 12th Biennial ASME Conference on Mechanical Vibration and Noise*. Montreal, Canada, 1989, pp. 17–22

[62] ULBRICH, H. ; CHAVEZ, A. ; GINZINGER, L. : Control of Impact Phenomena of a Rubbing Rotor. In: *Proceedings of the 3rd International Symposium on Stability Control of Rotating Machinery (ISCORMA-3)*. Cleveland, Ohio, September 19-23, 2005

[63] ULBRICH, H. ; FUERST, S. : Modeling and Active Vibration Control of Flexible Rotors. In: *Proceedings of the 7th World Congress on Theory of Machines and Mechanisms*. Sevilla, Spain, 1987, pp. 1739–1743

[64] ULBRICH, H. ; SCHWEITZER, G. ; BAUSER, E. : A Rotor supported without Contact - Theory and Application. In: *Proceedings of the 5th World Congress on Theory of Machines and Mechanisms*, 1979

[65] ULBRICH, H. : *Entwurf und Regelung einer berührungsfreien Magnetlagerung für ein Rotorsystem*, Technische Universität München, Dissertation, 1979

[66] ULBRICH, H. : Active Vibration Control of Rotors. In: *Proceedings of the Fifth International Conference on Rotor Dynamics, IFToMM*, 1998, pp. 16–31

[67] VON GROLL, G. ; EWINS, D. J.: A Mechanism of Low Subharmonic Response in Rotor/Stator Contact - Measurements and Simulations. In: *Journal of Vibration and Acoustics* 124 (2002), pp. 350–358

[68] WATANABE, Y. ; SHIRAKI, K. ; AWA, K. ; IWATSUBO, T. : Study of Rotor Vibration due to the Rubbing against Casing. In: *Proceedings of the 10th International Symposium on Transport Phenomena and Dynamics of Rotating Machinery (ISROMAC 10)*. Honolulu, Hawaii, March 7-11, 2004

[69] WEGENER, G. : *Elastische Fanglager zur Amplitudenbegrenzung elastischer Rotoren*, Technische Universität Darmstadt, Dissertation, 2000. – Fortschr.-Ber. VDI Reihe 11 Nr. 290. Düsseldorf: VDI Verlag 2000.

[70] WESENJAK, R. : *Simulation eines anstreifenden Rotors in Simpack*, Technische Universität München, Lehrstuhl für Angewandte Mechanik, Semesterarbeit, 2007

[71] WU, W. : *Aktive Dämpfung von Rotorschwingungen über regelbare Gleitlager*, Technische Universität München, Dissertation, 1999. – Fortschr.-Ber. VDI Reihe 11 Nr. 278. Düsseldorf: VDI Verlag 1999.

[72] YOUNAN, A. A. ; DIMOND, T. W. ; ALLAIRE, P. E.: Transient Drop Analysis of Auxiliary Bearings in Fluid Film/Magnetic Bearing Supported Rotor. In: *Proceedings of the 11th International Symposium on Magnetic Bearings (ISMB11)*, 2008

[73] ZANDER, R. ; SCHINDLER, T. ; FRIEDRICH, M. ; HUBER, R. ; FÖRG, M. ; ULBRICH, H. : Non-smooth dynamics in academia and industry: recent work at TU München. In: *Acta Mechanica*, Springer Wien, 2008

[74] ZANDER, R. : *Flexible Multi-Body Systems with Set-Valued Force Laws*, Technische Universität München, Dissertation, 2008. – Fortschr.-Ber. VDI Reihe 20 Nr. 420. Düsseldorf: VDI Verlag 2009.